All-Metal Aromaticity and Antiaromaticity

Alexander I. Boldyrev*

Department of Chemistry and Biochemistry, Utah State University, Logan, Utah 84322-0300

Lai-Sheng Wang*

Department of Physics, Washington State University, 2710 University Drive, Richland, Washington 99354, and W. R. Wiley Environmental Molecular Sciences Laboratory and Chemical Sciences Division, Pacific Northwest National Laboratory, MS K8-88, P.O. Box 999, Richland, Washington 99352

Received December 2, 2004

Contents

1. Introduction

Since its introduction by August Kekulé in 1865,[1] the concept of aromaticity has been continuously conquering new territories in chemistry (refs 2−20 are only a small fraction of the published articles, reviews, books, and conference proceedings on this subject). Initially, aromaticity was developed for the following classes of organic compounds: (i) monocyclic planar conjugate hydrocarbons and their ions with $(4n + 2)$ π electrons; (ii) polycyclic conjugate hydrocarbons—benzenoid hydrocarbons built of fused benzene rings; (iii) polycyclic conjugated carbocyclic hydrocarbons based on nonbenzenoid systems such as azulene and other conjugate hydrocarbons with four-, five-, seven-, and eight-membered rings.[2,4−17] Today, aromaticity has been extended to a highly diverse number of heterocyclic compounds,[3,8,13,15,17,21−23] as well as three-dimensional (3D) compounds, such as ferrocenes and related sandwich systems,[24−29]

* E-mail (A.I.B.) boldyrev@cc.usu.edu; (L.-S.W.) ls.wang@pnl.gov.

10.1021/cr030091t CCC: $53.50
Published on Web 09/28/2005

Alexander I. Boldyrev was born in Siberia, Russia (1951), and received his B.S./M.S. (1974) in chemistry from Novosibirsk University, his Ph.D. in physical chemistry from Moscow State University, and his Dr.Sci. in chemical physics from Moscow Physico-Chemical Institute (1984). He is currently a professor in the Department of Chemistry and Biochemistry at Utah State University. His current scientific interest is the development of chemical bonding models capable of predicting the structure, stability, chemical bonding, and other molecular properties of pure and mixed main group metal, nonmetal, and metalloid clusters, with the most recent accent on transition metal clusters.

Lai-Sheng Wang was born in Henan, China, in 1961 and received his B.S. in chemistry from Wuhan University, Wuhan, China (1982). After a brief stay at the Institute of Chemistry, Chinese Academy of Sciences in Beijing in 1982, he came to the University of California, Berkeley, and obtained his Ph.D. in physical chemistry in 1990. He was a postdoctoral research associate at Rice University from 1990 to 1992. In 1993, he took a joint position between Washington State University and the Pacific Northwest National Laboratory, where he conducts his research in the W. R. Wiley Environmental Molecular Sciences Laboratory. He is currently professor of physics and materials sciences at Washington State University and holds an affiliate senior chief scientist position at the Chemical Sciences Division, Pacific Northwest National Laboratory. His research interests include the study of size-dependent properties of atomic clusters using photoelectron spectroscopy, discovery of new chemical bonds in clusters, and cluster-assembled materials. His group has also developed experimental techniques to investigate multiply charged anions in the gas phase and is currently involved with the study of the microsolvation of complex anions and solution phase species in the gas phase. He has received a Sloan Research Fellowship and is a Fellow of the American Physical Society. He is currently holding a John Simon Guggenheim Fellowship.

pyramidal hydrocarbons,[8] boron hydrides, carbo- and heteroboranes,[30,31] and fullerenes.[32−34]

Compounds containing metal atoms have been found to be aromatic, too. In 1979, Thorn and Hoffmann[35] predicted that some hypothetical metallocycles should exhibit delocalized bonding and some aromatic characters. During the subsequent years from the initial proposal of Thorn and Hoffmann, approximately 25 metallobenzenes have been isolated and characterized.[36] The first example of a stable, isolabile metallobenzene—osmabenzene—was reported by Elliot et al. in 1982.[37] A large family of metallobenzenes—the iridabenzenes—was synthesized by Bleeke and co-workers,[38−40] whereas a series of dimetallobenzenes with two metal atoms incorporated into the benzene ring was synthesized and characterized by Rothwell et al.[41,42] Recent advances in metallobenzenes have been reviewed by Bleeke.[36]

The term "metalloaromaticity" was introduced by Bursten and Fenske[43] in 1979 to describe metal complexes of cyclobutadiene—aromatic compounds containing a metal atom coordinated to C_4H_4, which is the simplest and archetypal Hückel antiaromatic ($4n$ π electrons) molecule. Interestingly, a coordinated C_4H_4 often acts as if it were aromatic rather than antiaromatic.

The first organometallic compound containing an aromatic cycle completely composed of metal atoms was synthesized by Robinson et al.[44] in 1995. That aromatic compound, $Na_2(Mes_2C_6H_3)Ga]_3$ (Mes = 2,4,6-$Me_3C_6H_2$), contains a triangular aromatic Ga_3^{2-} ring embedded in a large organometallic molecule. In the follow-up publications, Robinson, in collaboration with Schaefer and others, proved computationally that the Ga_3^{2-} unit indeed has two completely delocalized π electrons similar to that in the hydrocarbon analogue $C_3H_3^+$.[45−48] The first π aromatic organometallic compound composed of four gallium atoms, in which an almost perfect square-planar gallium cluster Ga_4 was embedded in an organometallic environment in the $K_2[Ga_4(C_6H_3\text{-}2,6\text{-}Trip_2)_2]$ (Trip = C_6H_2-2,4,6-^{i}Pr$_3$) compound, was prepared by Twamley and Power.[49] Aromaticity in the Power compound was established computationally.[50−52] It was shown that the planar $-Ga_4-$ unit does possess two completely delocalized π electrons and is hence π aromatic, similar to that in the hydrocarbon analogue $C_4H_4^{2+}$.

A few solid compounds containing aromatic metalloid and metal clusters have been characterized as well. Among them, experimental characterization has been reported on aromatic square clusters, such as Se_4^{2+}, Te_4^{2+},[53−56] Sb_4^{2-}, and Bi_4^{2-},[57−59] which are valence isoelectronic to the prototypical aromatic hydrocarbon $C_4H_4^{2-}$, as well as planar pentagonal aromatic clusters, such as As_5^-,[60,61], Sn_5^{6-}, and Pb_5,$^{6-}$,[62] which are valence isoelectronic to the prototypical aromatic hydrocarbons $C_5H_5^-$.

King and Rouvray[30,63a] and Aihara[63b,c] advanced aromaticity in deltahedral boranes and in related compounds including deltahedral metal carbonyls, such as the octahedral clusters $Rh_6(CO)_{16}$, $Ru_6C(CO)_{17}$, and $Os_6(CO)_{18}^{2-}$.[30] King extended this treatment to Rh−Ni carbonyl clusters with structures related to deltahedral 3D aromatic systems such as boranes.[64] The deltahedral structure of the Rh−Ni carbonyl clusters can be explained on the basis of Wade's rules.[65] King also considered a variety of Zintl-like ions composed of metals, which are isolobal and essentially isostructural with the deltahedral boranes with the same number of vertices. Such bare metal cluster ions may be regarded as analogous 3D

aromatic systems, which also possess $2n + 2$ skeletal electrons and use three internal orbitals from each vertex atom.[30] Aromaticity in transition metal oxide structures, due to metal−metal interactions through M−O−M bridges, has also been considered by King[66] and Li.[67]

Despite the progress of synthesizing aromatic compounds with metal atoms being a part of the aromatic ring, the concept of aromaticity was not extended into gas-phase metal clusters and bulk metal alloys until very recently. In 2001 we made a series of bimetallic clusters, $LiAl_4^-$, $NaAl_4^-$, and $CuAl_4^-$, in the gas phase and obtained their photoelectron spectra.[68] Our theoretical studies showed that the most stable isomers of these bimetallic clusters all contain a square-planar Al_4^{2-} dianion, which was shown to be aromatic. Thus, we extended aromaticity to an all-metal (composed of metal atoms only) isolated Al_4^{2-} dianion and to bimetallic all-metal $LiAl_4^-$, $NaAl_4^-$, and $CuAl_4^-$ clusters. Since then aromaticity has been found in a large number of new gaseous all-metal or metalloid clusters: X_4^{2-} (X = B, Al, Ga, In, Tl),[52,68−71] Si_2X_2 (X = B, Al, Ga),[69] XAl_3^- (X = C, Si, Ge, Sn, Pb),[72] XGa_3^- (X = Si, Ge),[73] $NaGa_4^-$ and $NaIn_4^-$,[52,74] X_3^- and NaX_3 (X = Al, Ga),[75] Au_5Zn^+,[76] Cu_nH_n ($n = 3-6$),[77] sandwich structures of $[Al_4TiAl_4]^{2-}$ and $Na[Al_4TiAl_4]^-$,[78] $Al_2(CO)_2$,[79] X_4^{2-} and NaX_4^- (X = N, P, As, Sb, Bi),[80] and X_5^- (X = N, P, As, Sb, Bi).[81−84] Recently, aromaticity has also been extended into metal alloys.[85] It has been shown that all-metal aromatic systems tend to be more electron deficient compared to the corresponding aromatic hydrocarbons. The electron deficiency results in an interesting new feature in all-metal aromatic systems, which should be considered as having multiple aromaticity (π and σ), multiple antiaromaticity (π and σ), and conflicting aromaticity (simultaneous presence of π aromaticity and σ antiaromaticity or π antiaromaticity and σ aromaticity).

The multiple aromaticity (simultaneous presence of σ and π aromaticity) of the Al_4^{2-} dianion has been established with a variety of theoretical techniques: the maps of ring current,[86,87] the aromatic ring-current shielding (ARCS),[69] the nuclear-independent current shielding (NICS),[88] the valence bond (VB) assessment of σ and π aromaticity,[89] the bifurcation analysis of the electron localization function (ELF),[90] and resonance energy (RE) estimations.[70,71]

Following the discovery of the all-metal multiply aromatic Al_4^{2-}, we also experimentally and theoretically characterized an all-metal cluster with conflicting aromaticity (π antiaromaticity and σ aromaticity), Al_4^{4-} in the $Li_3Al_4^-$ bimetallic cluster.[91] The Al_4^{4-} unit is shown to possess four π electrons (π antiaromatic) and has a rectangular structure, analogous to the prototypical antiaromatic cyclobutadiene. However, the Al_4^{4-} tetraanion is still a doubly σ aromatic system. We claimed that the $Li_3Al_4^-$ bimetallic cluster is net antiaromatic[91] primarily on the basis of rectangular distortion of the Al_4 unit. The net antiaromatic nature of $Li_3Al_4^-$ was questioned by Schleyer and co-workers,[88] who concluded that the overall nature of this anion is aromatic rather than antiaromatic on the basis of a small negative value of the total ($\sigma + \pi$) NICS index. The controversy over the net aromatic or antiaromatic nature of the Al_4^{4-} system with simultaneous σ aromaticity and π antiaromaticity generated an interesting discussion in the literature.[92−95]

These new developments in the aromaticity and antiaromaticity in all-metal or metalloid cluster systems are important for developing a unified chemical bonding theory throughout chemistry and are the focus of the current review. Advances in metallobenzenes have been recently reviewed by Bleeke.[36] The topic of aromaticity has been comprehensively reviewed in two recent special issues of *Chemical Reviews*.[2,3]

2. What Is Aromaticity?

Aromaticity is still a rather fuzzy concept, despite being taught in general chemistry classrooms. It is certainly one of the most discussed concepts in the chemical literature, which is demonstrated by about 60000 references to the terms "aromaticity" or "aromatic" in the scientific literature between 1981 and 2000.[96,97] Many books[5,8−13,18,19] and numerous reviews[2−4,6,7,15,16] have been published, and several conferences[14,17,20] have been dedicated to deciphering aromaticity. Knowing that it is still somewhat controversial, we adopt a view of aromaticity with which we hope most chemists would agree. We believe that aromaticity is a qualitative concept that allows chemists to assign a large number of molecules to a certain class, in which all species have specific and similar molecular properties. These specific molecular properties should be different from standard molecular properties observed in classical molecules. We assign a molecule to be classical if we can characterize its chemical bonding using one Lewis structure with two-center two-electron (2c-2e) bonds and lone pairs. Correspondingly, we assign a molecule to be aromatic or antiaromatic if it cannot be characterized by that model and if it also satisfies most of the criteria for aromaticity or antiaromaticity. For example, propylene ($CH_3-CH=CH_2$), benzene (C_6H_6), and cyclobutadiene (C_4H_4) are considered to be classical, aromatic, and antiaromatic, respectively. As one can see, propylene can be easily described by the 2c-2e model, whereas benzene cannot. Many criteria have been proposed in the literature for aromaticity and antiaromaticity. We adopt a list of properties proposed by Krygowski et al.[96] with some small modifications and additions, which are summarized in Table 1.

These criteria have been proposed for π aromatic and π antiaromatic organic systems, but we will see that many of them are also applicable to σ aromatic and σ antiaromatic systems, as well as to a certain degree to all-metal aromatic systems—which exhibit multiple aromaticity, multiple antiaromaticity, and even conflicting aromaticity, although in the last case new criteria for net aromaticity or net antiaromaticity are also needed.

We should stress that one should not expect that aromaticity/antiaromaticity in all-metal systems will manifest itself exactly the same way as in organic chemistry. Many specific deviations are expected.

Table 1. Criteria for π-Aromaticity and π-Antiaromaticity (Adapted from Reference 96)

property	aromatic	olefinic/classical	antiaromatic
(i) electronic nature	$(4n + 2)$ π-electron cyclic conjugation	no cyclic conjugation	$4n$ π-electron cyclic conjugation
(ii) energy			
cyclic conjugation	stabilization	standard	destabilization
delocalization	enhanced	standard	decreased
HOMO−LUMO gap	large	standard	small
(iii) geometry			
bond lengths	equalization	alternation	alternation
(iv) magnetic properties			
anisotropy of diamagnetic susceptibility	enhanced		small
susceptibility exaltation	high		low
^{1}H NMR shifts	diatropic (low-field shift)		paratropic (high-field shift)
NICS (nucleus independent chemical shift)	large negative		large positive
(v) reactivity			
chemical structure	e.g., benzene	e.g., cyclohexadiene	e.g., cyclooctatetraene
retention of structure	electrophilic substitution	electrophilic addition	addition
(vi) spectroscopy			
UV spectra	high energy	standard	low energy
IR/Raman spectra	high symmetry		low symmetry
photoelectron spectra	high electron detachment energies	standard	low electron detachment energies

Nevertheless, we believe that the overall chemical bonding picture and most of the molecular properties in these new species should be explainable using the aromaticity/antiaromaticity concepts. With all that in mind, we now consider aromaticity/antiaromaticity in all-metal systems, starting with the experimental methods used in our laboratories to generate and characterize metal clusters.

3. Experimental Generation and Photoelectron Spectroscopy (PES) Characterization of All-Metal Aromatic/Antiaromatic Clusters

Experimental generation and characterization of all-metal aromatic/antiaromatic clusters are essential in this endeavor. All of the organic aromatic/antiaromatic molecules are known compounds that are either naturally occurring or have been synthesized. However, the all-metal aromatic/antiaromatic clusters that we focus on are gaseous species, which are ideal for theoretical studies but difficult to produce and characterize experimentally. These species are novel molecules and can be used to extend our understanding of chemical structures and chemical bonding. The experimental apparatus that we use in our laboratory involves a laser vaporization supersonic cluster source and a magnetic-bottle photoelectron spectrometer. Details of the experimental setup have been published previously.[98,99] We found that the laser vaporization supersonic beam technique is quite versatile, able to produce a variety of clusters, including the aromatic/antiaromatic all-metal clusters. PES is one of the most powerful techniques to probe the electronic structure of matter. The magnetic-bottle photoelectron spectrometer used in our laboratory is among the most sensitive experimental methods to characterize the electronic structure of gaseous cluster anions and is ideal for the experimental characterization of the all-metal aromatic/antiaromatic clusters.

Figure 1 shows a schematic overview of our experimental apparatus. Briefly, disk targets containing the appropriate atoms required to synthesize the desired clusters are vaporized by an intense pulsed

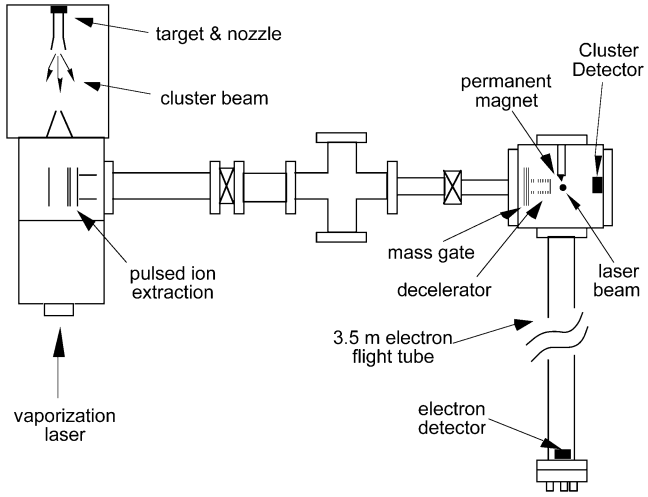

Figure 1. Schematic view of the laser vaporization magnetic-bottle time-of-flight photoelectron spectroscopy apparatus.

vaporization laser beam. The laser-induced plasma is cooled by a high-pressure helium carrier gas, initiating nucleation and formation of clusters. The nascent clusters are entrained in the helium carrier gas and undergo a supersonic expansion to form a collimated cluster beam. Negatively charged species are extracted from the collimated cluster beam perpendicularly and subject to a time-of-flight mass analysis.

Typically, complicated mass spectra with a variety of compositions are obtained. A mass gate is used to select the desired clusters to enter the interaction zone of the magnetic-bottle photoelectron analyzer. The selected clusters are subsequently decelerated before being detached by a laser beam.[98,99] A variety of detachment laser photon energies are available (532, 355, 266, and 193 nm). Photoemitted electrons are collected by the magnetic-bottle at nearly 100% efficiency and analyzed in a 3.5 m long electron time-of-flight tube. The photoelectron time-of-flight spectra are usually calibrated using the known spectra of Cu^- and converted to kinetic energy (KE) spectra. The reported binding energy (BE) spectra are obtained

Table 2. Experimental and Theoretical VDEs for $LiAl_4^-$, $NaAl_4^-$, and $CuAl_4^-$ [68]

species	expt	exptl VDE, eV	MO	$-\epsilon$ VDE, eV	ROVGF VDE,[a] eV	TD-B3LYP, VDE, eV	CCSD(T), VDE, eV	CASSCF/MRCI ADE,[b] eV
$LiAl_4^-$	X	2.15 ± 0.06	$3a_1$	1.94	2.09 (0.86)	1.98	2.22	
	A	2.20 ± 0.06	$1b_1$	2.17	2.17 (0.85)	2.12	2.21	
	B	2.82 ± 0.08	$2a_1$	2.46	2.69 (0.85)	2.68		
	C	3.09 ± 0.04	$1b_2$	2.85	2.97 (0.85)	3.08	3.00	
$NaAl_4^-$	X	2.04 ± 0.05	$3a_1$	1.85	1.92 (0.86)	1.85		1.47
	A	2.09 ± 0.05	$1b_1$	2.11	2.05 (0.85)	2.05		1.72
	B	2.70 ± 0.05	$2a_1$	2.24	2.52 (0.86)	2.58		
	C	2.96 ± 0.05	$1b_2$	2.79	2.86 (0.84)	3.00		
$CuAl_4^-$	X	2.32 ± 0.06	$4a_1$	1.99	2.31 (0.89)	2.14	2.34	
	A	2.35 ± 0.06	$2b_1$	2.18	2.31 (0.86)	2.10	2.31	
	B	3.24 ± 0.08	$2b_2$	3.09	3.25 (0.85)	3.31		
	C	3.84 ± 0.04	$3a_1$	3.11	3.71 (0.86)	3.66		

[a] VDEs were calculated at the OVGF/6-311+G(2df) level of theory. Numbers in parentheses indicate pole strength. [b] From ref 74.

by subtracting the KE spectra from the photon energy ($h\nu$) using Einstein's photoelectric equation: BE = $h\nu$ − KE. High photon energy spectra are particularly important because they reveal more electronic transitions, which are essential to facilitate comparisons with theoretical predictions. Low photon energies in general yield better-resolved spectra for the ground-state transitions, allowing more accurate determination of adiabatic detachment energies (ADEs) of the neutral species and vibrational resolution in favorable cases. The resolution of the apparatus is ΔKE/KE ~ 2.5%, that is, ~25 meV for 1 eV of electrons.

4. Photoelectron Spectroscopic and Theoretical Study of $M^+[Al_4^{2-}]$ (M = Li, Na, Cu)

The discovery of the all-metal aromatic cluster started from a combined PES and computational study of a series of bimetallic clusters, MAl_4^- (M = Li, Na, Cu).[68] These clusters were generated using the respective M/Al mixed samples as the laser vaporization targets.

4.1. Photoelectron Spectra of $M^+[Al_4^{2-}]$ (M = Li, Na, Cu)

The PES spectra of $M^+[Al_4^{2-}]$ (M = Li, Na, Cu) are shown in Figure 2 at two photon energies. The spectra of the three species are similar, each with an intense threshold peak (*X*&*A*) followed by two weaker features (*B* and *C*). The $CuAl_4^-$ anion has also been observed by Bowen and co-workers[100] at 355 nm only. The *X* and *A* features overlapped heavily and were only resolved in the 355 nm spectrum of $NaAl_4^-$ (Figure 2B). The vertical electron detachment energies (VDEs) of these features are measured from the peak maximum and compared to the results of ab initio calculations in Table 2.

4.2. Searching for Global Minimum Structures of $M^+[Al_4^{2-}]$ (M = Li, Na, Cu)

We performed ab initio calculations on a wide variety of structures in the search for the global minimum using three different theoretical methods: B3LYP/6-311+G*, MP2/6-311+G*, and CCSD(T)/6-311+G*. We found that the most stable structure for

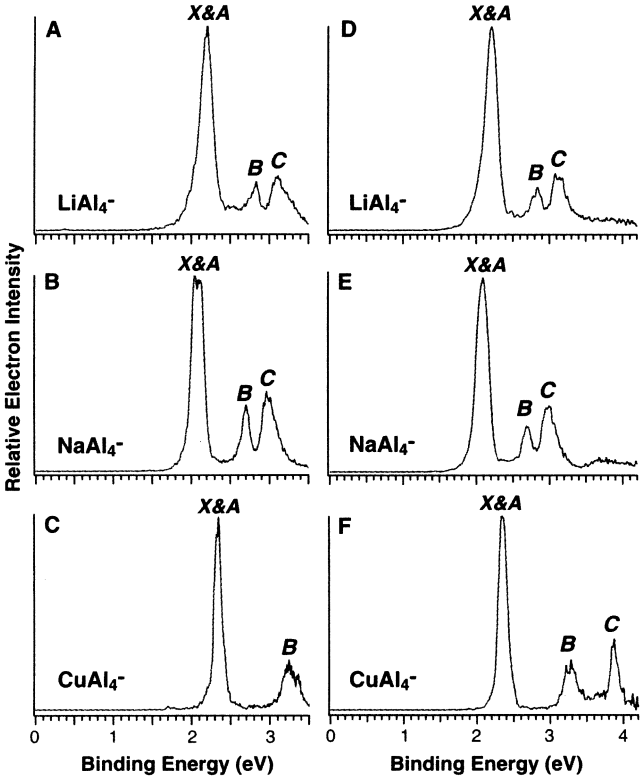

Figure 2. Photoelectron spectra at 355 nm for (A) $LiAl_4^-$, (B) $NaAl_4^-$, and (C) $CuAl_4^-$ and at 266 nm for (D) $LiAl_4^-$, (E) $NaAl_4^-$, and (F) $CuAl_4^-$.[68] The four detachment features are labeled *X*, *A*, *B*, and *C* (see also Table 2). (Reprinted with permission from *Science* (http://www.aaas.org), ref 68. Copyright 2001 American Association for the Advancement of Science.)

all three MAl_4^- species is a square pyramid (Figure 3) consisting of an M^+ cation coordinated to a square-planar Al_4^{2-} unit. All of the MAl_4^- species were also found to possess a fully planar low-lying isomer, with the M^+ cation coordinated to the edge of a square-planar Al_4^{2-} unit. The optimized geometries, vibrational frequencies, and relative energies agreed well at the three levels of theory used in this work for all three MAl_4^- species. The pyramidal structures were found to be more stable than the planar structures by 5.6, 7.6, and 7.6 kcal/mol [all data at CCSD(T)/6-311+G(2df)] for $LiAl_4^-$, $NaAl_4^-$, and $CuAl_4^-$, respectively. The preference of the pyramidal structure over

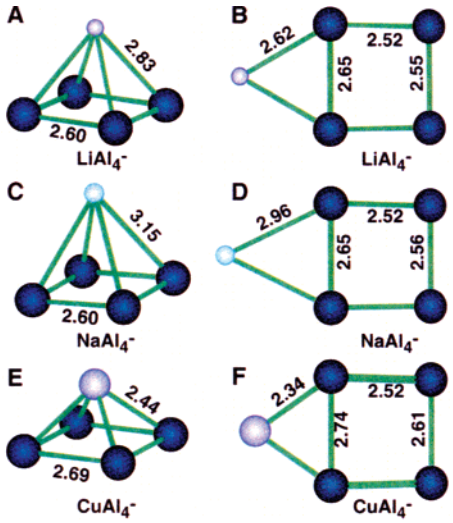

Figure 3. Optimized structures of $LiAl_4^-$ and $NaAl_4^-$ [at the CCSD(T)/6-311+G* level of theory] and $CuAl_4^-$ (at the MP2/6-311+G* level of theory): (A) square pyramidal $LiAl_4^-$ (C_{4v}, $^1A_1$); (B) fully planar $LiAl_4^-$ (C_{2v}, $^1A_1$); (C) square pyramidal $NaAl_4^-$ (C_{4v}, $^1A_1$); (D) fully planar $NaAl_4^-$ (C_{2v}, $^1A_1$); (E) square pyramidal $CuAl_4^-$ (C_{4v}, $^1A_1$); (F) fully planar $CuAl_4^-$ (C_{2v}, $^1A_1$).[68] Bond lengths are given in angstroms. (Reprinted with permission from *Science* (http://www.aaas.org), ref 68. Copyright 2001 American Association for the Advancement of Science.)

other isomers has been confirmed subsequently by several groups,[69,74,86,88,92,101−103] who used a variety of theoretical methods. In particular, we mention the work by Zhao and Balasubramanian,[74] who performed CASSCF calculations for $NaAl_4^-$ including all valence electrons and valence 4s4p2d basis sets. These types of calculations take into account multiconfiguration character of the wave function. They concluded that CASSCF, DFT, and CCSD(T) calculations for geometry and frequencies are in good agreement with each other for the electronic ground state.

To solidify our conclusion about the global minimum structures for the MAl_4^- species, we have recently developed a new tool in our group for global minimum searches. Today, when searching for the global minima of a new cluster, we use an ab initio gradient embedded genetic algorithm (GEGA) program, written by Alexandrova and described in detail in ref 104. The hybrid method, known as B3LYP,[105−107] with a relatively small basis set 3-21G, was employed throughout the execution of the GEGA.

Briefly, within the GEGA procedure, the initial geometries of individuals (structures) in the population (set of structures) are randomly generated and further optimized to the nearest local minima on the potential energy surface, using the Gaussian 03 package.[108] If a saddle point is encountered, the normal mode of the first imaginary frequency is followed until a local minimum is found. Furthermore, the population, composed of the thus selected good individuals (structures with lowest energies), undergoes breeding and mutations. The mating implemented in GEGA is performed on the basis of the robust technique originally proposed in 1995 by Deaven and Ho,[109] in which some of the geometrical features of good individuals in the population (parents) are combined and passed to new individuals (children). Parents are local minimum structures obtained during either the initial or subsequent iterations. Children are new structures made of two parent structures. Probabilities to be bred (to produce child structures) are assigned to parents according to the best-fit (lowest-energy) criterion. On the basis of the probabilities, couples of parents are randomly selected. The geometries of parents are cut by a random cutting plane (XY, YZ, or ZY), and the thus obtained halves (genes) are then recombined either in a simple or in a head-to-tail manner, forming a child. The number of atoms in the newly generated geometry is checked, and the child is optimized to the nearest local minimum. After the number of individuals in the population is doubled within the breeding process, the best-fit group is selected and convergence of the algorithm is checked. The GEGA is considered to be converged if the current lowest energy species (global minimum or at least very stable local minimum) remains leading for 20 iterations. If the convergence is not yet met, the highest energy species in the population undergo mutations. The mutation rate is set to 33.33%. Mutations are shifts of random atoms of a species in random directions, with the purpose of changing the initial geometry so as to push the structure out of the current local minimum to another well on the potential energy surface. Mutants are optimized to the nearest local minima. After that, the algorithm proceeds with the new cycle of breeding. All low-lying isomers are detected and stored throughout the execution, and they are reported to the user at the end of the run. A few runs of GEGA are done on the system to confirm the found global minimum structure.

We recently performed the GEGA search of the global minimum structure of the $LiAl_4^-$ anion[110] and confirmed that the pyramidal structure detailed in Figure 3A is indeed the global minimum for the $LiAl_4^-$ species.

4.3. Calculated Vertical Detachment Energies and Comparison with Experimental Data

The next step is to calculate the ab initio PES spectra, which will facilitate comparison with the experimental data. In the past, the assignment of molecular PES spectra was often based on molecular orbital (MO) calculations and Koopmans' theorem, according to which a negative value of a one-electron MO energy corresponds to the energy of the ionization process from the MO.[111] Unfortunately, ab initio Hartree−Fock (HF) orbital energies may produce large errors in ionization energies and completely misorder the final states in many cases. Therefore, HF orbital energies cannot be used for interpreting PES of our current new species. Quasiparticle approximations in electron propagator theory (EPT) are convenient generalizations of the Koopmans picture. In the quasiparticle approximations electrons assigned to canonical MOs are subjected to a correlated, energy-dependent potential. Earlier development of EPT was made by Linderberg and Ohrn,[112] Pickup and Goscinki,[113] and Simons and Smith,[114] who called

their theory the equations of motion (EOM) method. The most popular approximation of EPT, known as the restricted outer valence Green Function method (ROVGF), was developed by Cederbaum and co-workers for closed shell systems[115,116] and by Ortiz for open shell systems (UOVGF).[117−119] Both of these methods have been incorporated in Gaussian-98 by Ortiz and Zakrzewski.[117−119] OVGF belongs to the so-called direct methods, in which the ionization processes are considered as one-electron detachment processes. Corrections for electron correlation and relaxation are added directly to the one-electron MO energy. These methods allow one to perform calculations much more quickly and avoid spin-contamination when the initial state is a closed shell. Most importantly, these methods allow us to calculate one-electron VDEs from all occupied valence MOs, including transitions in final states that may have the same symmetry. The latter is a significant advantage compared to conventional methods to calculate VDEs at the MPn[120,121] and CCSD(T)[122−124] levels of theories, which use energy differences between a given anion and the various states of its corresponding neutral. These are known as indirect methods, in which only transitions to the lowest state for a given symmetry can be calculated.

We determined theoretically the four lowest lying vertical one-electron detachment processes for the pyramidal $LiAl_4^-$, $NaAl_4^-$, and $CuAl_4^-$, as summarized in Table 2. For the $NaAl_4^-$ species we also included the CASSCF/MRCI calculation performed by Zhao and Balasubramanian.[74] One can see that simple orbital energies (Koopmans' approximation) provide qualitatively correct theoretical PES, but to achieve quantitative agreement, one needs to use post HF methods, such as DFT, OVGF, or CCSD(T) methods. When many-electron effects are taken into account, excellent agreement was obtained for all three anions between the theoretical VDEs of the pyramidal structures and the experimental spectra. The predicted VDEs for the low-lying planar isomers do not agree well with the experimental data, suggesting that this isomer was not significantly populated in the experiment. The first VDEs for all three anions were found to be rather high (2.0−2.3 eV) as compared to VDEs of atomic anions: Li^- (0.618 eV), Na^- (0.548 eV), Cu^- (1.228 eV), and Al^- (0.441 eV). These high VDEs in the MAl_4^- species indicate appreciable stabilization due to the bonding characters of the HOMO, which is another spectroscopic signature of aromaticity in the MAl_4^- species.

We stress that the pole strength (see details in refs 112 and 119) presented in Table 2 in the OVGF results characterizes the validity of the one-electron detachment picture, which holds reasonably well (85% and more) for the four upper electron detachment energies. This indicates that one-electron detachment from a particular MO dominates the experimentally observed PES. The rather high values of the pole strengths may serve as a justification for using the MO picture in interpreting chemical bonding even when many-electron effects are explicitly included in ab initio calculations.

5. Multiple Aromaticity in the Al_4^{2-} Cluster

The local structure of the Al_4^{2-} unit appears to be similar or nearly identical in both the pyramidal global minima and the low-lying planar isomer of all three MAl_4^- species (Figure 3). The small changes in the Al_4^{2-} geometry in forming MAl_4^- molecules show its structural integrity, similar to benzene in the $M(C_6H_6)$ sandwich complexes. These observations stimulated our initial interest in understanding the nature of the chemical bonding in the isolated Al_4^{2-} species and led to the discovery of all-metal aromaticity. Isolated clusters composed of metal atoms represent an ideal starting point for the discussion of aromaticity/antiaromaticity in all-metal systems, because they are free from the influence of substituents (such as in Robinson's[44−48] or Power's[49−51] organometallic compounds) and crystal lattices or solvents. In this section, we will focus our discussion on Al_4^{2-} and its multiple aromaticity, a unique property for all-metal aromatic clusters that deserves to be discussed in more detail. Most organic and known inorganic aromatic molecules possess only one type of aromaticity, that is, π aromaticity. However, σ aromaticity has also been introduced in chemistry,[8,125−128] as has double (σ and π) aromaticity.[129−131] Whereas multiple aromaticity, multiple antiaromaticity, and conflicting aromaticity are very rare in organic and inorganic compounds, they seem to be much more common in all-metal aromatic systems.

5.1. Geometric Structure

Because of the coulomb repulsion between the two extra charges, the Al_4^{2-} dianion is not an electronically stable species toward spontaneous electron ejection, and its accurate theoretical treatment requires solution of the time-dependent Schrodinger equation. However, it was shown by Pyykko and co-workers[132−134] on numerous examples that conventional approximations of the time-independent Schrodinger equation could provide a reasonable description of molecular properties of multiply charged anions if one compares them to the properties of the same species stabilized by either solvent molecules or countercations in solids. The conventional quantum chemical approximations are meaningful because even being electronically unstable, a multiply charged anion corresponds to a local minimum on the potential energy surface separated by a repulsive coulomb barrier from dissociation or electron detachment.[135−138] Moreover, Wang and co-workers showed that even electronically unstable species can be experimentally observed if they have reasonable lifetimes.[135,136] Therefore, we believe that the use of conventional ab initio methods in describing properties of Al_4^{2-}, as well as other multiply charged anions, is justified.

We performed an extensive search for the global minimum structure of Al_4^{2-} using three theoretical methods: B3LYP/6-311+G*, MP2/6-311+G*, and CCSD(T)/6-311+G*. We found that the planar square structure D_{4h} ($^1A_{1g}$) is the most stable one. The alternative low-lying structures of Al_4^{2-} are shown in Figure 4.

The perfect square structure of the Al_4^{2-} global minimum is unexpected, because all of the alterna-

Table 3. Calculated Molecular Properties of Al_4^{2-}

method	E_{tot}, au	R(Al−Al),[d] Å	$\omega_1(a_{1g})$, cm^{-1}	$\omega_2(b_{1g})$, cm^{-1}	$\omega_3(b_{2g})$, cm^{-1}	$\omega_4(b_{2u})$, cm^{-1}	$\omega_5(e_u)$, cm^{-1}
B3LYP/6-311+G*[a]	−969.74053	2.592	294	132	307	115	272
MP2/6-311+G*[b]	−967.83597	2.585	314	117	315	87	370
CCSD(T)/6-311+G*[b]	−967.86648	2.582	310	98	318	65	293
CCSD(T)/aug-cc-pvdz[c]	−967.89464	2.639					
CCSD(T)/aug-cc-pvtz[c]	−967.95867	2.602					

[a] From refs 68 and 70. [b] From ref 69. [c] From ref 70, E(CCSD(T)/aug-cc-pVQZ) = −967.97579 au and E(CCSD(T)/CBS) = −967.98515 au. [d] R(Al−Al) = 2.601 Å at RHF/6-311+G(3df) (ref 86), R(Al−Al) = 2.589 Å at RHF/TZ2P, R(Al−Al) = 2.600 Å at MP2/TZ2P, R(Al−Al) = 2.578 Å at CCSD/TZ2P, R(Al−Al) = 2.602 Å at CCSD(T)/TZ2P, R(Al−Al) = 2.612 Å at RHF/TZ2P+diff, R(Al−Al) = 2.615 Å at MP2/TZ2P+diff, R(Al−Al) = 2.604 Å at CCSD/TZ2P+diff, R(Al−Al) = 2.618 Å at CCSD(T)/TZ2P+diff (all from ref 69).

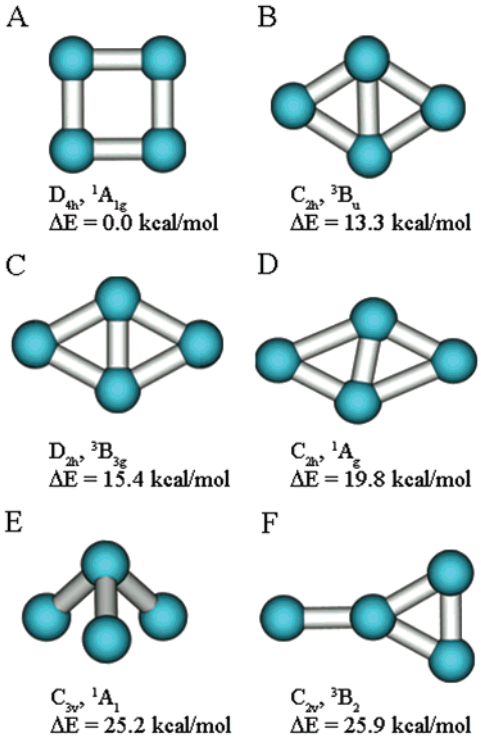

Figure 4. Optimized structures for the Al_4^{2-} dianion. Relative energies are given at the CCSD(T)/6-311+G(2df)//CCSD(T)/6-311+G* level of theory.

tive structures shown in Figure 3 would present better charge separation, which is expected to be important in determining the relative stability of the doubly charged anion. Our prediction that the planar square structure is the Al_4^{2-} global minimum has been confirmed in follow-up publications.[69,70,86−90] We summarized all published data on Al_4^{2-} in Table 3. As one can see from Table 3, all published data at various levels of theory agree reasonably well with each other. The question now is why the square-planar structure is so stable compared to the alternative structures, which provide better charge separation. There must be some unique features of chemical bonding in Al_4^{2-} that give rise to the stability of the favored square-planar structure. The perfect square structure of Al_4^{2-} provides tantalizing hints of aromaticity—which would explain its extra stability. However, to claim aromaticity in Al_4^{2-}, we need to check in detail a variety of molecular properties against the criteria summarized in Table 1. In the following, we first analyze the MOs of Al_4^{2-} and then present other evidence of aromaticity.

5.2. Molecular Orbital Analyses and Multiple Aromaticity

MO pictures for Al_4^{2-} are presented in Figure 5. The HOMO ($1a_{2u}$), HOMO-1 ($2a_{1g}$), and HOMO-2 ($1b_{2g}$) are completely bonding orbitals formed of 3p atomic orbitals (AOs) of Al and represent p_π (π orbitals perpendicular to the plane of the square from p_z-AOs), $p_{\sigma-r}$ (σ orbitals oriented radially toward the center of the square from the $p_{x,y}$-AOs), and $p_{\sigma-t}$ (σ orbitals oriented tangentially around the square from the $p_{x,y}$-AOs), respectively. The next four MOs are bonding, nonbonding, and antibonding orbitals formed primarily from the filled valence 3s orbitals of Al. When all bonding, nonbonding, and antibonding MOs composed of the same AOs (such as the 3s orbitals of Al in this case) are occupied, the net bonding effect is expected to be zero and this set of MOs can be viewed as atomic lone pairs. To illustrate that, we optimized the geometry for the planar square structure of Mg_4 with a valence electron configuration ($1a_{1g}^2 1e_u^4 1b_{1g}^2$) identical to the 3s set of MOs in Al_4^{2-}. Indeed, we found that the Mg_4 square planar structure is more stable than four isolated Mg atoms by only 1.4 kcal/mol at the CCSD(T)/6-311+G* level, clearly showing that bonding and antibonding interactions cancel each other quite well. Thus, the upper three MOs are primarily responsible for the chemical bonding in Al_4^{2-}. If we split the σ and π orbitals into two separate sets, we can represent the MOs formed by 3p-AOs of Al with the MO diagram shown in Figure 6.

For a more general discussion on the chemical bonding in the four-atom cyclic species of the main group elements, we also performed calculations on the square planar structure of Ar_4 (D_{4h}, $^1A_{1g}$) as a model system, and the pictorial representation of all resulting MOs is presented in Figure 7.

The lowest lying π-MO and the two lowest lying σ MOs (Figures 6 and 7) are completely bonding, whereas the highest lying ones are completely antibonding. The two MOs in the π set and the four MOs in the σ set that are located between the completely bonding and completely antibonding MOs are doubly degenerate with bonding/antibonding (or nonbonding) characters. The two types of $p_{\sigma-r}$ and $p_{\sigma-t}$ MOs are somewhat mixed, and that is why they are presented as one set in Figure 6. On the basis of these three distinct types of MOs, we can introduce three types of aromaticity: π aromaticity from the p_π MOs and two types of σ aromaticity from the $p_{\sigma-r}$ and $p_{\sigma-t}$ MOs, respectively. The occupation of all three bond-

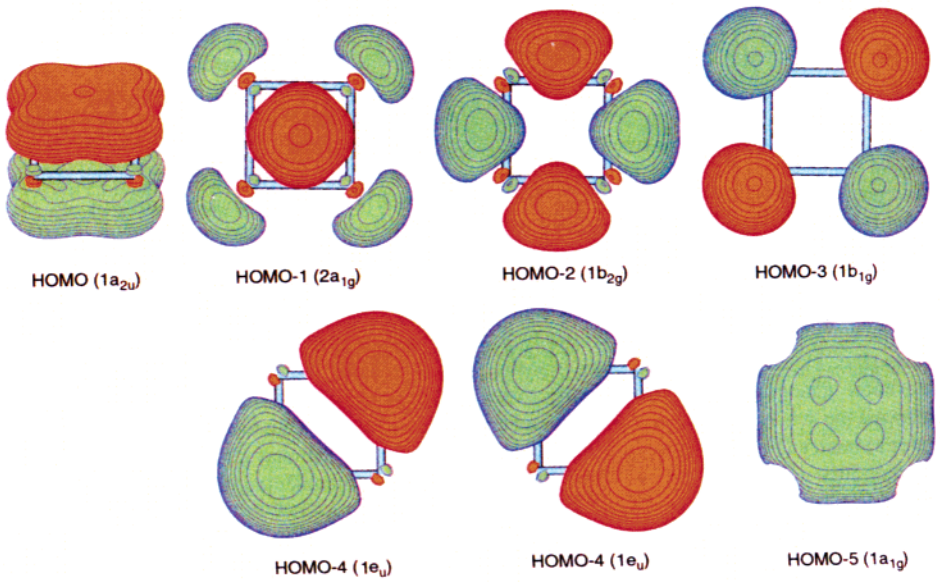

Figure 5. Valence molecular orbital pictures of the square planar Al_4^{2-}.[68] (Reprinted with permission from *Science* (http://www.aaas.org), ref 68. Copyright 2001 American Association for the Advancement of Science.)

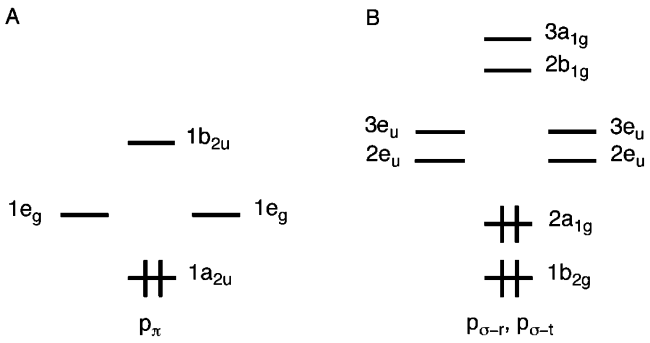

Figure 6. Molecular orbital diagram of the Al_4^{2-} dianion.

ing MOs in Al_4^{2-} makes it a perfect square shape and renders it triply aromatic nature on the basis of the MO analysis.

From comparison of the valence MOs of Al_4^{2-} (electronic configuration $1a_{1g}^2 1e_u^4 2a_{1g}^2 1b_{1g}^2 1b_{2g}^2 1a_{2u}^2$) with the valence MOs of the prototype hydrocarbon aromatic $C_4H_4^{2+}$ (electronic configuration $1a_{1g}^2 1e_u^4 2a_{1g}^2 1b_{1g}^2 1b_{2g}^2 2e_u^4 1a_{2u}^2$), we can see that these two ions differ by four valence electrons in the $2e_u$ MO. The $1a_{1g}^2 1e_u^4 2a_{1g}^2 1b_{1g}^2 1b_{2g}^2 2e_u^4$ electron set in $C_4H_4^{2+}$ can be localized by using any localization procedure into four 2c-2e C−H bonds and four 2c-2e C−C bonds. If we remove the $1a_{1g}^2 1e_u^4 1b_{1g}^2$ sets, which approximately correspond to four C−H bonds in $C_4H_4^{2+}$ and four $3s^2$ lone pairs in Al_4^{2-}, we can see that $C_4H_4^{2+}$ has the $2a_{1g}^2 1b_{2g}^2 2e_u^4 1a_{2u}^2$ set of MOs and that Al_4^{2-} has the $2a_{1g}^2 1b_{2g}^2 1a_{2u}^2$ set of MOs. In Al_4^{2-} the $1a_{2u}$ MO is occupied before the $2e_u$ MO. The $1a_{2u}$ MO is the completely bonding π MO in both cases. The $2a_{1g}^2 1b_{2g}^2 2e_u^4$ set in $C_4H_4^{2+}$ can be approximately localized into four 2c-2e C−C bonds. $C_4H_4^{2+}$ possesses only two delocalized π electrons in the $1a_{2u}$ MO, making it a classical π aromatic species. The $2e_u$ MO is empty in Al_4^{2-}. Therefore, it does not have enough electrons to complete its σ framework to form four 2c-2e Al−Al bonds. The two totally delocalized σ MOs ($2a_{1g}$ and $1b_{2g}$) in Al_4^{2-} make it doubly σ-aromatic, in addition to the π aromaticity derived from the $1a_{2u}$ MO.

The occupation of the π MO ($1a_{2u}$) in Al_4^{2-} before the completion of the classical σ framework (occupation of the $2e_u$ MO) is unusual and makes multiple aromaticity in the dianion possible. We believe that the reason the $1a_{2u}$ MO is occupied before the $2e_u$ MO is due to the lower valence charge of Al relative to C. Al simply cannot favorably support eight electrons in the σ framework (the $2a_{1g}^2 1b_{2g}^2 2e_u^4$ set) and instead the π MO ($1a_{2u}$) is occupied. The presence of multiple-fold aromaticity is a rather unusual phenomenon in chemistry, but it is typical for metal systems, as will be further shown below.

5.3. Electron Density Analyses

Aromaticity in Al_4^{2-} has also been studied using the electron localization function (ELF) by Santos et al.[90] The ELF was introduced[139−141] as an alternative method for analyzing chemical bonding using electron density, rather than molecular orbitals. According to the interpretation of the ELF, a region of the space with high value of ELF corresponds to a region where the probability to localize an electron or a pair of electrons is high. Local maxima, called attractors, of the ELF characterize these regions, and the volume enclosed by all gradient lines, which end up at one attractor, is called a basin. At low values of the ELF, the volume enclosed by the respective isosurface may contain more than one attractor, and eventually, for a sufficiently low value, all of the attractors will be contained in the isosurface. When the isosurface goes to larger values of the ELF, the basins begin to split and, finally, the respective isosurfaces show all of the basins separated. This process is conveniently followed by means of a bifurcation diagram. The bifurcation points have been interpreted as a measure of the interaction among the different basins and chemically as a

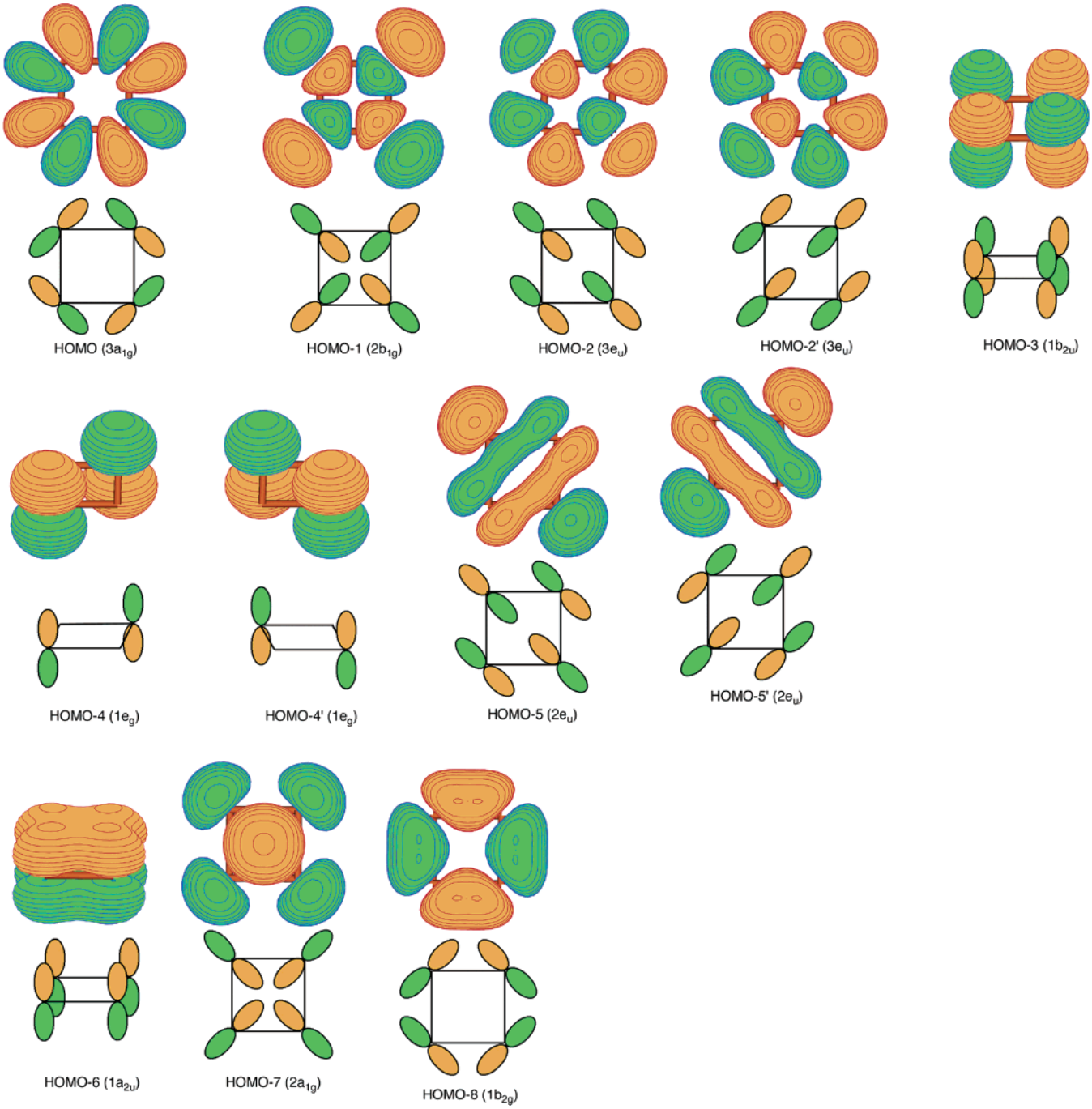

Figure 7. All occupied molecular orbitals formed by 3p-AOs of a square-planar Ar_4 (D_{4h}, $^1A_{1g}$) cluster.[153] (Reprinted with permission from ref 153. Copyright 2004 Wiley.)

measure of electron delocalization.[142,143] Santos et al.[90] were able to separate the ELF of Al_4^{2-} into its σ and π components and to perform the bifurcation analysis of the ELF. They found the highest total bifurcation value ($ELF_{tot} = 0.82$) for Al_4^{2-} among all 13 probed aromatic molecules including the prototypical benzene. The Al_4^{2-} dianion has the highest σ and π components of ELF ($ELF_\sigma = 0.88$ and $ELF_\pi = 0.99$). These numbers can be compared to the corresponding values for benzene: $ELF_{tot} = 0.68$, $ELF_\sigma = 0.76$, and $ELF_\pi = 0.91$. These results demonstrate that the σ delocalization in Al_4^{2-} is as important as the π delocalization, and indeed the Al_4^{2-} dianion is one of the most aromatic species on the basis of the bifurcation analysis of the ELF.

5.4. Resonance Energy Evaluations

The triple aromaticity found in Al_4^{2-} should result in a very high "resonance" or stabilization energy (RE). Because the isolated Al_4^{2-} dianion is electronically unstable, it is more convenient to evaluate the RE in the Al_4^{2-} unit when it is a part of a Na_2Al_4 molecule, which is a bound species. However, it is still difficult to evaluate accurately the RE in the Na_2Al_4 molecule due to the interaction of Na^+ and Al_4^{2-} and due to the problem of identifying a suitable reference molecule with an Al=Al double bond and an Al—Al single bond formed by aluminum atoms with valences I and II, respectively. Shaad and Hess[144] recently reviewed many approaches for cal-

culating RE in aromatic systems. They showed that the incorrect choices of reference structures may dramatically affect even the assignment of a molecule as aromatic or antiaromatic. Nevertheless, considering the importance of the RE within the concept of aromaticity, two groups recently endeavored to evaluate the RE in the all-metal triply aromatic systems. Boldyrev and Kuznetsov[71] evaluated the RE in neutral Na_2Al_4 and Na_2Ga_4 molecules, and Dixon et al.[70] evaluated the RE in the Al_4^{2-} dianion. Because of the difficulties in selecting good reference molecules with single and double Al−Al bonds, both groups could give only the upper and lower limits for the RE in Al_4^{2-} and Na_2Al_4.

Boldyrev and Kuznetsov[71] made several assumptions in their RE evaluations. First, they assumed that Al atoms have valence I, and there is little hybridization mixing between s and p AOs. Second, because they could not devise a molecule in which Al would have valence I with a double bond, they assumed that an Al=Al bond is equal in strength to two single Al−Al bonds. And, third, they assumed that the energy of the Na−Al_4 bond in Na_2Al_4 is approximately equal to the energy of the Na−Al bond in the NaAl diatomic molecule. On the basis of the MO analysis made for Al_4^{2-} above, the dianion has seven valence MOs: four $3s^2$ Al lone pairs, one completely bonding π MO, and two completely delocalized σ MOs. Only the latter three MOs are responsible for bonding. Therefore, in the reference structure one needs to have two σ and one π Al−Al bonds. Now the RE can be evaluated as follows:

$$\mathrm{RE} = E_{\mathrm{at}}(Na_2Al_4) - 2\mathrm{BE}(\mathrm{Na{-}Al}) - 3\mathrm{BE}(\mathrm{Al{-}Al}) \quad (1)$$

The Na_2Al_4 atomization energy was found from eq 2

$$Na_2Al_4\ (C_s, {}^1A') \rightarrow 2Na\ ({}^2S) + 4Al\ ({}^2P) \quad (2)$$

which is calculated to be $E_{\mathrm{at}} = 214$ kcal/mol at the CCSD(T)/6-311+G(2df) level of theory. This atomization energy is unusually high, hinting at extra stability due to aromaticity.

The energy of the Na−Al bond is 18 kcal/mol. The needed energy of the single Al−Al bond is not readily available. The dissociation energy of $H_2Al{-}AlH_2$ is not appropriate, because it involves dissociation of the Al−Al bond with two Al atoms in valence III rather than I. However, the Al−AlH_2 molecule contains an Al−Al bond, with one Al being in the valence I state and the other in valence III. The BE(Al−Al) in a hypothetical Al_2 molecule, which has a single Al−Al bond formed from only $3p_\sigma$ AOs, was evaluated from eq 3:

$$\mathrm{Al{-}Al} + H_2Al{-}AlH_2 \rightarrow 2Al{-}AlH_2 \quad (3)$$

It should be pointed out that Al_2 has a triplet ground electronic state ($^3\Pi_u$)[71] with one electron occupying a σ MO and another in a π MO. Therefore, BE(Al_2, $^3\Pi_u$) is not appropriate. Assuming that the energy of reaction 3 is zero, and using our ab initio data for Al−AlH_2 and $H_2Al{-}AlH_2$, the calculated energy of the desirable single Al−Al bond is 27 kcal/mol (all of these numbers have been corrected for ZPE). Using eq 1 and all available numbers, one finds RE = 97 kcal/mol. The result is certainly unexpectedly high on the basis of the value of the RE in benzene, $E_{\mathrm{res}} =$ 20 kcal/mol.[8]

The RE could be substantially reduced if we take into account the s−p hybridization of Al atoms in Na_2Al_4. The influence of the s−p hybridization on the Al−Al bond energy can be obtained from the $H_2Al{-}AlH_2$ molecule, where the dissociation energy into two AlH_2 groups takes place. The new BE(Al−Al) is now 60 kcal/mol. With the new BE(Al−Al), the RE in Na_2Al_4 is now −2 kcal/mol. Certainly the last number is unrealistically low, because Al atoms in Na_2Al_4 are not sp^2 hybridized as in Al_2H_4. Boldyrev and Kuznetsov proposed to the use a compromise—the average value of these two numbers—as the RE for Na_2Al_4, which is 48 kcal/mol.

Dixon et al.[70] used a different approach. They started with the number of bonding electron pairs in Al_4^{2-}, which they denoted $m(Al_4^{2-})$, the reference bond energy of a localized Al−Al bond BE(Al−Al), and the total bond energy (the atomization enthalpy change from Al_4^{2-} to 4Al + 2e). Then the RE can be evaluated from eq 4

$$\mathrm{RE}(Al_4^{2-}) = \Delta E(Al_4^{2-} \rightarrow 4Al + 2e) - m(Al_4^{2-})\mathrm{BE}(\mathrm{Al{-}Al}) \quad (4)$$

with $\Delta E(Al_4^{2-} \rightarrow 4Al + 2e) = 149$ kcal/mol and BE(Al−Al) = $\Delta E[Al_2(^1\Sigma_g) \rightarrow 2Al] = 26$ kcal/mol. They predicted $\mathrm{RE}(Al_4^{2-}) = 73$ kcal/mol, where all data are at the CCSD(T) level of theory using the complete basis set extrapolation and with corrections on core−valence electron correlation, scalar relativistic effects, spin−orbit effects, and zero-point energy. When they used BE(Al−Al) = $\Delta E[Al_2(^3\Pi_u) \rightarrow 2Al] = 32$ kcal/mol, the $\mathrm{RE}(Al_4^{2-})$ was found to be 53 kcal/mol. The last number is close to the average RE = 48 kcal/mol found by Boldyrev and Kuznetsov in Na_2Al_4.[71] Although the RE values found in both studies were dispersed over a wide energy range, they are consistently very high as compared to the RE of C_6H_6 (20 kcal/mol). The high RE value for Al_4^{2-} clearly supports the triple aromaticity proposed on the basis of the MO analysis.

Zhao and Balasubramanian[74] calculated the dissociation energy of $NaAl_4^-$ into Al_4^- and Na. One could think that a neutral Na atom may form only a weak van der Waals complex with the already negatively charged Al_4^- anion. Yet, they found that the dissociation energy of $NaAl_4^-$ into Al_4^- and Na is 36 kcal/mol at the MRCISD/$4s4p2d_{Al}$+$7s5p1d_{Na}$-level, clearly indicating strong bonding. They also calculated the dissociation energy of $NaAl_4^-$ into Al_4^{2-} and Na^+ using the MRCISD/$4s4p2d_{Al}$+$7s5p1d_{Na}$ level of theory ($D_e = 196$ kcal/mol) and a simple point-charge electrostatic model at the computed equilibrium distance ($D_e \approx 208$ kcal/mol). Because these two numbers are close to each other, they concluded that the interaction between Na and Al_4 in $NaAl_4^-$ is ionic (Na^+ and Al_4^{2-}) with some back charge transfer from Al_4^{2-} to Na^+. This conclusion is in agreement with our natural population analysis (NPA): $Q(\mathrm{Na}) = 0.55$

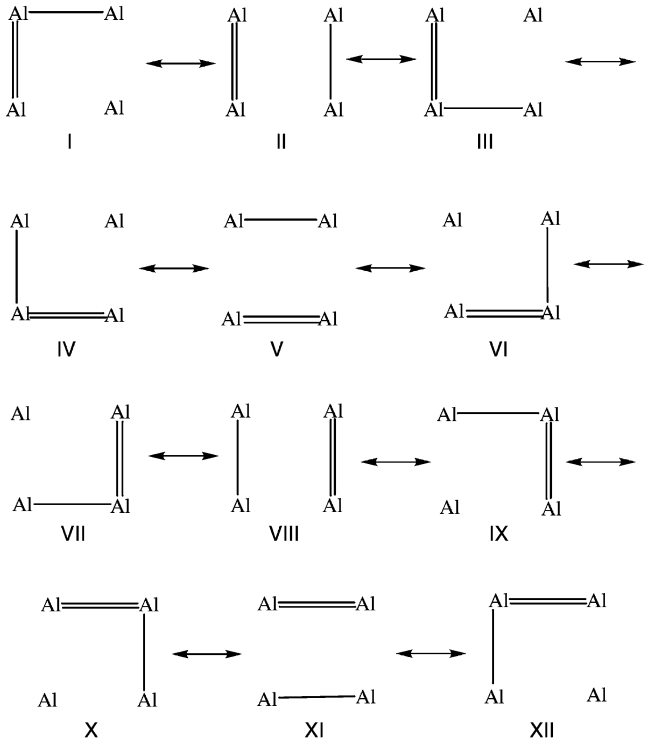

Figure 8. Twelve resonance structures representing bonding in Al_4^{2-}.[50] (Reprinted with permission from ref 50. Copyright 2001 American Chemical Society.)

|e| and $Q(Al) = -0.39$ |e| (at the MP2/6-311+G* level).[68] This additional transfer of electron density from Na to Al_4^- during the formation of $NaAl_4^-$ is a further manifestation of the extra stability of Al_4^{2-}.

5.5. Valence Bond Treatment of Al_4^{2-}

Two types of resonance structures have been proposed for describing the bonding in Al_4^{2-}. Kuznetsov et al.[50] proposed 12 resonance structures to describe the bonding in Al_4^{2-}, as shown in Figure 8. Every structure has one double bond and one single bond to represent the single π MO and the two bonding σ MOs. From these resonance structures one can find the average Al−Al bond order in the cluster is 0.75, with 0.50 coming from the two σ bonds and 0.25 from the π bond. These results are consistent with the bond order found on the basis of the three bonding MOs (two σ and one π) divided among the four Al−Al bonds in Al_4^{2-}.

Alternatively, Dixon et al.[70] proposed to use 64 resonant bonding structures to describe the σ and π bonds localized along the line of centers between adjacent Al atoms in Al_4^{2-}. The 16 resonance structures representing the resonance of only one σ and one π orbital is shown in Figure 9, where the σ bond is represented by a straight line and the π bond by a wavy line.

If the third bond (the second σ bond) is included, these 16 bonding structures will become 64 potential resonance structures. The number of resonance structures in the Dixon et al. approach is substantially higher than that in the Kuznetsov and Boldyrev approach, because Dixon et al. included resonance structures with dangling π bonds, which do not have σ bonds between the same pair of atoms.

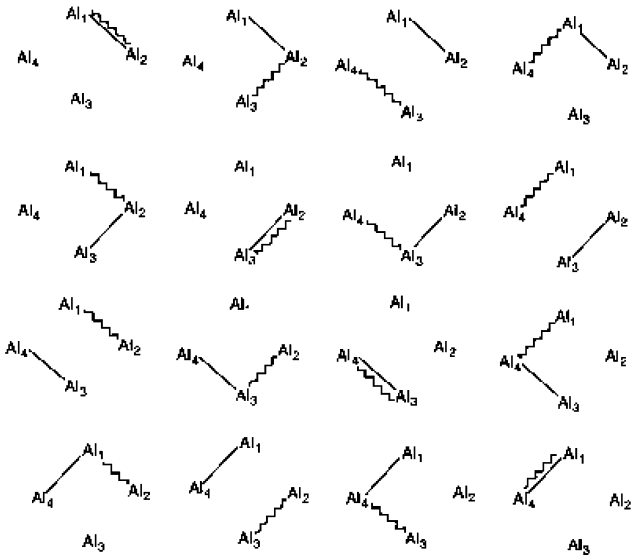

Figure 9. Sixteen resonance structures derived from a π and σ bond in Al_4^{2-}. When a second σ bond is considered, a total of 64 resonance structures is obtained.[70] (Reprinted with permission from ref 70. Copyright 2002 American Chemical Society.)

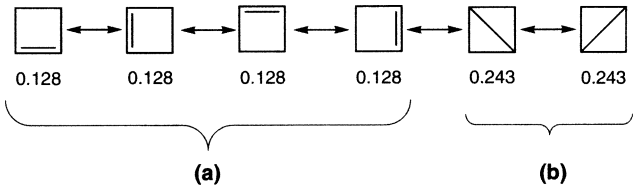

Figure 10. Weights of the six different π Lewis structures, calculated using the local orbital approach.[89] (Reprinted with permission from ref 89. Copyright 2004 Elsevier.)

To resolve this issue, Havenith and van Lenthe[89] performed ab initio VB calculations, which is a natural way to incorporate resonance structures in ab initio calculations. They used two different orbital optimization models: (i) all orbitals were kept strictly atomic, and (ii) the orbitals were kept predominantly atomic in nature but were allowed to delocalize. The π and σ systems were treated separately: in the π VB calculations, the σ skeleton was described by a HF core, that is, doubly occupied orthogonal MOs. In the VB calculations for the σ system, the situation was reversed. The π system of Al_4^{2-} was described using the six possible VB structures, shown in Figure 10 together with their weights in the (local) VB wave function.

Surprisingly, Havenith and van Lenthe found that the Dewar-like resonance structures with the diagonal bond have the highest weight. The Pauling RE (the energy difference between the total VB energy and the energy of the most stable structure) was found to be 45 kcal/mol using the local approach and 39 kcal/mol using the delocalizing approach. This number is substantially higher than the Pauling RE obtained for benzene using the same approach (20 kcal/mol), but it is substantially lower than the RE obtained for $C_4H_4^{2+}$ (167 kcal/mol).

The σ aluminum valence bonds were made up of singly occupied orbitals. Two spin-coupling schemes were probed, which are presented in Figure 11. The first spin-coupling mode consists of localized Al−Al

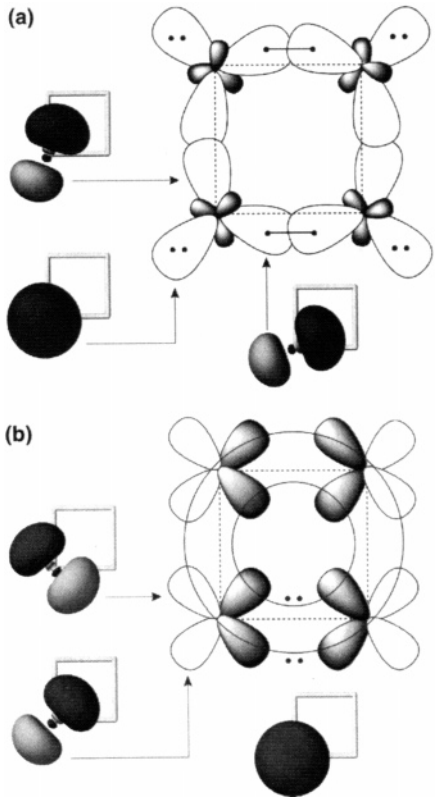

Figure 11. Schematic representation of the spin-coupling schemes and contour plots of the optimized orbitals using the local approach for (a) the spin-coupling mode that represents localized Al−Al bonds and for (b) the spin-coupling mode that represents the two independent delocalized σ systems.[89] (Reprinted with permission from ref 89. Copyright 2004 Elsevier.)

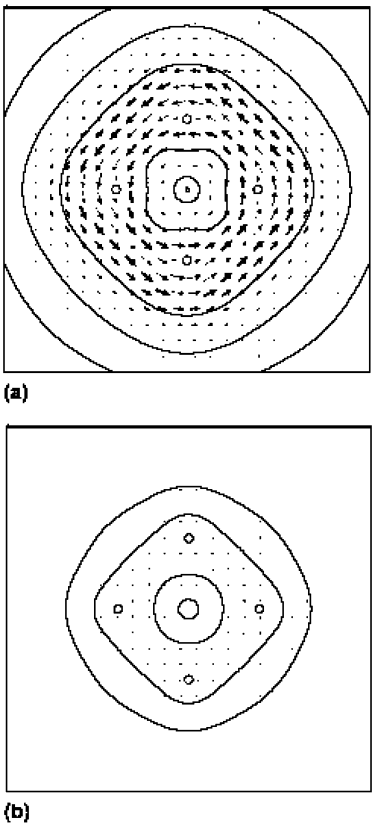

Figure 12. Relative contributions of σ and π orbitals to the total ring current in Al_4^{2-}: (a) total σ valence current density; (b) π current density. Both plots refer to plotting plane at a height of 1.63 a_0 above the molecule, in which the π current density reaches its maximum value. Over 80% of the total current density in this plane arises from the σ electrons.[86,87] (Reprinted with permission from ref 86. Copyright 2001 Elsevier.)

bonds made up of sp^2-like hybrids, with four Al lone pairs (Figure 11a). The second coupling mode consists of two separate σ systems, each with two electrons that are made up from the radial and tangential π orbitals on each aluminum atom, with four Al lone pairs (Figure 11b). The calculated RE for the first coupling scheme was found to be 2.6 kcal/mol, compared to the 123.2 kcal/mol for the second coupling scheme. Havenith and van Lenthe concluded that the much lower total energy (and much higher RE) for the second scheme suggests that the σ skeleton of the Al_4^{2-} anion is best described as two different delocalized systems, a radial and a tangential one, with each system holding two electrons.

Thus, the VB calculations showed that conventional chemical wisdom, that is, that bonding between two neighboring atoms is dominant in chemical bonding, failed in the case of Al_4^{2-}. In the all-metal Al_4^{2-} dianion the Dewar-like resonance structures with diagonal bonding have higher contribution than the conventional Kekulé resonance structures with neighboring Al−Al bonding. We feel, however, that more work needs to be done in VB studies on all-metal aromatic systems. In particular, it would be interesting to check if the extra charges (2−) may influence the dominance of the Dewar resonance structures over the Kekulé ones in Al_4^{2-}, because in the Dewar structure the diagonal position of extra charges is more favorable that in the Kekulé structures, where they are located at the edge. An extensive VB study of all-metal systems with multiple aromaticity will help develop new resonance structure languages for these new species, which eventually will help to develop a unified chemical bonding theory throughout chemistry.

5.6. Ring Current and Magnetic Criteria

In aromatic molecules, an external magnetic field creates a ring current. The ring current induces a secondary magnetic field perpendicular to the current loop and opposite to the applied magnetic field. This secondary magnetic field can be experimentally observed as resonance shifts of a few parts per million in the ^1H NMR spectra and computationally as a long-range magnetic shielding. The application of the NICS index in deciphering aromaticity and antiaromaticity is reviewed by Heine et al. in the current issue. We therefore will discuss here only the application of these two approaches to the characterization of aromaticity in Al_4^{2-} and recommend the above reviews to readers interested in more details on these methods.

Fowler et al.[86,87] constructed current density maps for Al_4^{2-} separately for the σ and π orbitals, as presented in Figure 12. The current density maps were computed using the ipsocentric continuous transformation of origin of current density−diamag-

netic zero formulation of coupled HF theory and the 6-311++G(3df) basis set. They found that the contribution to the current from the π electrons is rather weak compared to the contribution from the σ electrons. The strong diatropic σ ring current confirms the presence of σ aromaticity in Al_4^{2-}, whereas the combination of σ and π diatropic ring current (although the latter being a weak one) confirms the multiple aromatic character of Al_4^{2-}.

Sundholm et al.[69] used the aromatic ring-current shielding (ARCS) method to probe the aromaticity in Al_4^{2-} using a variety of theoretical methods starting from HF to CCSD(T) and using two different basis sets: a split-valence basis set augmented with polarization functions (SVP) and a triple-ζ quality basis set plus double-polarization functions (TZ2P). The magnetic shieldings, $\sigma(z)$, were calculated at selected points along a line perpendicular to the molecular plane starting at the center of the molecular ring. From the calculations it was concluded that the $\sigma(z)$ calculated at the HF, CCSD, and CCSD(T) levels are similar and clearly show the strong presence of aromaticity in Al_4^{2-}. However, the shielding function calculated at the MP2 level shows the wrong sign at small z. The $\sigma(z)$ calculated at the MP2 level even suggests that the Al_4^{2-} ring is antiaromatic. They also calculated the ring current susceptibility for the Al_4^{2-} dianion, which was found to be $\sim$9−12 nA·T^{-1}, which can be compared to 8 nA·T^{-1} for benzene. In summary, Sundholm et al. concluded that the Al_4^{2-} dianion sustains a large diatropic ring current in an external magnetic field, and thus on the basis of this criterion it should be considered to be aromatic.

Schleyer and co-workers[88] tested aromaticity in the Al_4^{2-} dianion using NICS proposed by him and coworkers in 1996.[145] Today, this index has become a popular probe of aromaticity in a variety of molecules, as is shown in Schleyer's review in the current issue. Negative NICSs denote aromaticity, whereas positive NICSs denote antiaromaticity. For the prototypical aromatic and antiaromatic molecules, the NICS(0) indices calculated at the center of the ring were found to be −9.7 ppm (C_6H_6) and 27.6 ppm (C_4H_4) (at the B3LYP/6-31+G* level of theory). In a recent work, Schleyer and co-workers were able to calculate NICS indices of each canonical MO (NICS-CMO) individually.[88] The NICS(0)/B3LYP/6-311+G* analysis performed at the center of the Al_4^{2-} ring is presented in Figure 13. One can see that NICS-CMO confirmed that not only the diatropic π MO (−17.8 ppm) but also the σ MOs (sum −11.1 ppm) contribute importantly to the considerable aromaticity. The total NICS(0) = −30.9 ppm value for Al_4^{2-} is appreciably higher than the NICS(0) = −9.7 ppm for the prototypical aromatic benzene molecule. Thus, all magnetic probes (NICS and ARCS) as well as the maps of total and σ- and π-induced ring current clearly indicate not only the presence of π aromaticity in the Al_4^{2-} dianion but also σ aromaticity.

From the above discussion one can see that the Al_4^{2-} dianion satisfies many criteria proposed for aromaticity (Table 1) and thus can be considered as aromatic with certainty. Moreover, this discussion clearly shows the presence of multiple (σ and π) aromaticity in the dianion. The success of the multiple-aromaticity model in explaining a variety of molecular properties of Al_4^{2-}, MAl_4^-, and M_2Al_4 (M = Li, Na, Cu) demonstrates a great potential of the model for other metal, metalloid, and nonmetal clusters. We should mention that there were also attempts to explain the enhanced stability of $NaAl_4^-$ and Na_2Al_4 using the jellium model,[102] which was very successful in explaining extra stability of so-called "magic" clusters of alkali metal clusters. However, Dhavale et al.[102] concluded that the enhanced stability of the $NaAl_4^-$ and Na_2Al_4 species cannot be explained on the basis of a simple jellium model.

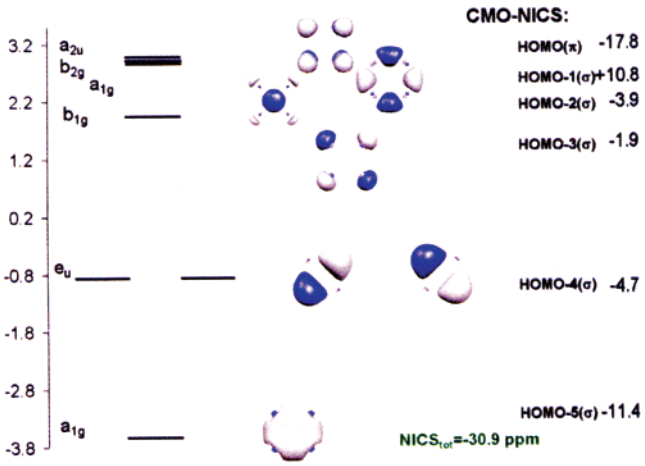

Figure 13. NICS(0)-CMO analysis at the ring center of Al_4^{2-} (D_{4h}).[88] (Reprinted with permission from ref 88. Copyright 2003 American Chemical Society.)

6. Other Multiply Aromatic Clusters

6.1. Valence Isoelectronic Species of Al_4^{2-}: X_4^{2-} (X = B, Ga, In, Tl)

Since the discovery of aromaticity in Al_4^{2-}, we have also extended the concept to the heavy congeners Ga_4^{2-} and In_4^{2-} in $NaGa_4^-$ and $NaIn_4^-$, which were experimentally characterized using PES.[50] Several computational studies have also been reported focusing on the aromaticity in other group III valence isoelectronic dianions, M_4^{2-}.[69,71,74] The most accurate ab initio data obtained by Sundholm et al.[69] for the B_4^{2-}, Ga_4^{2-}, In_4^{2-}, and Tl_4^{2-} doubly charged anions are summarized in Table 4. Although the authors studied only D_{4h} structures for the four dianions, they found that all of them have a valence electronic configuration of $1a_{1g}^2 1e_u^4 1b_{1g}^2 1b_{2g}^2 2a_{1g}^2 1a_{2u}^2$ similar to that of Al_4^{2-} and that the square structures are true minima on their potential energy surfaces. The square structure of all four dianions and the same set of MOs indicate that these systems are aromatic as well. To test aromaticity in these systems further, they calculated the ring-current susceptibilities at the HF level of theory. For Ga_4^{2-}, In_4^{2-}, and Tl_4^{2-}, the susceptibilities were found to be equal and somewhat larger than for benzene. For B_4^{2-}, the obtained ring-current susceptibility of 7.4 nA·T^{-1} is only 10% smaller than that for benzene. These results support the assignment of these dianions as aromatic species.

Similar to the case of the bare Al_4^{2-} dianion, all bare X_4^{2-} (X = B, Ga, In, Tl) dianions are not

Table 4. Ab Initio Molecular Parameters of B_4^{2-}, Ga_4^{2-}, In_4^{2-}, Tl_4^{2-} [69]

molecule	level of theory	R(X−X), Å	$\omega_1(a_{1g})$, cm^{-1}	$\omega_2(b_{1g})$, cm^{-1}	$\omega_3(b_{2g})$, cm^{-1}	$\omega_4(b_{2u})$, cm^{-1}	$\omega_5(e_u)$, cm^{-1}
B_4^{2-}	CCSD(T)/TZV2P	1.668	881	375	903	286	709
Ga_4^{2-}	CCSD(T)/SVP	2.540	201	92	204	78	183
In_4^{2-}	CCSD(T)/3VE-sp2df	2.970	122	49	124	44	113
Tl_4^{2-}	CCSD(T)/3VE-sp2df	3.047	81	36	82	34	76

electronically stable species toward spontaneous electron detachment, and they correspond to a metastable local minimum on their corresponding potential energy surface. This makes the experimental study of these species very challenging. However, capping these dianions by an alkali metal cation makes the resulting species electronically stable and accessible experimentally, as was demonstrated in the case of Al_4^{2-}.[68] In our work on $NaGa_4^-$ and $NaIn_4^-$,[50] the species were generated in the molecular beam, and their electronic structure was probed using PES. We optimized the geometries for the two lowest energy structures using three ab initio methods [B3LYP, MP2, and CCSD(T)] and 6-311+G* basis sets for Na and Ga and the CEP-121G+spd basis set together with the pseudopotential for core electrons on In. We also calculated frequencies of these two species using the first two levels of theory. As in $NaAl_4^-$, the pyramidal structure was found to be more stable than the fully planar structure for $NaGa_4^-$ and $NaIn_4^-$ (Figure 14). In the same investigation, we also found and confirmed that Power's $-Ga_4-$ organometallic compound is in fact aromatic, as will be discussed later in section 8.2.

$NaGa_4^-$ and $NaIn_4^-$ were also calculated by Zhao and Balasubramanian[74] using the CASSCF/4s4p2dGa,In+7s5p1dNa level of theory. They found that the pyramidal (C_{4v}, $^1A_1$) structure is the most stable for both anions at the multiconfigurational level of theory with geometric parameters and harmonic frequencies consistent with our data.

We also calculated the relative energies (compared to the global minimum structure) for the neutral Na_2Ga_4 molecule, and their structures and relative energies are also presented in Figure 14. The three lowest energy singlet structures identified correspond to an octahedral-type structure (D_{4h}, $^1A_{1g}$, Figure 14g) with two Na^+ cations coordinated to the π MO on the opposite sides of planar Ga_4^{2-}, an edge-capped square pyramid structure (C_s, $^1A'$, Figure 14i), with one Na^+ coordinated to the π MO and another one to the σ MO, and a fully planar structure (C_{2v}, $^1A_1$, Figure 14j) with two Na^+ cations coordinated to the σ MO. Interestingly, in the global minimum structure of Na_2Ga_4, one cation is coordinated to the π aromatic MO and another one to the σ aromatic MO (Figure 14i). When two cations are coordinated to the same π or σ MO, the resulting structures are less stable.

The structure of the Ga_4^{2-} dianion in $NaGa_4^-$ and Na_2Ga_4, as well as the structure of the In_4^{2-} dianion in $NaIn_4^-$, is somewhat distorted from a perfect square, but the distortion is modest and the geometric integrity of the aromatic dianions is clearly seen. Experimental PES spectra on $NaGa_4^-$ and $NaIn_4^-$ allow us to test the calculated electronic structure of these anions, as summarized in Table 5. The calculated VDEs are in better agreement with the experimental peaks for the pyramidal structure rather than for the fully planar structures, thus confirming the theoretical prediction of the global minimum structures. The B_4^{2-}, Ga_4^{2-}, In_4^{2-}, and Tl_4^{2-} dianions are all multiply aromatic on the basis of the MO analysis, square planar structure, and the high ring-current susceptibility, as found in the Al_4^{2-} dianion.

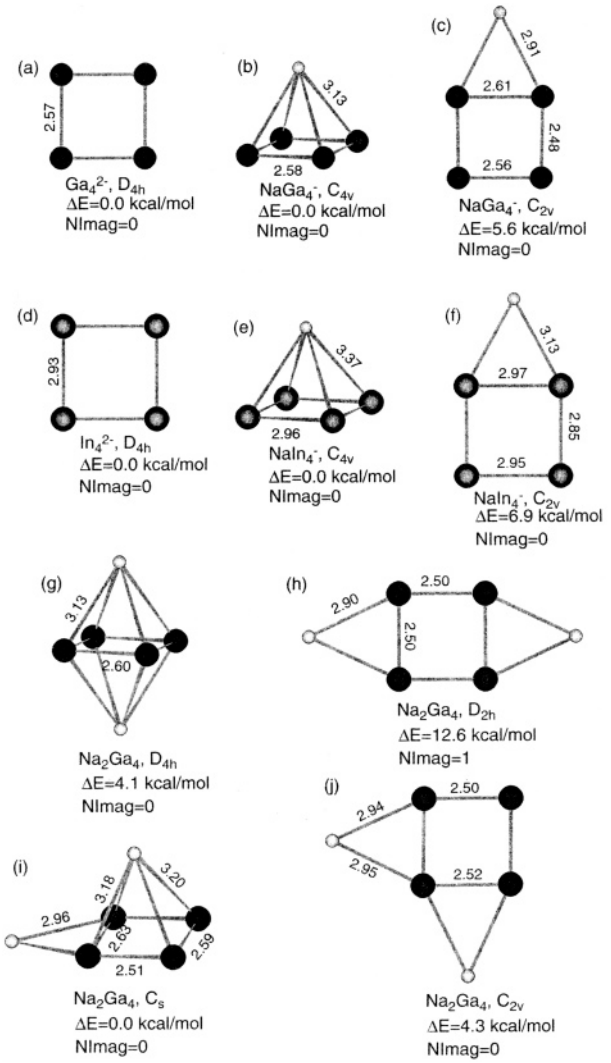

Figure 14. Optimized structures of (a) Ga_4^{2-}, (b) $NaGa_4^-$ (C_{4v}), (c) $NaGa_4^-$ (C_{2v}), (d) In_4^{2-}, (e) $NaIn_4^-$ (C_{4v}), (f) $NaIn_4^-$ (C_{2v}), (g) Na_2Ga_4 (D_{4h}), (h) Na_2Ga_4 (D_{2h}), (i) Na_2Ga_4 (C_s), and (j) Na_2Ga_4 (C_{2v}).[50] (Reprinted with permission from ref 50. Copyright 2001 American Chemical Society.)

6.2. Mixed Valence Isoelectronic Species: MAl_3^- (M = C, Si, Ge, Sn, Pb), M′Al$_3$ (M′ = P, As, Bi), and $Si_2M''_2$ (M″ = B, Al, Ga)

The substitution of one X in X_4^{2-} (X = B, Al, Ga, In, Tl) by a group IV atom M (M = C, Si, Ge, Sn, Pb) creates valence isoelectronic species MX_3^-, which are singly charged and can be produced and studied

Table 5. Experimental and Theoretical VDEs (in eV) for $NaGa_4^-$ and $NaIn_4^-$ [50]

species	exptl feature	exptl VDE	C_{4v} MO	C_{4v} VDE (theor)[a]	C_{4v} VDE (theor)[b]	C_{2v} MO	C_{2v} VDE (theor)[a]
$NaGa_4^-$	X	1.90 ± 0.06	$3a_1$	1.84 (0.87)	1.87	$1b_1$	1.75 (0.85)
	A	2.02 ± 0.05	$1b_1$	1.99 (0.85)	1.89	$4a_1$	1.80 (0.86)
	B	2.58 ± 0.05	$2a_1$	2.43 (0.86)	2.68	$3a_1$	2.29 (0.86)
	C	3.73 ± 0.15	$1b_2$	3.59 (0.84)	3.69	$2b_2$	3.51 (0.83)
$NaIn_4^-$	X	1.93 ± 0.06	$3a_1$	1.82 (0.87)		$1b_1$	1.70 (0.85)
	A	2.08 ± 0.06	$1b_1$	1.93 (0.86)		$4a_1$	1.78 (0.86)
	B	2.60 ± 0.05	$2a_1$	2.39 (0.87)		$3a_1$	2.29 (0.87)
	C	3.95 ± 0.15	$1b_2$	3.84 (0.83)		$2b_2$	3.77 (0.83)

[a] VDEs were calculated at the OVGF/6-311+G(2df) level of theory. Numbers in parentheses indicate pole strength. [b] VDEs calculated at UCCSD(T)/4s4p2d_{Ga}+7s5p1d_{Na} level of theory (ref 74).

experimentally by PES. The substitution of one X in X_4^{2-} (X = B, Al, Ga, In, Tl) by a group V atom M′ (M′ = N, P, As, Sb, Bi) or two X in X_4^{2-} by two group IV atoms M″ (M″ = C, Si, Ge, Sn, Pb) produces valence isoelectronic neutral species, which may be studied by IR or Raman spectroscopy in matrix isolation experiments or in the gas phase by photoionization spectroscopy. Chemical bonding in the mixed isoelectronic species is free from cation influence, such as in $NaAl_4^-$, providing new opportunities to explore aromaticity.

We studied experimentally and theoretically a series of MAl_3^- (M = C, Si, Ge, Sn, Pb) anions,[72] which allowed us to investigate systematically how the delocalization, and thus aromaticity, affects relative stability and other properties of heterocyclic (aromatic) and pyramidal (classical) structures. Optimized structures for the heteroclusters MAl_3^- (M = Si, Ge, Sn, Pb) are presented in Figure 15. According to our calculations, the cyclic MAl_3^- structure is the global minimum for these anionic species, with the pyramidal structure being appreciably higher in energy.

Experimental investigation by PES was performed to test this ab initio prediction.[72] The MAl_3^- (M = C, Si, Ge, Sn, Pb) anions were produced by laser vaporization, and their PES spectra were obtained at two detachment laser wavelengths (355 and 266 nm), as shown in Figure 16.

Four main spectral bands (X, A, B, C) were observed for each species. The first two features (X and A) were very close in binding energies and were only barely resolved in the 355 nm spectrum of $PbAl_3^-$ (Figure 16g). The third band (B) also has a binding energy very close to that of band A, but the separation increases going down the periodic table to Si to Pb. Weak signals at the low binding energy side were due to structural isomers, which were more visible in the spectra of $SiAl_3^-$ and $GeAl_3^-$. We also calculated ab initio VDEs for these four species, which are compared to the experimental results in Table 6.

The weak and low binding energy features in the spectra of $SiAl_3^-$ and $GeAl_3^-$ (Figure 16) suggest a significant population of the C_{3v} isomer. Similar lower binding energy features seemed also to exist in the spectra of $SnAl_3^-$ and $PbAl_3^-$, but they weakened significantly along the $SiAl_3^-$–$GeAl_3^-$–$SnAl_3^-$–$PbAl_3^-$ series. This experimental observation is in complete agreement with the results of the ab initio calculations, which show that the relative stability of the aromatic cyclic structure steadily increases along the same direction. This observation and the excellent agreement between the calculated spectra of the cyclic structures and the experimental spectra provide conclusive evidence for the cyclic global minima structure of the MAl_3^- (M = Si, Ge, Sn, Pb) species.

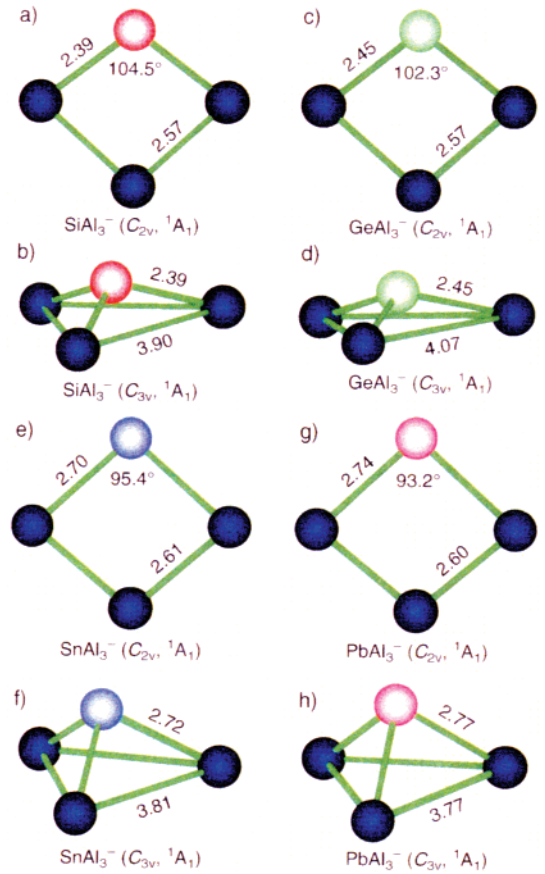

Figure 15. Optimized structures of MAl_3^- at the CCSD(T)/6-311+G* and CCSD(T)/4s4p1d levels of theory. Bond length are give in angstroms and bond angles in degrees.[72] (Reprinted with permission from ref 72. Copyright 2001 Wiley.)

The stability of the cyclic structure relative to the pyramidal structure is related to the π $1b_1$-MO in XAl_3^- (Figure 17). In the $SiAl_3^-$ the electron density is heavily concentrated on the Si site. When Si is substituted by the more metallic Ge, Sn, or Pb atom, the electron density is steadily extended toward the terminal Al atom (Figure 17). Consequently, the cyclic isomer becomes more stable relative to the

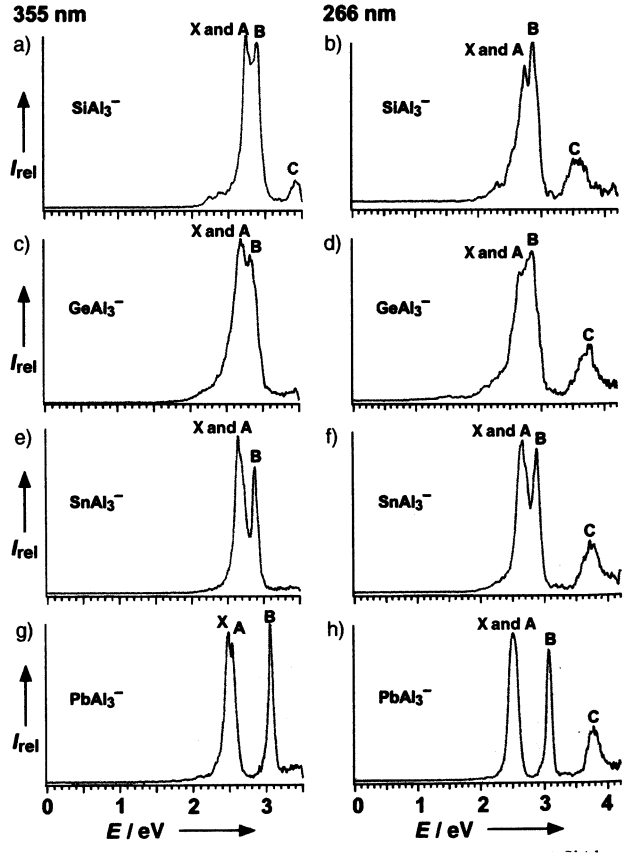

Figure 16. Photoelectron spectra of MAl_3^- (X = C, Si, Ge, Sn, Pb) at 355 and 266 nm.[72] (Reprinted with permission from ref 72. Copyright 2001 Wiley.)

Table 6. Experimental and Theoretical VDEs (in eV) for MAl_3^- (M = Si, Ge, Sn, Pb) (Adapted from Reference 72)

		C_{2v} ($^1A_1$)		C_{3v} ($^1A_1$)	
exptl feature	exptl VDE	MO	VDE, theor[a]	MO	VDE, theor[a]
		$SiAl_3^-$			
X&A	2.73 ± 0.08	$4a_1$	2.64 (0.86)	2e	2.48 (0.86)
		$1b_1$	2.70 (0.86)	$3a_1$	2.72 (0.86)
B	2.88 ± 0.05	$2b_2$	2.82 (0.86)	$2a_1$	4.64 (0.80)
C	3.54 ± 0.10	$3a_1$	3.33 (0.86)		
		$GeAl_3^-$			
X&A	2.70 ± 0.09	$4a_1$	2.61 (0.87)	2e	2.46 (0.86)
		$1b_1$	2.65 (0.86)	$3a_1$	3.56 (0.86)
B	2.83 ± 0.08	$2b_2$	2.81 (0.86)	$2a_1$	4.66 (0.79)
C	3.65 ± 0.18	$3a_1$	3.43 (0.86)		
		$SnAl_3^-$			
X	2.66 ± 0.04	$4a_1$	2.47 (0.86)	2e	2.24 (0.86)
A	2.70 ± 0.04	$1b_1$	2.51 (0.86)	$3a_1$	3.43 (0.86)
B	2.88 ± 0.02	$2b_2$	2.71 (0.86)	$2a_1$	5.10 (0.79)
C	3.72 ± 0.06	$3a_1$	3.63 (0.86)		
		$PbAl_3^-$			
X	2.484 ± 0.020	$4a_1$	2.36 (0.86)	2e	2.11 (0.86)
A	2.538 ± 0.020	$1b_1$	2.41 (0.86)	$3a_1$	3.33 (0.86)
B	3.054 ± 0.010	$2b_2$	2.61 (0.86)	$2a_1$	5.79 (0.79)
C	3.76 ± 0.06	$3a_1$	3.74 (0.86)		

[a] Theoretical results were calculated at the ROVGF/6-311+G(2df) or ROVGF/4s4p2d1f level of theory. Numbers in parentheses indicate pole strength.

pyramidal structure. When Si is substituted by the more electronegative C atom, the two π electrons are almost completely localized on the C atom, which substantially destabilizes the cyclic structure. Indeed, the photoelectron spectra of CAl_3^- are very different from those of the heavy XAl_3^- congeners shown in Figure 16,[146] suggesting that the CAl_3^- cluster has a different structure. All attempts to locate the cyclic CAl_3^- structure led to the pyramidal structure, the calculated VDEs of which are in good agreement with the experimental PES data.[146] The series of XAl_3^- species provides unequivocal evidence that the delocalization of the π electrons is responsible for the C_{2v} cyclic aromatic structure.

Recently, a series of MGa_3^- (M = Si, Ge) anions and their neutral derivatives $LMGa_3$ (L = Li, Na, K, Cu; M = Si, Ge) have been studied theoretically by Chi and co-workers.[73] They used a variety of density functional methods, as well as the MP2 method and the 6-311+G(3df) basis sets, for geometry optimization and frequency calculations. They found that as in the XAl_3^- series, the C_{2v} cyclic aromatic structure is the most stable for $SiGa_3^-$ and $GeGa_3^-$, with the pyramidal C_{3v} structure being the next local minimum. $SiGa_3^-$ and $GeGa_3^-$ have similar molecular orbitals as the XAl_3^- series and are aromatic. At the B3LYP/6-311+G(3df) level of theory the cyclic structures were found to be more stable than the pyramidal structures by 9.3 kcal/mol ($SiGa_3^-$) and by 11.6 kcal/mol ($GeGa_3^-$), which is again consistent with better delocalization of the two π electrons in $GeGa_3^-$ compared to $SiGa_3^-$. For the neutral $LMGa_3$ species Chi and co-workers[73] found the pyramidal and fully planar structures (Figure 18), analogues of the C_{4v} and C_{2v} structures discussed above for LAl_4^- (L = Li, Na, Cu) species. The pyramidal-type structures were found to be slightly more stable than the planar structures, similar to the LAl_4^- anions discussed above. They also pointed out the structural integrity of the MGa_3^- anions in the corresponding neutral $LMGa_3$ species.

Isoelectronic neutral species $M'Al_3$ (M′ = P, As) and $M'Ga_3$ (M′ = P, As) have been also studied computationally. Feng and Balasubramanian[147] reported a pyramidal C_{3v} ($^1A_1$) structure to be the ground electronic state of the PAl_3 molecule using the CASSCF/MRSDCI/$4s4p1d_{Al}$+$4s4p2d_P$ level of theory and the relativistic core potentials for both atoms. Archibong et al.[148] found two low-lying isomers for PAl_3 [at the CCSD(T)/6-311+G(2df) level of theory], which are the same as in the MAl_3^- and MGa_3^- anions: the planar cyclic C_{2v} ($^1A_1$) structure and the pyramidal C_{3v} ($^1A_1$) structure. At the CCSD(T)/6-311+G(2df) level of theory the pyramidal structure was found to be more stable than the cyclic structure by 1.5 kcal/mol. Thus, both groups reported the same ground state for PAl_3. Feng and Balasubramanian,[149] using the same level of theory as for PAl_3, predicted that PGa_3 has the same global minimum pyramidal C_{3v} ($^1A_1$) structure. Archibong et al.[150] found two low-lying isomers for PGa_3 [at the CCSD(T)/6-311+G(2df) level of theory], with the pyramidal C_{3v} ($^1A_1$) structure being more stable than the cyclic C_{2v} ($^1A_1$) structure by 3.1 kcal/mol. This is in accord with the previous data on the XAl_3^- and XGa_3^- anions. The larger difference in the electronegativity favors the pyramidal structure, because that favors the localization

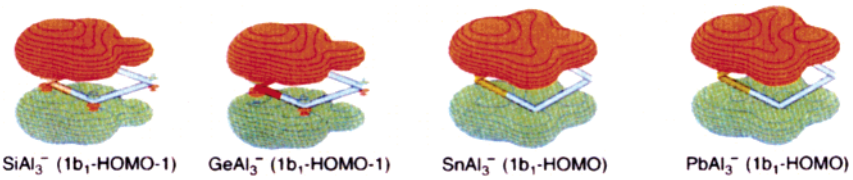

Figure 17. Delocalized π ($1b_1$) orbitals for the MAl_3^- anions.[72] ((Reprinted with permission from ref 72. Copyright 2001 Wiley.)

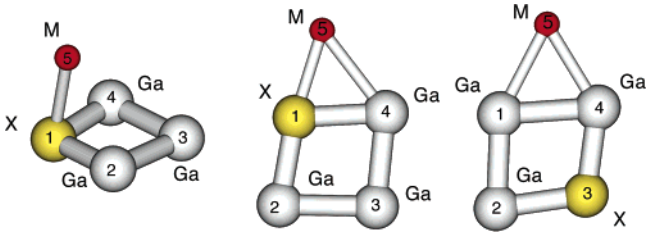

Figure 18. Three stable structures of $LMGa_3$, L = Li, Na, K, Cu and M = Si and Ge, calculated at B3LYP, B3PW91, and PW91PW91/6-311G(3df) levels of theory.[73] ((Reprinted with permission from ref 73. Copyright 2004 Elsevier.)

of the π electrons on the electronegative atom, similar to that in CAl_3^-.[146]

The interesting transformation occurs in the $AsAl_3$ species. Archibong and St-Amant[151] predicted that the cyclic C_{2v} ($^1A_1$) structure is now more stable (by 4.2 kcal/mol) than the pyramidal C_{3v} ($^1A_1$) one. Thus, the less electronegative As (compared to P) reverses the stability of the aromatic and classical structures. For $AsGa_3$, the two groups do not agree. Archibong et al.[150] reported that the cyclic C_{2v} structure is more stable than the pyramidal C_{3v} one. However, their results vary depending on the basis set. At CCSD(T)/6-311+G(2d) the pyramidal structure was found to be more stable by ~1.0 kcal/mol, but the cyclic structure became more stable at the CCSD(T)/6-311+G(2df)//CCSD(T)/6-311+G(2d) and CCSD(T)/6-311+G(3df)//CCSD(T)/6-311+G* levels of theory by 1.3 and by 1.1 kcal/mol, respectively. Balasubramanian and Zhu[152] reported that the pyramidal C_{3v} structure is the most stable one at the DFT/4s4p2d, CASSCF/4s4p2d, and MRCISD/4s4p2d levels of theory. However, it is not clear from the Balasubramanian and Zhu paper[152] if they considered the cyclic isomer. Certainly, more calculations need to be done to resolve this controversy. Aromaticity in cyclic structure of the neutral species $M'Al_3$ (M′ = P, As) and $M'Ga_3$ (M′ = P, As) can easily explain its appearance and its relative stability compared to the pyramidal classical structure. It would also be interesting to consider substitution by other more electropositive group V atoms, Sb and Bi. It is anticipated that the aromatic cyclic structures should be more favored.

Sundholm et al.[69] computationally studied another set of Al_4^{2-} isoelectronic neutral species, B_2Si_2, Al_2Si_2, and Ga_2Si_2, using the HF, B3LYP, and CCSD(T) levels and the SVP and TZVPP basis sets. There are two possible cyclic geometries for these species, the trans (denoted t-Al_2Si_2) and cis (denoted c-Al_2Si_2) isomers. For the planar t-Al_2Si_2 and c-Al_2Si_2 isomers all frequencies were found to be real, and thus they are true minima. At their highest level of theory [CCSD(T)/TZVPP] the c-Al_2Si_2 isomer is more stable than t-Al_2Si_2 by 2.1 kcal/mol. Because the vibrational frequencies and the molecular structure for Al_2Si_2 were not sensitive to the level of correlation treatment, t-B_2Si_2 and t-Ga_2Si_2 were studied only at the HF and B3LYP levels. At these levels of theory t-B_2Si_2 and t-Ga_2Si_2 are planar stable molecules. According to the ARCS calculations all of these cyclic species show a large diatropic ring current induced by a magnetic field, and thus these molecules can be considered to be aromatic.

Sundholm et al.[69] also studied c-B_2C_2 and t-B_2C_2 species. They found that the geometry optimization starting from the c-B_2C_2 isomer results in a ring opening and that it has a triplet ground state with two nearly degenerate minima. One minimum corresponds to a short C−C distance, and another minimum corresponds to a short B−B distance. They obtained similar results for Al_2C_2. Thus, when there is a significant difference in the electronegativity, the cyclic aromatic structures for the mixed isovalent clusters are no longer favored.

We recently studied a fully silicon analogue of Al_4^{2-}—a dication Si_4^{2+}.[153] As expected, the square structure was found to be the most stable as for Al_4^{2-}, even if alternative structures provided better charge separation. The square structure is most stable again due to the presence of π and σ aromaticity in the dication.

The above discussion demonstrates that the concept of multiple aromaticity introduced initially for Al_4^{2-} is capable of explaining the preference of the cyclic structure for a variety of tetraatomic molecules with 14 valence electrons. If all atoms in a molecule have similar electronegativity, which favors delocalization, the aromatic cyclic structure can be predicted to be the global minimum.

6.3. X_3^- and NaX_3 (X = B, Al, Ga) Clusters

The simplest all-metal aromatic clusters are composed of only three atoms. Two groups considered aromaticity in X_3^- (X = B, Al, and Ga) clusters. Kuznetsov and Boldyrev[75] studied bare X_3^- and dressed NaX_3 clusters using two theoretical methods [B3LYP/6-311+G* and CCSD(T)/6-311+G*] for geometry optimization and frequency calculations. They also used a few theoretical methods: ROVGF/6-311+G(2df), TD-B3LYP/6-311+G(2df), and CCSD(T)/6-311+G*(2df) for ab initio calculations of photoelectron spectra of X_3^- anions. Dixon et al.[70] used the CCSD(T)/aug-cc-pVDZ and CCSD(T)/aug-cc-pVTZ methods and studied a variety of low-lying states for the Al_3 and Al_3^- species. Recently the B_3^- anion has been studied experimentally and theoretically by Zhai et al.[158] All groups predicted that a perfect triangular D_{3h} ($^1A_1'$) structure is the global minimum for Al_3^- and for X_3^- species in general.

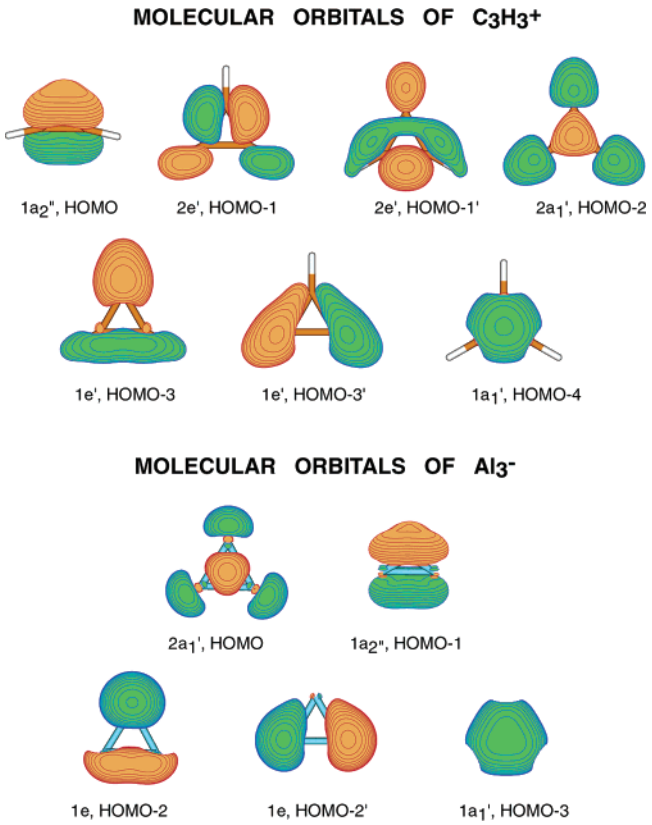

Figure 19. Molecular orbital pictures of $H_3C_3^+$ and Al_3^-.[75] (Reprinted with permission from ref 75. Copyright 2002 Springer.)

Molecular orbital analysis reveals the presence of multiple aromaticity in the X_3^- species. The multiple aromaticity can be understood by comparing the molecular orbitals of the X_3^- anions with those of the prototypical aromatic hydrocarbon cation $C_3H_3^+$, as shown in Figure 19 for Al_3^-. The HOMO ($1a_{2u}$) of $C_3H_3^+$ is a π bonding orbital formed from the out-of-plane 2p orbitals. The next six MOs are linear combinations of hybridized sp^2-AOs of C and 1s-AOs of H. These MOs can be transformed by some localization procedure into three C−H σ bonds and three C−C σ bonds, justifying the classical (2c-2e) description of the σ framework of the $C_3H_3^+$ cation. Thus, $C_3H_3^+$ is a classical 2 π electron aromatic species.

The HOMO ($2a_1'$) of Al_3^- is a σ-bonding MO formed from the in-plane $3p_r$ orbitals. The HOMO-1 ($1a_{2u}$) is a π-bonding orbital formed from the out-of-plane $3p_z$ orbitals. The following three MOs are bonding−antibonding (nonbonding 1e) and bonding ($1a_1'$) orbitals formed primarily from the filled valence 3s orbitals of Al with rather small contributions from 3p orbitals of Al, and thus the net bonding effect from these MOs is expected to be close to zero and they can be viewed as lone pairs.

The surprising result from the comparison is the earlier appearance of the π MO ($1a_2''$) in the X_3^- anions before the pair of σ MOs (2e) is occupied. The presence of the $1a_2''$-MO in B_3^-, Al_3^-, and Ga_3^- is a violation of the canonical order of the molecular orbitals observed in the $C_3H_3^+$ cation. What is even more surprising is that the π MO is the lowest bonding MO. As in the case of Al_4^{2-} and other valence isoelectronic aromatic species, we believe that the earlier occupation of the $1a_2''$ π MO in the X_3^- anions is due to the low valence charge of B, Al, and Ga, which cannot support additional electrons in the σ MOs, as in $C_3H_3^+$. Therefore, it is more favorable to occupy the π MO.

The HOMO ($2a_1'$) and HOMO-1 ($1a_2''$) are responsible for chemical bonding in the X_3^- anions. Their completely bonding nature results in the characteristics of σ and π double aromaticity for the X_3^- species. Kuznetsov and Boldyrev also calculated the neutral species NaX_3 (X = B, Al, Ga). They found that these species are highly ionic, Q(Na) = 0.88 |e| (NaB_3), Q(Na) = 64 |e| ($NaAl_3$), and Q(Na) = 0.65 |e| ($NaGa_3$), compared to the diatomic molecules NaX, Q(Na) = 0.33 |e| (NaB), Q(Na) = 0.07 |e| (NaAl), and Q(Na) = 0.09 |e| (NaGa) (all are NPA effective charges at the MP2/6-311+G* level). Optimized geometric parameters and harmonic frequencies of the bare X_3^- anions or inside the NaX_3 species are very similar. Thus, the X_3^- species preserve their electronic and geometric integrity in the NaX_3 neutral species.

The unusual ordering of the MOs in the X_3^- species have been verified by comparing ab initio VDEs with available photoelectron spectra,[154−156] as shown in Table 7). Agreement between the experimental and theoretical results is very reasonable. The theoretical data for Al_3^- also agree well with the best ab initio data reported by Baeck and Bartlett.[157] We also point out that the measured first VDEs of the X_3^- species B_3^- (VDE = 2.82 ± 0.02 eV), Al_3^- (VDE = 1.925 ± 0.050 eV), and Ga_3^- (VDE = 1.95 ± 0.10 eV) are substantially higher than the VDEs of the corresponding atomic anions: B^- (VDE = 0.277 ± 0.010 eV), Al^- (VDE = 0.441 ± 0.010 eV), and Ga^- (VDE = 0.30 ± 0.15 eV). This provides another piece of evidence for the bonding and aromatic nature of the HOMO in the X_3^- anions.

The resonance energy for the Al_3^- species has been evaluated by Dixon et al.[70] using eq 5:

$$RE(Al_3^-) = \Delta E(Al_3^- \rightarrow 3Al + e) - 2\Delta E(Al_2\ (^1\Sigma_g^+) \rightarrow 2Al) \quad (5)$$

The calculations at the CCSD(T) level of theory using the complete basis set extrapolation and with corrections on core−valence electron correlation, scalar relativistic effects, spin−orbit effects, and zero-point energy gave $RE(Al_3^-)$ = 79.3 kcal/mol. This is an upper limit for $RE(Al_3^-)$. When they used $\Delta E[Al_2\ (^3\Pi_u) \rightarrow 2Al]$ instead of $\Delta E[Al_2\ (^1\Sigma_g^+) \rightarrow 2Al]$, they obtained $RE(Al_3^-)$ = 65.8 kcal/mol, which is a lower limit for $RE(Al_3^-)$. In any case, the $RE(Al_3^-)$ is very high, consistent with its double aromaticity.

We have also examined the aromaticity in X_3^- and NaX_3 using NICS indices.[159] We computed NICS indices at the center of the X_3^- cycle and below the center of the X_3^- cycle by 0.5 and 1.0 Å (on the opposite side of the X_3 plane in the NaX_3 species). Results of these calculations are summarized in Table 8. As one can see, all species are highly aromatic according to the NICS values. The largest NICS values are found for the boron species. These

Table 7. Experimental and ab Initio Photoelectron Spectra of X_3^- (X = B, Al, Ga) Anions[75]

B_3^- exptl spectrum		theor spectrum			
			VDE		
band	VDE	final state	ROVGF/6-311+G(2df)[a]	TD-B3LYP/6-311+G(2df)	RCCSD(T)/6-311+G(2df)
X	2.82 ± 0.02	$^2A_1'$, $1a_1'^2 1e'^4 1a_2''^2 2a_1'^1 2e'^0$	2.72 (0.87)	2.66	2.88
A	3.56 ± 0.03	$^2A_2''$, $1a_1'^2 1e'^4 1a_2''^1 2a_1'^2 2e'^0$	3.57 (0.88)	3.60	3.54
B	4.55 ± 0.03	$^2E'$, $1a_1'^2 1e'^4 1a_2''^2 2a_1'^0 2e'^1$		4.49	4.70
		$^2E''$, $1a_1'^2 1e'^4 1a_2''^1 2a_1'^1 2e'^1$		4.67	
C	5.58 ± 0.03	$^2E'$, $1a_1'^2 1e'^3 1a_2''^2 2a_1'^2 2e'^0$	5.31 (0.83)	5.38	

Al_3^- exptl spectrum		theor spectrum			
			VDE		
band	VDE	final state	ROVGF/6-311+G(2df)[a]	TD-B3LYP/6-311+G(2df)	RCCSD(T)/6-311+G(2df)
X	1.925 ± 0.050	$^2A_1'$, $1a_1'^2 1e'^4 1a_2''^2 2a_1'^1 2e'^0$	1.73 (0.87)	1.69	1.86
A	2.165 ± 0.050	$^2A_2''$, $1a_1'^2 1e'^4 1a_2''^1 2a_1'^2 2e'^0$	2.02 (0.88)	1.99	2.11
B	2.65 ± 0.10	$^2E'$, $1a_1'^2 1e'^4 1a_2''^2 2a_1'^0 2e'^1$		2.56	
C	4.34 ± 0.10	$^2E''$, $1a_1'^2 1e'^4 1a_2''^2 2a_1'^0 2e'^0 1e''^1$		4.41?	
D	4.66 ± 0.10	$^2E'$, $1a_1'^2 1e'^3 1a_2''^2 2a_1'^0 2e'^0$	4.66 (0.76)	4.52	

Ga_3^- exptl spectrum		theor spectrum			
			VDE		
band	VDE	final state	ROVGF/6-311+G(2df)[a]	TD-B3LYP/6-311+G(2df)	RCCSD(T)/6-311+G(2df)
X	1.95 ± 0.10	$^2A_1'$, $1a_1'^2 1e'^4 1a_2''^2 2a_1'^1 2e'^0$	1.69 (0.87)	1.67	1.77
A	2.18 ± 0.10	$^2A_2''$, $1a_1'^2 1e'^4 1a_2''^1 2a_1'^2 2e'^0$	1.94 (0.88)	1.90	1.99
		$^2E'$, $1a_1'^2 1e'^4 1a_2''^2 2a_1'^0 2e'^1$		2.48	
		$^2E''$, $1a_1'^2 1e'^4 1a_2''^2 2a_1'^0 2e'^0 1e''^1$		4.44	

[a] At the CCSD(T)/6-311+G* geometry. Pole strength is given in parentheses.

Table 8. NICS Indices Calculated at the B3LYP/6-311+G* Level of Theory[75]

molecule	R(bq), Å	NICS, ppm	molecule	R(bq), Å	NICS, ppm
B_3^-	0.0	−73.6	NaB_3	0.0	−73.4
	0.5	−57.9		0.5	−57.7
	1.0	−22.6		1.0	−26.6
Al_3^-	0.0	−35.8	$NaAl_3$	0.0	−36.7
	0.5	−33.8		0.5	−38.2
	1.0	−24.8		1.0	−33.5
Ga_3^-	0.0	−27.3	$NaGa_3$	0.0	−30.4
	0.5	−26.9		0.5	−28.7
	1.0	−22.6		1.0	−21.9

NICS indices are all substantially higher than those in benzene, consistent with the multiple aromaticity in X_3^- and NaX_3. Table 8 also shows that the Na^+ coordination to X_3^- does not affect the NICS indices.

6.4. Pure σ Aromatic/Antiaromatic Metal Clusters

The aromaticity/antiaromaticity concept has also been extended to metal clusters with σ electrons only. In such clusters only valence s-AOs are involved in chemical bonding. The simplest metal cluster is Li_3^+, which is known to have a triangular global minimum structure.[160] It has only one completely delocalized bonding σ molecular orbital, as shown in Figure 20.[161]

The $1a_1'$-MO is the sum of the 2s-AOs of the three lithium atoms and is very similar to the completely delocalized π MO in the $C_3H_3^+$ cation (Figure 19). The only difference is that the π MO is the sum of $2p_z$-AOs of carbons with a nodal plane. The delocalized π MO in $C_3H_3^+$ renders its π aromaticity according to the $4n + 2$ Huckel rule. On the basis of the analogy between the π-delocalized MO in $C_3H_3^+$ and the

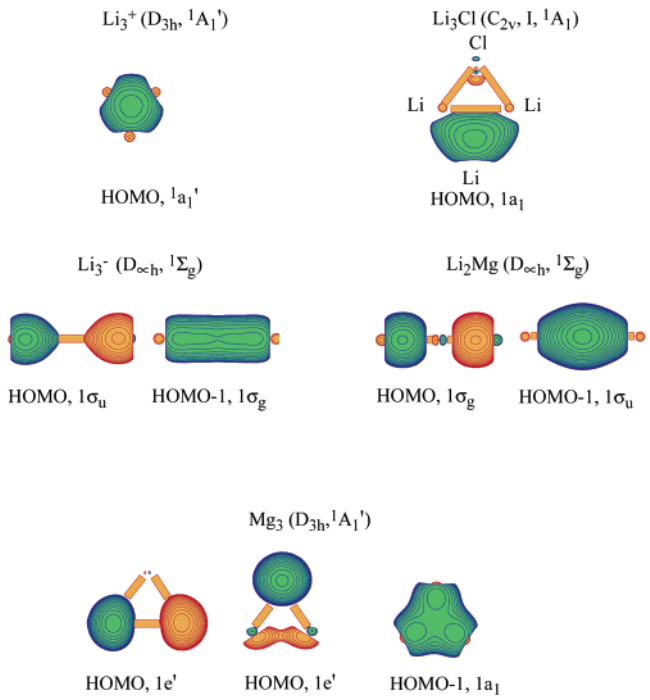

Figure 20. Molecular orbitals of the triatomic σ aromatic and σ antiaromatic clusters.[161a] (Reprinted with permission from ref 161a. Copyright 2003 American Chemical Society.)

σ-delocalized MO in Li_3^+, the latter cation should be called σ aromatic.[161a]

If the Li_3^+ cation is σ aromatic, it should have a special stability relative to nonaromatic reference molecules, but it is inconvenient to work with a cation. Instead, a Li_3Cl neutral molecule, containing the Li_3^+ cation and a Cl^- anion, was considered by Alexandrova and Boldyrev[161a] for RE calculations. It was found that the bidentate structure (C_{2v}, I, $^1A_1$,

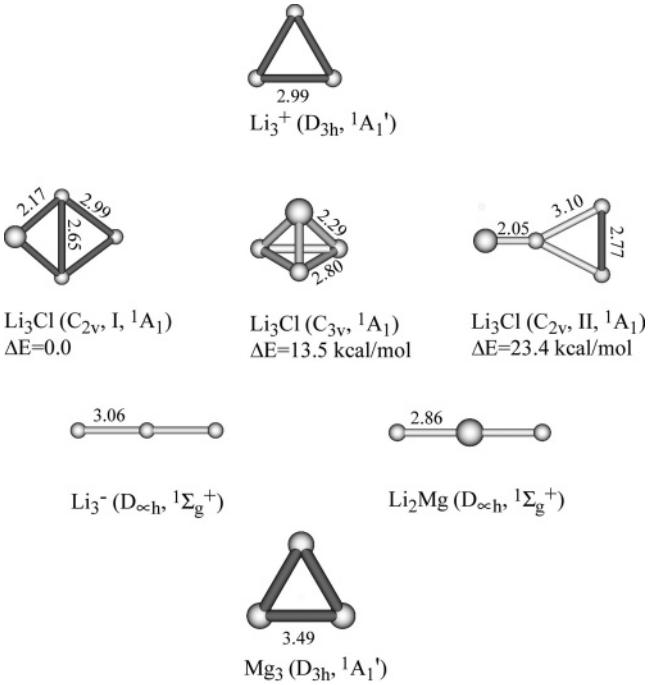

Figure 21. Optimized structures of selected triatomic σ aromatic and σ antiaromatic clusters.[161a] (Reprinted with permission from ref 161a. Copyright 2003 American Chemical Society.)

Figure 21) with the Cl^- coordinated to the edge of the Li_3^+ triangle is the global minimum, in agreement with previous calculations.[162]

The Cl^- anion only slightly perturbs the σ aromatic HOMO in Li_3Cl when compared to the isolated Li_3^+ cation, as can be seen in Figure 20. The σ RE in the Li_3^+ cation can be calculated as the energy of the reaction

$$Li_3Cl\ (C_{2v}, {}^1A_1) \rightarrow Li_2 + LiCl \qquad (6)$$

where Li_2 and LiCl are reference classical molecules (i.e., are represented by a single Lewis structure). At the highest level of theory [CCSD(T)/6-311+G(2df)//CCSD(T)/6-311+G*+ZPE/CCSD(T)/6-311+G*] the RE(Li_3^+) was found to be 35.7 kcal/mol.[161a] The calculated RE is certainly very high compared to the Li_2 dissociation energy (23.1 kcal/mol). Thus, Alexandrova and Boldyrev concluded that the introduction of the σ aromaticity in the Li_3^+ cation is justified. Fowler and co-workers in their recent paper[161b] dispute the σ aromaticity in the Li_3^+ cation. They calculated current density maps for Li_3^+ and H_3^+ ions, and on the basis of these maps they concluded that H_3^+ shows a marked diatropic ring current and can be considered to be σ aromatic on the magnetic criterion. Li_3^+ shows no global current and thus is nonaromatic on this criterion, despite highly negative values of calculated NICS(0) for the both species: H_3^+ [NICS(0) = −33.6 ppm] and Li_3^+ [NICS(0) = −11.2 ppm].

The counting rule for σ electrons is $4n + 2$ if only the s-AOs are responsible for bonding. For σ antiaromatic species the counting rule is then $4n$, analogous to the Huckel rules for π antiaromaticity. The Li_3^- anion is a good example of a σ antiaromatic system with four σ electrons.[161a] The electronic configuration for the singlet state of Li_3^- at the D_{3h} symmetry is $1a_1'^2 1e'^2$, and the triangular structure with this electronic configuration is subject to Jahn−Teller distortion. Indeed, it is known that Li_3^- is linear.[163] Two σ-delocalized MOs (Figure 20) can be approximately localized into two 2c-2e bonds, and the linear structure of Li_3^- can be formally considered as a classical structure. This situation is similar to the antiaromatic cyclobutadiene structure, which can be considered as having two double and two single carbon−carbon bonds, thus being formally a classical structure.

When two more electrons are added, the number of σ electrons again satisfies the $4n + 2$ rule, and the corresponding cluster is expected to be aromatic again. However, the corresponding Mg_3 cluster is a weakly bound van der Waals complex (the atomization energy was found to be just 5.2 kcal/mol). We believe that this does not contradict the aromaticity concept. As one can see in Figure 20, in Mg_3 all bonding, nonbonding, and antibonding MOs, composed of the 3s atomic orbitals, are occupied, and in such a case the net bonding effect is expected to be close to zero.

A similar approach can be used to explain aromaticity and antiaromaticity in tetraatomic clusters. The Li_4^{2+} dication is the simplest tetraatomic metal cluster with just two σ electrons, and it is aromatic.[161a,165] Whereas the Li_4^{2+} dication is not expected to be stable because of the Coulomb repulsion, it does have a local minimum at the tetrahedral structure. Indeed, the calculated dissociation energy is negative, showing its instability:

$$Li_4^{2+}\ (T_d, {}^1A_1) \rightarrow 2Li\ ({}^2S) + 2Li^+\ ({}^1S)$$
$$\Delta E = -169.3\ \text{kcal/mol} \qquad (7)$$

To evaluate RE(Li_4^{2+}), one needs to subtract the destabilizing effect of the Coulomb repulsion from the two extra positive charges. One way to do this is to assume that the Coulomb repulsion of the two extra charges in Li_4^{2+} can be approximately evaluated by placing one point charge of 0.5 |e| on each of the four Li nuclei. After subtraction of the repulsion energy thus calculated (269.5 kcal/mol) from the atomization energy in reaction 7, one obtains a value of 98.9 kcal/mol. Using this value and the dissociation energy of Li_2, one arrives at a quite high RE(Li_4^{2+}) value of 75.8 kcal/mol.[161a]

When two more electrons are added, the neutral Li_4 molecule with four σ electrons is expected to be antiaromatic and rectangular, as is known for C_4H_4.[8] However, a rhombus structure is known to be the global minimum for Li_4.[164] Thus, the σ antiaromatic molecules have a rhombus distortion rather than the expected rectangular distortion.[161a] We will see later that this can also be true for σ antiaromatic molecules with p-AOs responsible for bonding.

The next tetraatomic system considered with six σ electrons is Mg_4^{2+}. It is a metastable species with a local minimum at the planar square geometry (Figure 22), which is similar to that of the π aromatic $C_4H_4^{2-}$ hydrocarbon.[166−168] The linear structure of

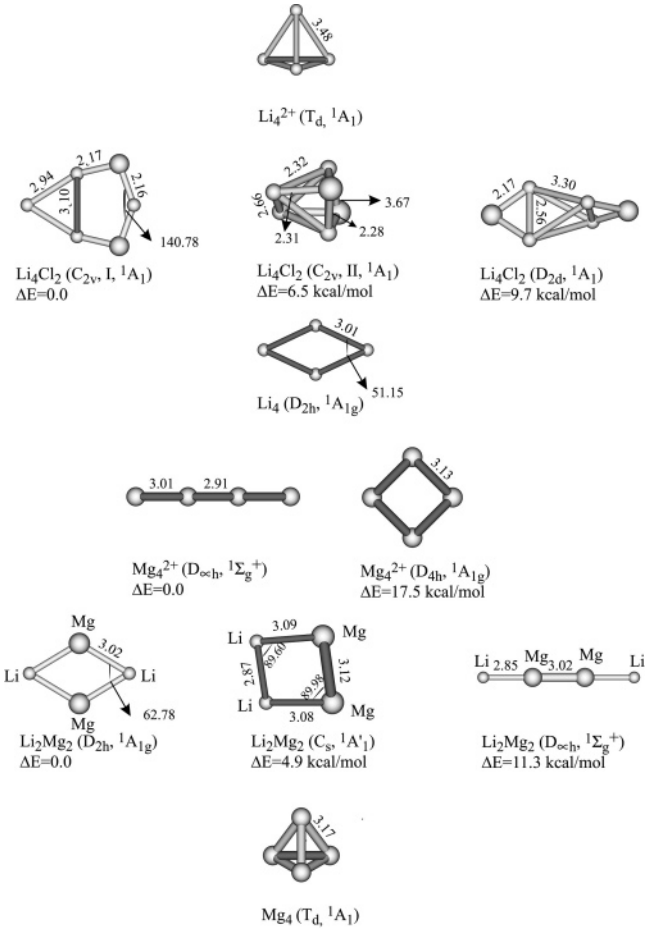

Figure 22. Optimized structures of selected tetraatomic σ aromatic and σ- antiaromatic clusters.[161a] (Reprinted with permission from ref 161a. Copyright 2003 American Chemical Society.)

Mg_4^{2+} (Figure 22) is, however, more stable because it minimizes the Coulomb repulsion. To avoid dealing with doubly charged species, the Mg_2Li_2 molecule was studied, which has six σ electrons and is supposed to be σ aromatic. As is shown in Figure 22, the cyclic Mg_2Li_2 aromatic structures are indeed more stable than the linear Li−Mg−Mg−Li classical structure.[161a] The higher stability of the σ aromatic structures of Mg_2Li_2 provides us with an additional justification for the introduction of the σ aromaticity concept into metal clusters. The Mg_4 cluster, in analogy with Mg_3, is supposed to be a weakly bound van der Waals complex. However, with the increase of the size of a cluster, the s−p hybridization starts to play a more important role, which leads to a rather high atomization energy for Mg_4 (22.4 kcal/mol).

σ aromaticity can also be responsible for enhanced stability in transition metal clusters formed by group IB atoms.[76,77] In such clusters s electrons are primarily responsible for chemical bonding similar to alkali metal clusters. Lievens and co-workers[76a] recently explained the enhanced intensity of the Au_5Zn^+ cluster (Figure 23) generated from a laser vaporization cluster source using the idea of σ aromaticity. They found three stable isomers for Au_5Zn^+ using ab initio calculations, as shown in Figure 24. Molecular orbital analysis (Figure 25) reveals that the Au_5Zn^+ cluster has three σ MOs, which are rather similar in

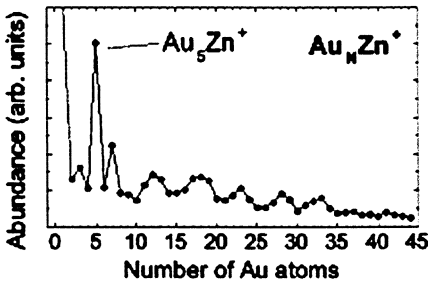

Figure 23. Mass abundance spectrum of Au_5Zn^+ clusters.[76] (Reprinted with permission from ref 76. Copyright 2003 American Chemical Society.)

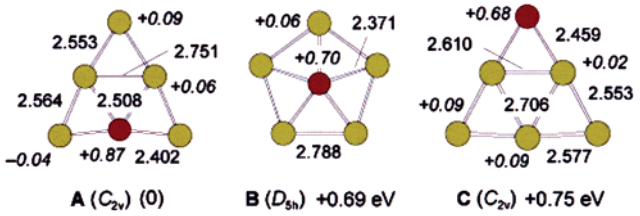

Figure 24. Optimized structures, effective atomic charges, and relative stabilities of Au_5Zn^+ calculated at the MP2 level of theory. Bond distances are in angstroms.[76a] (Reprinted with permission from ref 76a. Copyright 2003 American Chemical Society.)

all three isomers, with HOMO-2 being completely bonding and HOMO and HOMO-1 being partially bonding. Six σ electrons occupying these MOs satisfy the $4n + 2$ rule for σ aromaticity, and thus the Au_5Zn^+ cluster is σ aromatic. Lievens and co-workers[76a] performed also NICS calculations and found that all three isomers have high negative NICS values at the ring center, thus providing additional support that this cluster is aromatic. The Au_5Zn^+ cluster is the first experimentally observed and theoretically proved example of all-metal aromatic cluster formed by transition metal atoms.

Alexandrova et al.[76b] claimed that a highly unusual sandwich anion $Cu_3C_4^-$ is also aromatic. In the most stable structure a Cu_3^{3+} triangular group is sandwiched by two C_2^{2-} units lying parallel to the plain of Cu_3^{3+}. A comparison of ab initio PES spectra with the experimental data showed that the sandwich $Cu_3C_4^-$ structure was solely responsible for the observed spectra. The calculated NICS at the centrum and above the Cu_3 fragment were found to be negative (−7.1 ppm at $z = 0$ Å, −7.9 ppm at $z = 0.4$ Å, and −17.0 ppm at $z = 0.8$ Å), showing the presence of aromaticity on the basis of this criterion. We think that the back-donation of the electron density from C_2^{2-} units to the completely bonding aromatic MO of Cu_3^{3+} could be responsible for the presence of aromaticity in this cluster.

Schleyer and co-workers[76c] recently presented evidence of aromaticity in a series of interesting all-metal clusters M_4Li_2, where M = Cu, Ag, and Au. The calculated NICS(0) were found to be −14.5 ppm (Cu_4Li_2), −14.1 ppm (Ag_4Li_2), and −18.6 ppm (Au_4Li_2) for the most stable square bipyramidal (D_{4h}, $^1A_{1g}$) structure. The calculated charge separation in Cu_4Li_2 is close to the ideal Li^+ and Cu_4^{2-}. If one assumes that primarily s-AOs of Cu participate in the Cu_4^{2-} chemical bonding, than we have six σ electrons and

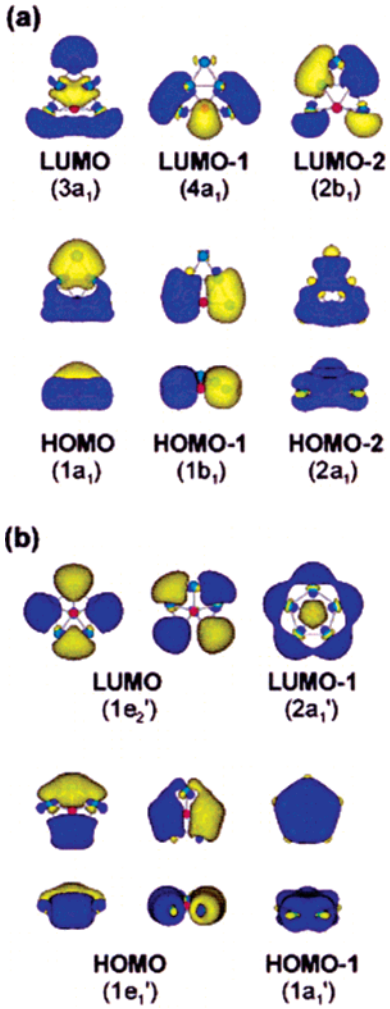

Figure 25. HOMOs and LUMOs of isomers A (a) and B (b) in Figure 24.[76a] (Reprinted with permission from ref 76a. Copyright 2003 American Chemical Society.)

the system should be σ aromatic and adapt a planar square structure similar to that of the Mg_4^{2+} cluster[161a] discussed above. Schleyer and co-workers,[76c] however, concluded that d orbitals of Cu contributed to aromaticity in this cluster on the basis of diatropic d orbital contributions to the total NICS.

Another interesting class of transition metal clusters, which was claimed to be aromatic, is a series of cyclic hydrocoppers. Tsipis and Tsipis[77] optimized geometries for $(CuH)_n$, $n = 3-6$, as well as for $(CuX)_3$, X = CH_3, NH_2, OH, and PH_2 using the B3LYP/6-311+G** level of theory. The hydrocopper clusters can be considered as analogues of the organocopper-(I) compounds, which are known to form planar cyclic structures such as the cyclic Cu_4R_4 (R = CH_2SiMe_3). They found that the 3D structures are less stable than the corresponding planar cyclic structures by 46.4 kcal/mol (Cu_4H_4), by 27.5 kcal/mol (Cu_5H_5), and by 29.8 kcal/mol (Cu_6H_6). The calculated structures of the $(CuH)_n$, $n = 3-6$, species are shown in Figure 26. Tsipis and Tsipis[77] proposed to use aromaticity to explain the preference of planar cyclic structures over the 3D structures. They found that all cyclic structures are very stable toward dissociation into CuH molecules: $\Delta E = E(CuH)_3 - 3E(CuH)$, 81.5 kcal/mol; $\Delta E = E(CuH)_4 - 4E(CuH)$, 137.0 kcal/mol; $\Delta E = E(CuH)_5 - 5E(CuH)$, 180.1 kcal/mol; and $\Delta E =$

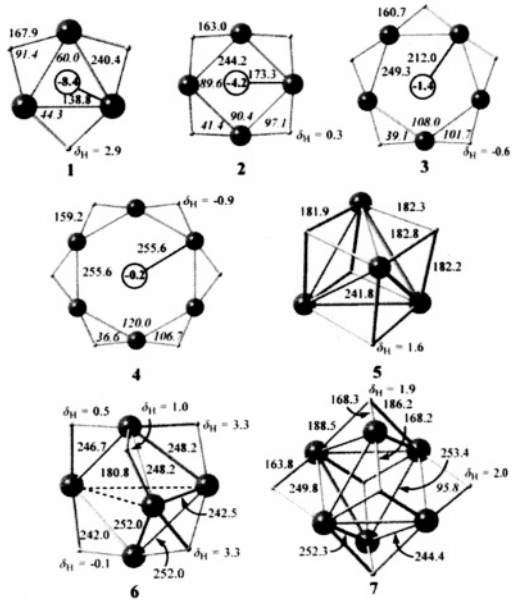

Figure 26. Selected geometric parameters for the cyclic planar and cubic Cu_nH_n molecules computed at the B3LYP/6-311+G** level of theory.[77] (Reprinted with permission from ref 77. Copyright 2003 American Chemical Society.)

$E(CuH)_6 - 6E(CuH)$, 217.5 kcal/mol (all at B3LYP/6-311+G**). Calculated NICS indices were found to be negative at the center of the cycle, while they were decreasing from −8.4 ppm in Cu_3H_3 to −0.02 ppm in Cu_6H_6, primarily due to the increase of the cyclic radius. All of these data indicate that aromaticity could be responsible for the stability and cyclic structures of these species.

6.5. Aromatic Metal Clusters with Only π Bond

There could be metal clusters in which π bonding occurs without the formation of the σ-bonding framework. Kuznetsov and Boldyrev[169] recently have shown that three, four, or five metal atoms can be held together by a single π bond in the Mg_3^-, $NaMg_3^-$, and Na_2Mg_3 clusters. In both the $NaMg_3^-$ and Na_2Mg_3 species, the basic structural unit is an unusual Mg_3^{2-} trigonal planar cluster, which exhibits properties of aromaticity, because it satisfies the $4n + 2$ rule for π electrons and it is an equilateral triangle. Natural population analysis shows that the Na atomic orbitals contribute to the formation of the π-bonding MO, and thus all four atoms in $NaMg_3^-$ or all five atoms in Na_2Mg_3 are involved in chemical bonding. In these clusters, π aromaticity occurs without a σ framework.

The Be_3^- and Mg_3^- species have been shown previously to be bound by a single π bond. Ab initio calculations[170−172] and a photoelectron spectroscopic study[173] show that the Be_3^- and Mg_3^- clusters have a $^2A_2''$ ground state. As we discussed in section 6.4 above, an isolated Mg_3 ($^1A_1'$, D_{3h}) is a weakly bound van der Waals complex. In the ground state of the Mg_3^- ($^2A_2''$, D_{3h}) anion, the HOMO is a half-occupied π MO, which is solely responsible for bonding in Mg_3^-. Molecular orbitals for Mg_3^- are presented in Figure 27. The three bottom MOs are the complete bonding, nonbonding, and antibonding combinations of the valence Mg 3s electrons. Their net bonding effect is zero, and the Mg 3s atomic orbitals can be

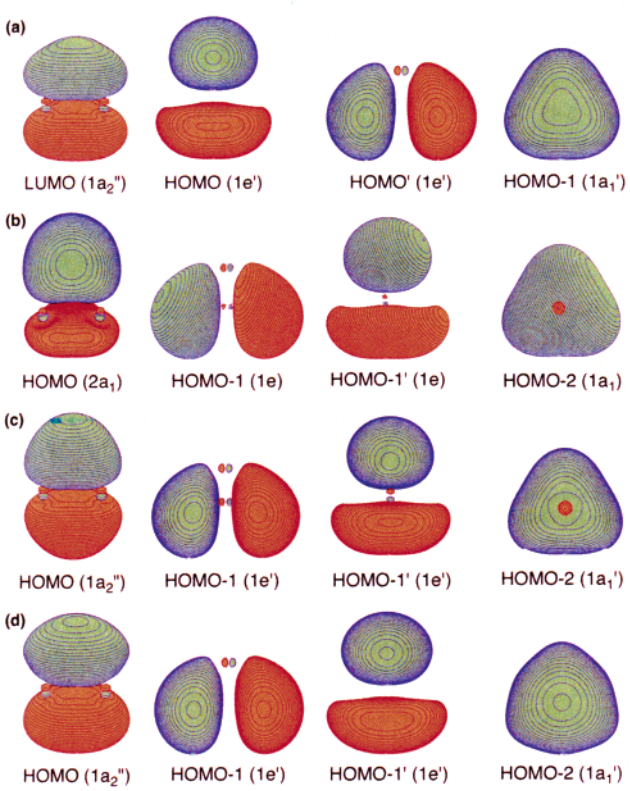

Figure 27. Valence molecular orbitals of Mg_3^- (a), $NaMg_3^-$ (b), Na_2Mg_3 (c), and $Mg_3^{2-}(Z^+)_2$ (d).[169] (Reprinted with permission from ref 169. Copyright 2004 Elsevier.)

Table 9. Calculated and Experimental Photoelectron Spectra of Mg_3^- and $NaMg_3^-$ (Adapted from Reference 169)

	VDE, theor OVGF/ 6-311+G(2df)[a]	VDE, theor CCSD(T)/ 6-311+G(2df)[a]	VDE, exptl
Mg_3^-, (D_{3h}, $^2A_2''$)			
$1a_2''$	0.84 (0.88)	0.80	0.85[b]
$1e'$	2.35 (0.82)		2.20[b]
$NaMg_3^-$, (C_{3v}, $^1A_1$)			
$2a_1$	1.13 (0.86)	1.29	
$1e$	2.31 (0.81)		

[a] At CCSD(T)/6-311+G* geometry. Pole strength is given in parentheses. [b] Evaluated from Figure 2 in ref 173.

essentially considered as lone pairs. The HOMO ($1a_2''$) in Mg_3^- is a π-bonding orbital formed by p orbitals of the three Mg atoms and is solely responsible for bonding in Mg_3^-. The calculated atomization energy for the reaction

$$Mg_3^- (D_{3h}, {}^2A_2'') \rightarrow 3Mg ({}^1S) + e \qquad \Delta E = 22.2 \text{ kcal/mol} \quad (8)$$

clearly shows an appreciable chemical bonding in the Mg_3^- species. Thus, three metal atoms can be held together by a single π bond without appreciable σ bonding. The calculated photoelectron spectrum of Mg_3^- is in good agreement with Bowen's experimental PES spectrum[173] (Table 9), lending credence to this description of chemical bonding in Mg_3^-.

Kuznetsov and Boldyrev[169] also tested if the $NaMg_3^-$ and Na_2Mg_3 species could be viable molecules. They found that the most stable structure for the $NaMg_3^-$ species was the C_{3v} singlet trigonal pyramid structure (Figure 28c). The C_{3v} triplet trigonal pyramid structure (Figure 28d) was found to be the second low-lying isomer. At the highest level of theory, the global minimum structure was found to be more stable than the triplet isomer by 13.4 kcal/mol. The calculated energies of the following reactions

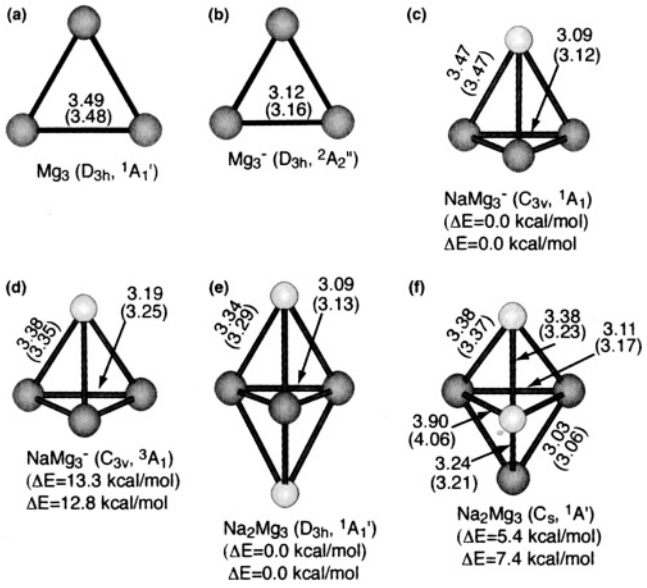

Figure 28. Optimized structures of magnesium species at the B3LYP/6-311+G* and CCSD(T)/6-311+G* levels of theory: (a) trigonal planar Mg_3 (D_{3h}, $^1A_1'$); (b) trigonal planar Mg_3^- (D_{3h}, $^2A_2''$); (c) trigonal pyramid $NaMg_3^-$ (C_{3v}, $^1A_1$); (d) trigonal pyramid $NaMg_3^-$ (C_{3v}, $^3A_1$); (e) trigonal bipyramid Na_2Mg_3 (D_{3h}, $^1A_1'$); (f) trigonal bipyramid Na_2Mg_3 (C_s, $^1A'$). Bond lengths are given in angstroms. Data at the B3LYP/6-311+G* level of theory are given in parentheses.[169] (Reprinted with permission from ref 169. Copyright 2004 Elsevier.)

$$NaMg_3^- (C_{3v}, {}^1A_1) \rightarrow Na ({}^2S) + Mg_3^- (D_{3h}, {}^2A_2'') \qquad \Delta E = 28.3 \text{ kcal/mol} \quad (9)$$

$$NaMg_3^- (C_{3v}, {}^1A_1) \rightarrow Na^- ({}^1S) + Mg_3 (D_{3h}, {}^1A_1') \qquad \Delta E = 32.9 \text{ kcal/mol} \quad (10)$$

clearly show that $NaMg_3^-$ is a chemically bound species.[169] Molecular orbitals of $NaMg_3^-$ shown in Figure 27b look very similar to MOs of Mg_3^-. The HOMO ($2a_1$) is a bonding π orbital formed by the $3p_z$ AOs of the Mg atoms. Therefore, on the basis of the MO analysis it was concluded that $NaMg_3^-$ does not possess σ chemical bonds, but rather the four metals atoms are held together by a single π bond.[169]

The most stable structure of the Na_2Mg_3 species was found to be the D_{3h} trigonal bipyramidal structure (Figure 28e).[169] The C_s trigonal bipyramid structure is the lowest isomer (Figure 28f). At the highest level of theory, the global minimum D_{3h} trigonal bypiramidal structure was found to be more stable than the C_s trigonal bipyramidal structure by 8.0 kcal/mol, as found for the following calculated reaction energy:

$$Na_2Mg_3 (D_{3h}, {}^1A_1') \rightarrow 2Na ({}^2S) + 3Mg ({}^1S) \qquad \Delta E = 54.1 \text{ kcal/mol} \quad (11)$$

Table 10. Calculated NICS Values for Na_2Mg_3 (D_{3h}, $^1A_1'$) and Mg_3^{2-} (D_{3h}, $^1A_1'$), with Point Charges, and Mg_3 (D_{3h}, $^1A_1'$) (Adapted from Reference 169)

	NICS (ppm) at the B3LYP/6-311+G* level of theory[a]		
distance (R) from the Mg_3 ring center, Å	Na_2Mg_3 (D_{3h}, $^1A_1'$)	$Mg_3^{2-}(Z^+)_2$ (D_{3h}, $^1A_1'$)	Mg_3 (D_{3h}, $^1A_1'$)
0.0	−29.8	−30.4	1.7
0.2	−29.6	−30.2	1.6
0.4	−29.0	−29.6	1.0
0.6	−28.0	−28.6	0.4
0.8	−26.6	−27.2	−0.4
1.0	−24.9	−25.4	−1.2

[a] Geometry at the CCSD(T)/6-311+G* level of theory.

Na_2Mg_3 is clearly a chemically bound species with quite high atomization energy. Molecular orbitals of Na_2Mg_3 shown in Figure 27c again are very similar to those of Mg_3^-. Natural population analysis, however, shows that there is little charge transfer from Na to Mg [Q(Na) = 0.086 |e| and Q(Mg) = −0.057 |e| at QCISD/6-311+G*] and that the Na atomic orbitals contribute significantly to the $1a_2''$-HOMO. However, despite the significant contribution from the Na atomic orbitals to the $1a_2''$-MO, it remains a π MO. To prove that, Kuznetsov and Boldyrev[169] calculated molecular orbitals for a model system $Mg_3^{2-}(Z^+)_2$, with two point charges (1) located at the positions of the sodium atoms (Figure 28d). One can see that the HOMO in the $Mg_3^{2-}(Z^+)_2$ model system looks exactly the same even though it has a composition in its $1a_2''$-HOMO completely different from that of Na_2Mg_3, which has large contributions from the Na atomic functions. Thus, the Na_2Mg_3 species is an intriguing example of five atoms bonded by a single π bond. In both the $NaMg_3^-$ and Na_2Mg_3 species, the basic unit can be formally considered as Mg_3^{2-}, which is aromatic: it obeys the $4n + 2$ rule for π electrons and is an equilateral triangle.

Kuznetsov and Boldyrev[169] further tested aromaticity in these species using NICS calculations (Table 10). One can see that both $Mg_3^{2-}(Z^+)_2$ and Na_2Mg_3 are highly aromatic, whereas the Mg_3 neutral species is nonaromatic. Thus, metal clusters offer us an extraordinary type of aromaticity, where π aromaticity occurs without the initial formation of a σ framework.

6.6. Sandwich Complexes Based on All-Metal Aromatic Clusters

Mercero and Ugalde[78] reported computational prediction of the first transition metal sandwich complex based on the all-metal aromatic Al_4^{2-} cluster, $[Al_4TiAl_4]^{2-}$, in analogy to similar transition metal benzene complexes. They obtained a staggered (D_{4d}, $^1A_1$) structure for the doubly charged $[Al_4TiAl_4]^{2-}$ complex, as shown in Figure 29. The eclipsed structure, which corresponds to the transition state for the staggered isomer's interconversion, is only 5 kcal/mol higher in energy. The Al_4^{2-} aromatic units maintain the square-planar structure with the Al−Al bond length being elongated by 0.14 Å upon complexation.

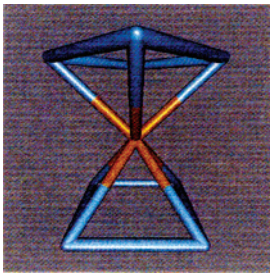

Figure 29. Optimized $[Al_4TiAl_4]^{2-}$ structure at the B3LYP/6-311G level of theory.[78] (Reprinted with permission from ref 78. Copyright 2004 American Chemical Society.)

They also computed the dissociation energy for the following reaction:

$$[Al_4TiAl_4]^{2-} \rightarrow 2[Al_4^{2-}] + Ti^{2+} \qquad (12)$$

A very high dissociation energy for reaction 12 was found, ~610 kcal/mol. This value is similar to metallocene binding energies. The ferrocene experimental energy is 636 ± 6 kcal/mol, and the calculated energy is 656 kcal/mol at a similar level of theory. Mercero and Ugalde[78] also used NICS to probe the aromaticity in $[Al_4TiAl_4]^{2-}$. They found that NICS(0) = −39.0 ppm and NICS(1) = −16.9 ppm in $[Al_4TiAl_4]^{2-}$ compared to the NICS(0) = −28.5 ppm and NICS(1) = −24.2 ppm in free Al_4^{2-} using the B3LYP/6-311G level of theory. On the basis of these results Mercero and Ugalde[78] concluded that the aromatic nature of the Al_4^{2-} square complex remains intact upon complexation. Because the isolated dianion $[Al_4TiAl_4]^{2-}$ is not electronically stable due to the strong coulomb repulsion, they also studied $Na[Al_4TiAl_4]^-$ and $Na_2[Al_4TiAl_4]$, in which the dianions are stabilized by the Na^+ counterions. The Na^+ cations only slightly deformed the Al_4^{2-} rings, providing an opportunity for experimental study of novel sandwich complexes.

7. All-Metal Clusters with Conflicting Aromaticity: Antiaromaticity in $Li_3Al_4^-$

7.1. General Considerations

As discussed above, the Al_4^{2-} dianion is an all-metal triply aromatic system. The triple aromaticity comes from three types of MOs formed by the three 3p AOs of Al (Figure 5): p_π (π orbitals perpendicular to the plane of the square from p_z AOs), $p_{\sigma-r}$ (σ orbitals oriented radially toward the center of the square from the $p_{x,y}$ AOs), and $p_{\sigma-t}$ (σ orbitals oriented tangentially around the square from the $p_{x,y}$ AOs). These MOs can be separated in a square structure into two sets: σ MOs and π MOs (Figure 6). We conjectured that if a cluster containing Al_4^{4-} could be made, it would be a good candidate to be the first net antiaromatic all-metal cluster,[91] because the additional electron pair could occupy one of the degenerate π ($1e_g$) or σ ($2e_u$) MOs (Figure 30), thus making it either π antiaromatic or σ antiaromatic. In both cases the system will possess conflicting aromaticity, for example, being σ aromatic and π antiaromatic in the first case and being σ antiaromatic and π aromatic in the second case. For molec-

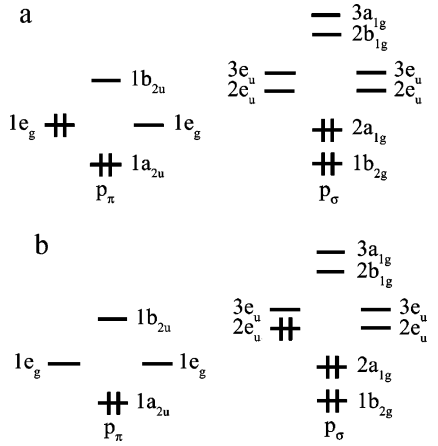

Figure 30. Molecular orbital schemes for the π antiaromatic Al_4^{4-} structure (a) and the σ antiaromatic Al_4^{4-} (b).

ular systems with conflicting aromaticity it is difficult to predict in advance if aromaticity or antiaromaticity will win, and thus the system will be net aromatic or net antiaromatic, respectively. Moreover, different criteria of aromaticity may signal different net conclusions. From the geometric point of view if the two additional electrons enter a π orbital (Figure 30a), the system would be net antiaromatic if the Al_4^{4-} framework would assume a rectangular shape in contrast to the square shape of Al_4^{2-}, or if the two additional electrons enter a σ orbital (Figure 30b), the system would be net antiaromatic if the square would distort to a rhombus shape.

An Al_4^{4-} tetraanion is expected to be highly electronically unstable due to the enormous coulomb repulsion as well as highly unstable toward dissociation. Therefore, we again used alkali cations as a stabilizer and considered a singly charged $Li_3Al_4^-$ anion and the neutral Li_4Al_4. The singly charged $Li_3Al_4^-$ anion can be produced experimentally similar to the $LiAl_4^-$ anion and can be investigated by photoelectron spectroscopy, thus facilitating comparisons between theory and experiment.[91]

7.2. Search for the Global Minimum Structures

We performed ab initio calculations on a wide variety of structures for $Li_3Al_4^-$ in search of the global minimum using two different theoretical methods: B3LYP/6-311+G* and CCSD(T)/6-311+G*. We found many isomers for the $Li_3Al_4^-$ species lying very close to each other near the global minimum (Figure 31).[91] At the B3LYP/6-311+G* level of theory the most stable structure was found to be the "fork" structure (Figure 31D). However, at the highest level of theory, CCSD(T)/6-311+G(2df), the most stable structure was found to be the capped octahedral singlet structure (Figure 31B) with the four low-lying isomers in the following order: the capped octahedron triplet structure (Figure 31C), the "fork" singlet structure (Figure 31D), the "hood" singlet structure (Figure 31E), and the "scooter" singlet structure (Figure 31F). Numerous other isomers were also located for $Li_3Al_4^-$, but at all levels of theory they have higher energies than the five low-lying structures shown in Figure 31. The ground state of $Li_3Al_4^-$ (Figure 31B) indeed

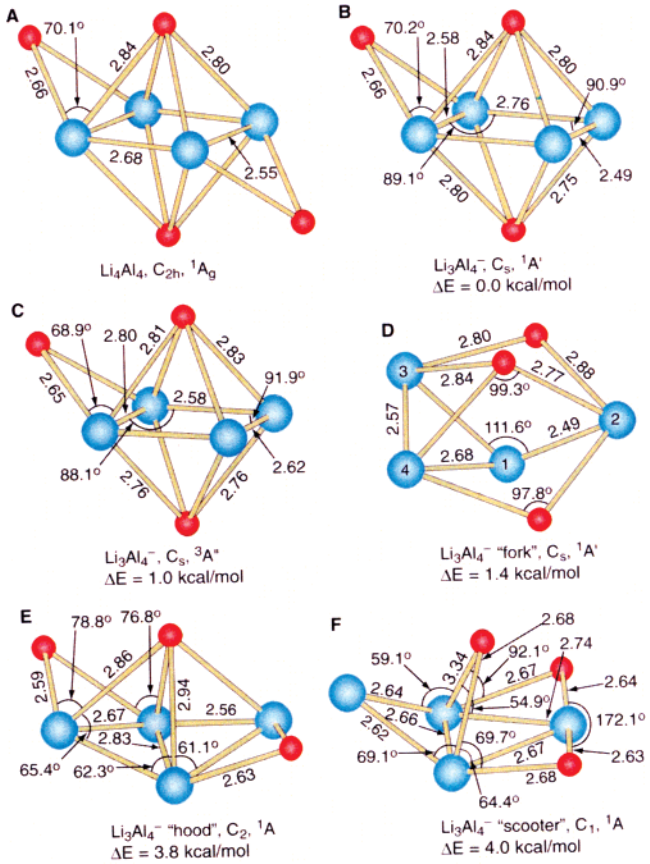

Figure 31. Optimized structures of Li_4Al_4 and $Li_3Al_4^-$: (A) Li_4Al_4; (B) capped octahedral singlet $Li_3Al_4^-$ (C_s, $^1A'$); (C) capped octahedral triplet $Li_3Al_4^-$ (C_s, $^3A''$; (D) "fork" $Li_3Al_4^-$ (C_s, $^1A'$); (E) "hood" $Li_3Al_4^-$ (C_2, ^1A); (F) "scooter" $Li_3Al_4^-$ (C_1, ^1A). Structural parameters given in angstroms, and degrees are at the B3LYP/6-311+G* level of theory. The relative energies for the isomers of $Li_3Al_4^-$ are at the CCSD(T)/6-311+G(2df) level of theory.[91] (Reprinted with permission from *Science* (http://www.aaas.org, ref 91. Copyright 2003 American Association for the Advancement of Science.)

possesses a slightly distorted rectangular Al_4 framework; the distortion is caused by the asymmetric capping of the third Li atom. The neutral Li_4Al_4 cluster (Figure 31) has been optimized, too, and found indeed to contain a rectangular Al_4 framework, as expected if the two extra electrons enter the second π orbital ($1e_g$ MO, Figure 30A). The neutral Li_4Al_4 cluster has been recently studied by Chacko et al.[174] with molecular dynamics within the framework of density functional theory. A similar capped octahedron with four Al atoms forming a perfect rectangular framework was shown to be the most stable structure. We recently performed a new search for local minimum structures of $Li_3Al_4^-$ using ab initio gradient embedded genetic algorithm (GEGA program)[110] and the B3LYP/3-21G level of theory. Although we found more local minima for this anion, the few most stable structures were found to be the same as reported before.

7.3. Photoelectron Spectroscopy of $Li_3Al_4^-$ and Comparison between Experiment and Theory

To confirm the theoretical predictions of the global minimum structure of $Li_3Al_4^-$ and explore the anti-

Table 11. Experimental Vertical Electron Detachment Energies (VDE) (in eV) of $Li_3Al_4^-$, Compared to Calculated VDEs for the Ground State and Four Low-Lying Isomers of $Li_3Al_4^-$ (Adapted from Reference 91)

		C_s, ^{1}A′, capped octahedron		C_s, ^{3}A″, capped octahedron		C_s, ^{1}A′, "fork"		C_2, ^{1}A, "hood"		C_1, ^{1}A, "scooter"	
	VDE (exptl)	MO	VDE (theor)[a]	MO	VDE (theor)[b]	MO	VDE (theor)[a]	MO	VDE (theor)[a]	MO	VDE (theor)[a]
X	1.39 ± 0.07	6a′	1.34 (0.86) [1.35 (0.86)]	3a"	1.21 (0.89)	6a′	1.66 (0.85)	3b	1.40 (0.86)	8a	1.37 (0.85)
				6a′	1.34 (0.90)						
A	1.92 ± 0.06	5a′	1.85 (0.85) [1.86 (0.85)]	5a′	1.66 (0.88)	5a′	1.88 (0.85)	5a	1.66 (0.85)	7a	2.00 (0.85)
				4a′	1.90 (0.88)						
B	2.39 ± 0.05	4a′	2.39 (0.84) [2.37 (0.84)]	3a′	2.18 (0.87)	2a″	2.15 (0.84)	4a	2.21 (0.84)	6a	2.08 (0.84)
C	2.91 ± 0.08	3a′	2.92 (0.83) [2.91 (0.83)]	2a″	2.61 (0.86)	4a′	2.56 (0.84)	3a	2.52 (0.84)	5a	2.47 (0.84)
		2a″	2.96 (0.82) [3.00 (0.83)]								
		1a″	6.32 (−0.01) [6.33 (0.00)]			3a′	4.10 (0.79)	2a	3.53 (0.77)	4a	3.69 (0.75)

[a] VDEs were calculated at the ROVGF/6-311+G(2df)//B3LYP/6-311+G* level of theory. Numbers in parentheses indicate pole strength, which characterizes the validity of the one-electron detachment picture. VDEs in brackets were calculated at the ROVGF/6-311+G(2df)//CCSD(T)/6-311+G* level of theory. The first VDE for the global minimum structure was calculated to be 1.42 eV [CCSD(T)/6-311+G(2df)//CCSD(T)/6-311+G*]. [b] VDEs were calculated at the UOVGF/6-311+G*//B3LYP/6-311+G* level of theory.

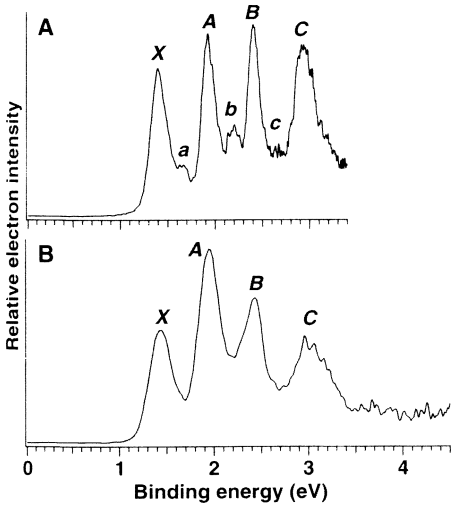

Figure 32. Photoelectron spectra of $Li_3Al_4^-$ (a) at 355 nm (3.496 eV) and (b) at 193 nm (6.424 eV). The vertical detachment energies for the four major detachment features (*X*, *A*, *B*, *C*) are given in Table 11.[91] (Reprinted with permission from *Science* (http://www.aaas.org, ref 91. Copyright 2003 American Association for the Advancement of Science.)

aromaticity in Al_4^{4-}, we studied the $Li_3Al_4^-$ species experimentally. The $Li_3Al_4^-$ anions were produced using laser vaporization of a LiAl alloy target (see section 3) and probed using PES. The PES spectra of $Li_3Al_4^-$ are shown in Figure 32 at two photon energies. The spectra exhibit four major detachment features (*X*, *A*, *B*, *C*) and three weak features (*a*, *b*, *c*). Band C is fairly broad and may contain two detachment channels. This was revealed more clearly in the 193 nm spectrum (Figure 32b), and thus the 3 eV band is labeled C&D to indicate that it contains two overlapping bands. The vertical electron detachment energies of these features are measured from the peak maxima and compared to the results of ab initio calculations in Table 11.

There is an excellent agreement between the first five vertical detachment channels calculated for the ground-state structure (Figure 31b) and the four major experimental peaks (*X*, *A*, *B*, *C*). The calculated detachment energies from the 3a′ and 2a″ orbitals are very close, in agreement with the experimental observation that the 3 eV band contains two detachment channels. Ab initio calculations predict that there are no one-electron detachment channels between 3.0 and 6.3 eV, consistent with the absence of any major peaks beyond 3 eV in the $Li_3Al_4^-$ spectrum at 193 nm (Figure 32b). The other three low-lying singlet isomers all have a major transition between 3.5 and 4.5 eV (Table 11) and thus can be excluded from being contributors to the major observed spectral features. However, there are minor features (*a*, *b*, *c*) in the spectra of $Li_3Al_4^-$, seen more clearly at 355 nm (Figure 32a). They could be due to either impurities or isomers of $Li_3Al_4^-$. We could rule out contributions from impurities because the mass selection was quite clean. Thus, the minor peaks are most likely due to the presence of minor isomers of $Li_3Al_4^-$, consistent with the theoretical predictions. The best agreement for these minor peaks was found for the "fork" isomer (Table 11), which is the lowest lying singlet isomer. Contributions from the two other singlet isomers (Figure 31E,F) are expected to be small due to their higher relative energies. We did not observe much contribution from the triplet capped octahedron structure, the first vertical detachment energy of which is rather low (Table 11).

7.4. Molecular Orbital Analyses and Antiaromaticity in Al_4^{4-}

The rectangular framework of the Al_4 fragment in $Li_3Al_4^-$ and Li_4Al_4 already hints at the presence of net antiaromaticity, as was initially suspected. The rectangular distortion suggests that the two extra electrons enter the π orbital in Al_4^{4-} (Figure 30a). To

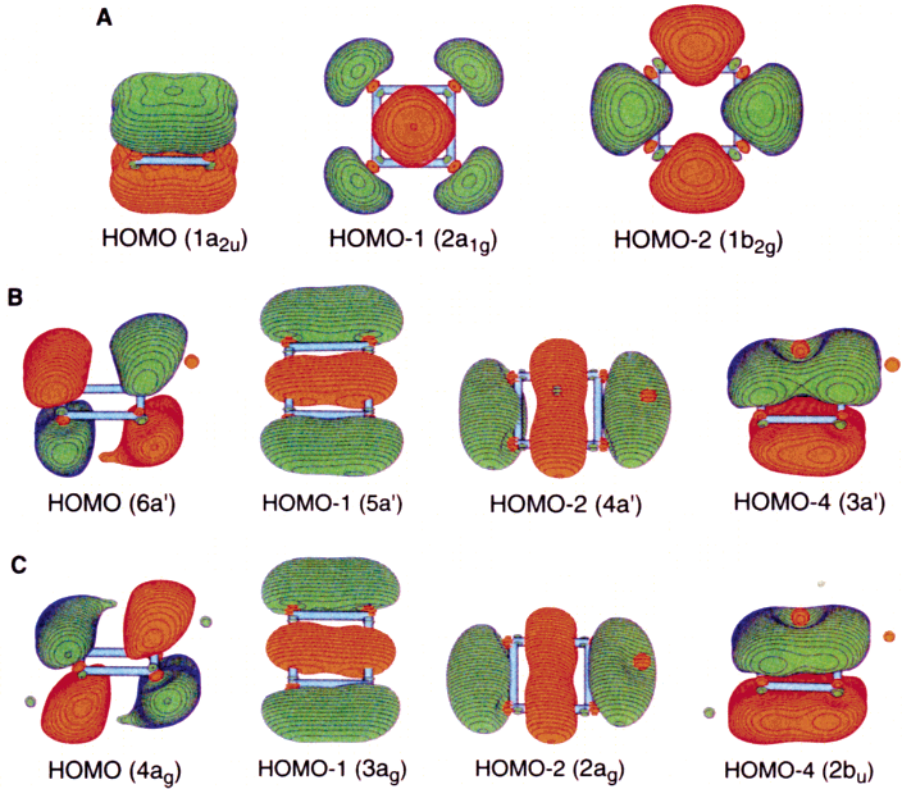

Figure 33. Molecular orbital pictures: (A) Al_4^{2-} (D_{4h}, $^1A_{1g}$); (B) capped octahedral singlet $Li_3Al_4^-$ (C_s, $^1A'$); (C) Li_4Al_4 (C_{2h}, ^1A_g).[91] (Reprinted with permission from *Science* (http://www.aaas.org, ref 91. Copyright 2003 American Association for the Advancement of Science.)

provide further proof, we need to analyze the molecular orbitals and see if Al_4^{4-} possesses four π electrons. The MOs of $Li_3Al_4^-$ and Li_4Al_4 are shown in Figure 33. For comparison we also present the MOs of Al_4^{2-} (Figure 33A). The MOs of $Li_3Al_4^-$ and Li_4Al_4 are nearly identical, even though the Al_4 framework in $Li_3Al_4^-$ is slightly distorted from a perfect rectangle due to the asymmetric capping by the Li atoms. Clearly the Li atoms substantially donate electron density and the two clusters can be viewed approximately as $Li^+{}_3Al_4^{4-}$ and $Li^+{}_4Al_4.^{4-}$ Those MOs that are similar to those of Al_4^{2-} can be recognized in Al_4^{4-}: the completely delocalized π MO (HOMO-4) is considerably stabilized in Al_4^{4-}, and the two delocalized σ MOs (HOMO-1 and HOMO-2) correspond to the same set in Al_4^{2-} (Figure 33A). The extra pair of electrons enters the HOMO of Al_4^{4-}, which is indeed a π MO. This π HOMO of Al_4^{4-} is bonding within the two shorter Al−Al bonds, but antibonding between the two pairs of Al (Figure 33B), resulting in the rectangular shape, is responsible for the antiaromatic characters of Al_4^{4-}. Both the π bonding patterns and the rectangular shape of Al_4^{4-} are analogous to the prototypical antiaromatic organic molecule cyclobutadiene. Thus, Al_4^{4-} is the first all-metal π antiaromatic species ever made,[175] even though it still possesses σ aromaticity derived from the two delocalized σ bonding MOs; thus, the whole system has conflicting aromaticity, but it is net antiaromatic from the geometric point of view.

The triplet isomer C_s ($^3A''$) (Figure 31C) with two electrons in the same spin occupying the $1e_g$ π MO (Figure 30a) is very interesting. This suggests that this isomer should be aromatic because the π electron count for aromaticity for triplet species is $4n$.[176] Thus, the Al_4 framework should again be square in this isomer. Indeed, Figure 31C shows that the three Al−Al bonds that are not coordinated by Li^+ are almost equal (2.58 versus 2.62 Å), which is quite different from the rectangular distortion in the antiaromatic ground-state structure (Figure 31B). The aromaticity of the triplet isomer explains why it is so stable and only 1.0 kcal/mol higher than the singlet ground state. To confirm this observation and eliminate the structural complication caused by the asymmetric Li^+ coordination in $Li_3Al_4^-$, we computed an isoelectronic and symmetric species $Li_2Al_4^{2-}$, in which one Li^+ is coordinated above and the other Li^+ is coordinated below the Al_4 plane.[159] We found indeed that in the singlet $Li_2Al_4^{2-}$ an ideal rectangular Al_4 framework is obtained, whereas in the triplet $Li_2Al_4^{2-}$ a perfect square Al_4 framework is obtained. This result demonstrates unequivocally the net antiaromaticity in the singlet Al_4^{4-} and the net aromaticity in the triplet Al_4^{4-}, similar to cyclobutadiene.

The chemical bonding in other low-lying isomers can be explained starting from the Al_4^{2-} dianion (Figure 4). The fork isomer (C_s, $^1A'$) can be traced to the pyramidal structure (C_{3v}, $^1A_1$) of Al_4^{2-} (Figure 4E). In the dianion the pyramidal isomer was substantially less stable (~25.2 kcal/mol higher in energy) than the aromatic square structure. In the fork isomer of $Li_3Al_4^-$ the additional electron pair resulted in the formation of an Al−Al bond, providing considerable stabilization, which is manifested by the close energetics between the fork isomer and the ground state (Figure 31). Thus, the stabilization of the fork isomer relative to the rectangular isomer is because

of the relative destabilization of the latter due to the occupation of the partially antibonding $1e_g$ MO in the square and due to the occupation of a partially bonding MO in the pyramidal isomer. The hood and scooter isomers (Figure 31E,F) originate from the square structure of Al_4^{2-} upon occupation of one of the degenerate $2e_u$ σ MOs (Figure 30b), resulting in rhombus distortions. These two isomers simply reflect two different ways to cap the rhombus Al_4^{4-} tetraanion. The rhombus structures are π aromatic, but σ antiaromatic, and thus the system has conflicting aromaticity. We see that these π aromatic and σ antiaromtic $Li_3Al_4^-$ isomers are very close in energy to the π antiaromatic and σ aromatic ground state. This is not the case for the Si_4 cluster, which is isoelectronic to Al_4^{4-}. Raghavachari and Logovinski[177] first predicted computationally that the Si_4 cluster has a rhombus structure, which was confirmed experimentally.[178−180] The rhombus shape of the Si_4 cluster is due to its π aromatic and σ antiaromatic nature, as we elucidated recently.[153] An alternative σ aromatic and π antiaromatic rectangular structure for Si_4 was found to be substantially higher in energy (~46 kcal/mol) than the rhombus one. The higher valence atomic charge of Si relative to Al allows silicon clusters to have more electrons in the σ framework.

7.5. Is $Li_3Al_4^-$ Antiaromatic or Aromatic? The Controversy over the Net Antiaromaticity of $Li_3Al_4^-$

Immediately after the publication of the all-metal antiaromatic $Li_3Al_4^-$,[91] Schleyer and co-workers published a paper disputing the net antiaromaticity in $Li_3Al_4^-$.[88] Schleyer and co-workers confirmed the ground-state structures that we identified for $Li_3Al_4^-$ and Li_4Al_4 and calculated the NICS indices for several isomers of $Li_3Al_4^-$, as well as for Li_4Al_4. They further confirmed that both the $Li_3Al_4^-$ and Li_4Al_4 ground states contain the rectangular Al_4^{4-} tetraanion with four π electrons, which give positive (paramagnetic) contributions to the NICS indices, that is, strong π antiaromaticity. They also obtained negative NICS indices for the σ electrons, confirming the σ aromaticity in these all-metal clusters. However, when they added all of the NICS indices from both π and σ electrons, they obtained an overall negative value because the magnitude of the NICS index from the σ electrons is higher than that from the π electrons. The total NICS values obtained are $NICS(Li_3Al_4^-) = -4.8$ ppm and $NICS(Li_4Al_4) = -11.4$ ppm, from which they concluded that both systems should be considered to be net aromatic rather than net antiaromatic.[88] This controversy was extended into a discussion on the overall aromaticity or antiaromaticity in all-metal systems when both $\sigma(\pi)$ aromaticity and $\pi(\sigma)$ antiaromaticity are present simultaneously and was reported in a feature article by Ritter in *Chemical & Engineering News*.[95]

In this discussion we maintained that the singlet $Li_3Al_4^-$ isomer with the rectangular Al_4^{4-} tetraanion should be considered to be net antiaromatic on the basis of the rectangular distortion, which is exactly analogous to the structural distortion in the prototypical antiaromatic C_4H_4 molecule. We argued that if the aromaticity from σ electrons overwhelms the antiaromaticity from π electrons, the overall structure of Al_4^{4-} should be square-planar, like Al_4^{2-} in the $LiAl_4^-$ anion. We also pointed out that the first vertical electron detachment energy in $Li_3Al_4^-$ (1.39 eV)[91] is substantially smaller than that in $LiAl_4^-$ (2.15 eV),[68] consistent with one additional (spectroscopic) criterion for antiaromaticity in $LiAl_4^-$.[95] Schleyer and co-workers argued that the alteration in the Al−Al distances in Al_4^{4-} is small percentagewise compared to the same difference in C_4H_4 and that the smaller first VDE in $Li_3Al_4^-$ compared to the VDE in $LiAl_4^-$ is simply a reflection of the presence of more highly charged species (Al_4^{4-} compared to Al_4^{2-}) in the $Li_3Al_4^-$ and $LiAl_4^-$ anions, respectively.[95] We continue to believe that because we have an alteration in bond length we cannot call $Li_3Al_4^-$ aromatic and the low VDE is a reflection of the partially antibonding nature of its HOMO. We felt that the perfect rectangular shape of Al_4^{4-} in the singlet $Li_2Al_4^{2-}$ species and the perfect square shape of Al_4^{4-} in the triplet $Li_2Al_4^{2-}$ provide unequivocal evidence for their antiaromatic and aromatic nature, respectively. Furthermore, we found that the Al−Al bond length in the triplet $Li_2Al_4^{2-}$ is exactly the average of the Al−Al bond lengths in the rectangular singlet $Li_2Al_4^{2-}$,[159] similar to the cases of the triplet aromatic C_4H_4 and the singlet antiaromatic C_4H_4.[181] Apparently, these two camps were not able to reach any consensus.[95]

The other participants in the debate were split.[95] Fowler proposed simply to call $Li_3Al_4^-$ π antiaromatic and σ aromatic, without trying to assign net aromaticity or antiaromaticity to the system. Shaik and Hiberty stated that even if there is a distortion from the square structure in $Li_3Al_4^-$, it is a net aromatic system on the basis of their previous publications on the distortive nature of π electrons.[182] Frenking concluded that if one uses an energetic rather than a magnetic criterion, then the π antiaromaticity overwhelms the σ aromaticity in $Li_3Al_4^-$ because of the obvious rectangular structural distortion. Sundholm used the method of aromatic ring-current shielding to show that Al_4^{4-} is antiaromatic and concluded that the normally reliable NICS calculations failed in this case.

7.6. More Recent Works on the Net Antiaromaticity of $Li_3Al_4^-$ and Related Species

Since the appearance of the Ritter article in *Chemical & Engineering News*,[95] several new studies have been published on $Li_3Al_4^-$,[92,94] Li_4Al_4,[92,94,174,183] $Na_3Al_4^-$,[93] Na_4Al_4,[93,102,183] and K_4Al_4.[183] Fowler and coworkers[92] analyzed induced current density maps in $Li_3Al_4^-$, C_s (Figure 34), and in Li_4Al_4, C_{2h} (Figure 35). They showed that in the Al_4 plane both systems exhibit a strong diatropic σ current. At 1 a_0 above the Al_4 plane, the total current is of mixed character, with competing diatropic and paratropic subpatterns, and at 2 a_0 above the Al_4 plane, the current in $Li_3Al_4^-$ is purely paratropic.

They stated that the question of aromaticity/antiaromaticity is complicated in these species by the

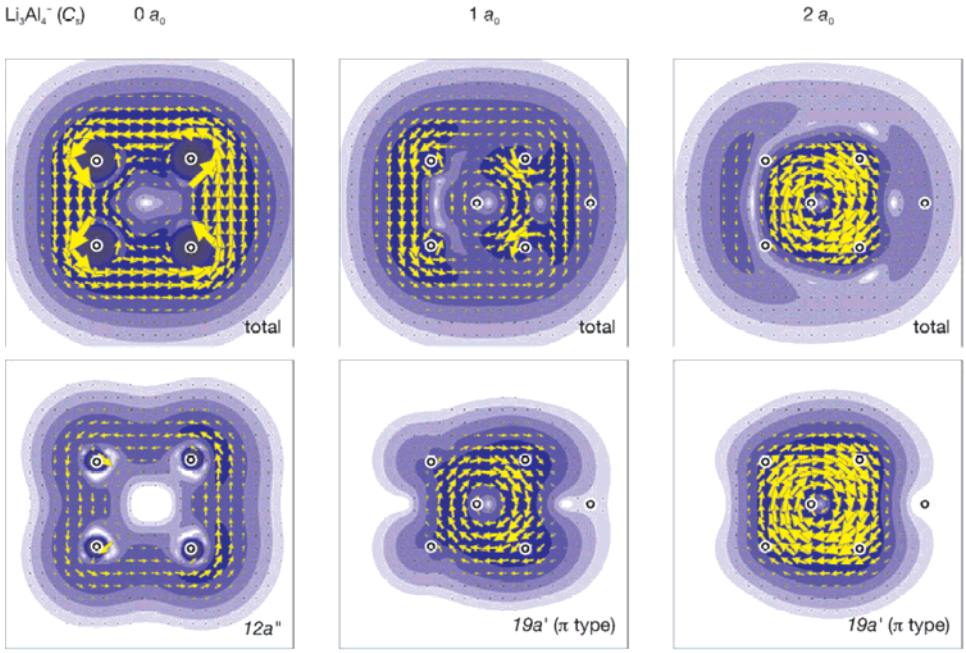

Figure 34. Total induced current density and orbital contributions to the current density for $Li_3Al_4^-$ C_s, plotted at different heights above the Al_4 square.[92] (Reprinted with permission from ref 92. Copyright 2004 Royal Society of Chemistry.)

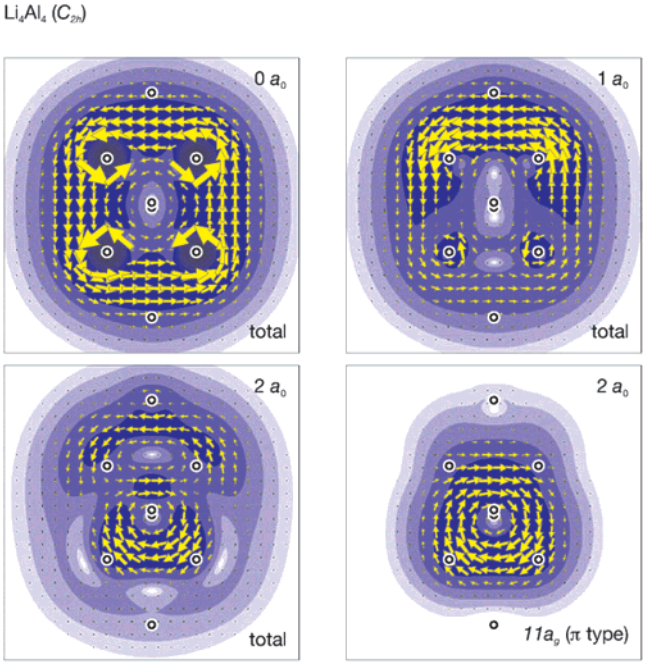

Figure 35. Total induced current density and orbital contributions to the current density for Li_4Al_4 C_{2h}, plotted at different heights above the Al_4 square.[92] (Reprinted with permission from ref 92. Copyright 2004 Royal Society of Chemistry.)

cancelation of currents.[92] The current in $Li_3Al_4^-$ is diatropic in the plane but paratropic out of the plane. Li_4Al_4 is a less clear-cut case in which the current is initially diatropic in plane and remains mixed out of plane. Chacko and co-workers[174] concluded that the C_{2h} singlet structure (found as the global minimum structure in their Born−Oppenheimer molecular dynamic calculations within the framework of density functional theory) is antiaromatic on the basis of the presence of four π electrons. Datta and Pati[183a] investigated the linear and nonlinear electric polarizibilities of the M_4Al_4 (M = Li, Na, K) clusters. From their quantum chemical calculations they showed that these species exhibit an exceptionally high magnitude of linear and nonlinear optical coefficients that are orders of magnitude higher than conventional π conjugate systems of similar sizes. They attributed such phenomenal increase to non-centrosymmetricity incorporated in the systems by the alkali atoms surrounding the ring, leading to charge transfer with small optical gap and low bond length alteration. However, they concluded that these species are aromatic in character on the basis of the low magnitude of the bond length alteration. From our point of view, extremely high linear and nonlinear optical coefficients are excellent proof that these species are actually antiaromatic.

Recently, Santos and co-workers[90,94] proposed to use ELF to probe aromaticity and antiaromaticity in organic and inorganic compounds, including $Li_3Al_4^-$ and Li_4Al_4 species. As in the case of Al_4^{2-} considered above (section 5.3), Santos and co-workers separated ELF into ELF_σ and ELF_π and then used bifurcation points as an aromatic scale for a series of chemical compounds presented in Figure 36. Results of their calculations are summarized in Table 12, from which one sees clearly that for conventional π aromatic molecules (I−XI), the σ bifurcation occurs at ELF_σ values of ~0.75 and the π bifurcation occurs at ELF_π values from 0.70 to 0.91, with the highest value of 0.91 being for the classical aromatic molecule benzene. Conventional π antiaromatic molecules (XII−XIV) also have the σ bifurcation points at ELF_σ values of ~0.75, but the π bifurcation occurs at much lower ELF_π values ranging from 0.11 to 0.35, with the lowest value, 0.11, for the classical antiaromatic molecule cyclobutadiene. The all-metal triple-aromatic Al_4^{2-} has the highest ELF_σ and ELF_π values, as well as the highest average ELF value (0.94),

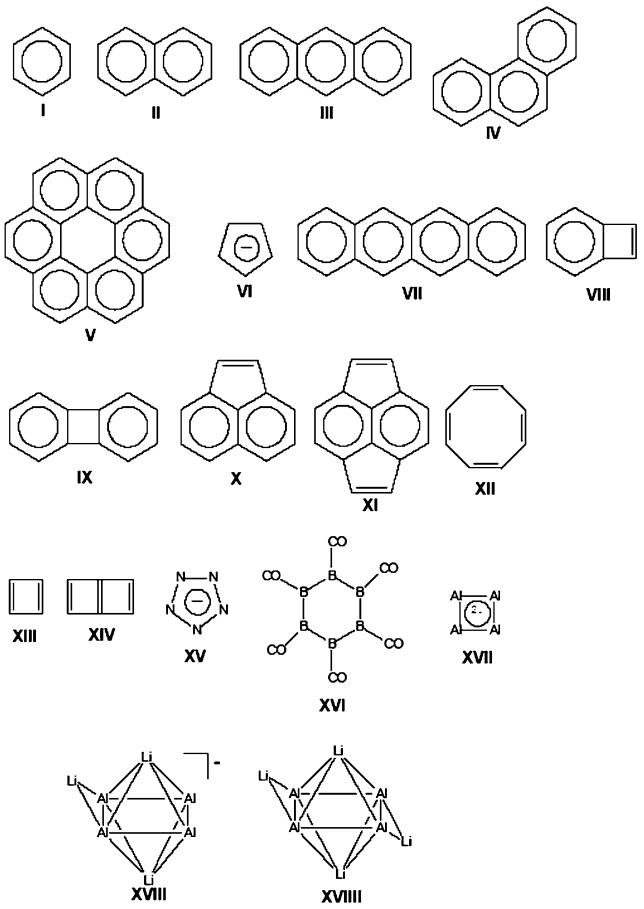

Figure 36. Molecules analyzed by the bifurcation ELF_σ and ELF_π.[94] (Reprinted with permission from ref 94. Copyright 2005 American Chemical Society.)

Table 12. Bifurcation Values of ELF_σ, ELF_π, and Their Average for Analyzed Molecules (Adapted from Reference 94)

molecule	ELF_σ	ELF_π	av	molecule	ELF_σ	ELF_π	av
I	0.76	0.91	0.84	XI	0.77	0.71	0.74
II	0.76	0.78	0.77	XII	0.73	0.35	0.54
III	0.77	0.70	0.74	XIII	0.79	0.11	0.45
IV	0.75	0.64	0.70	XIV	0.78	0.15	0.47
V	0.76	0.75	0.76	XV	0.81	0.78	0.80
VI	0.75	0.82	0.79	XVI	0.68	0.85	0.77
VII	0.74	0.69	0.72	XVII	0.88	0.99	0.94
VIII	0.76	0.72	0.74	XVIII[a]	0.86	0.08	0.47
IX	0.76	0.74	0.75	XVIII[b]	0.86	0.41	0.64
X	0.76	0.75	0.76	XIX	0.87	0.24	0.56

[a] Above the plane of Al_4. [b] Below the plane of Al_4.

reflecting the presence of multiple aromaticity as discussed in section 5.3.

For $Li_3Al_4^-$ Santos and co-workers[94] calculated bifurcation points above and below the Al_4 ring. The first bifurcation (0.08) corresponds to the separation of the basins above the plane of the ring, and the other bifurcation (0.41) corresponds to the separation of the basins below the plane, reflecting the asymmetric capping by the lithium atoms. Consequently, there are two average ELF values: 0.47 and 0.64. For the symmetric cluster Li_4Al_4 (XIX) they obtained the first bifurcation at 0.24, which is close to the average value of the first bifurcation points from the above two cases (0.08 and 0.41). The average ELF values for $Li_3Al_4^-$ (0.47 and 0.64) and Li_4Al_4 (0.56) are very close to the average ELF value of the prototypical antiaromatic molecules C_8H_8 (0.54) and C_4H_4 (0.45), thus clearly confirming the overall antiaromatic nature of $Li_3Al_4^-$ and Li_4Al_4. We believe the new ELF-based analysis proposed by Santos and co-workers[94] has great potential for the characterization of molecules with multiple aromaticity, multiple antiaromaticity, and conflicting aromaticity.

A few papers on aromaticity in $Li_3Al_4^-$ have been published after submission this paper. Sundholm and co-workers[69b] calculated magnetically induced densities in the four-membered ring Al_4^{2-} and Al_4^{4-} species at the CCSD level of theory by applying the gauge-including magnetically induced current (GIMIC) method. The GIMIC calculations support the earlier notion that Al_4^{2-} with formally two π electrons sustains a net diatropic ring current. The diatropic contribution to the ring-current susceptibility is carried by the electrons in both the σ (16.7 nA/T) and π (11.3 nA/T) orbitals. The induced ring current in the Al_4^{4-} compounds with four π electrons consists of about equally strong diatropic σ and paratropic π currents of about 14 and -17 nA·T^{-1}, respectively. The net current susceptibilities obtained for Al_4Li^-, Al_4Li_2, $Al_4Li_3^-$, and Al_4Li_4 at the CCSD level of theory using a triple-ζ basis set augmented with polarization functions are 28.1, 28.1, -5.9, and -3.1 nA·T^{-1}, respectively. The corresponding diatropic (paratropic) contributions to the ring-current susceptibilities are 32.4 (0.0), 36.7 (0.0), 18.9 (-19.9), and 18.6 (-16.8) nA·T^{-1}, respectively. On the basis of these data, Sundholm and co-workers concluded that the Al_4^{4-} species are nonaromatic or slightly antiaromatic.

Datta and Pati[183b] computationally demonstrated that similar to the transformation of C_4H_4 from being antiaromatic and rectangular (Δr = 0.24 Å) in the isolated state to being aromatic and almost square (Δr = 0.005 Å) in the η^4-(C_4H_4)−$Fe(CO)_3$ complex, the antiaromatic Al_4Li_4 species with rectangular Al_4 (Δr = 0.13 Å) unit becomes aromatic with an almost square Al_4 (Δr = 0.03Å) unit in the η^4-(Al_4Li_4)−$Fe(CO)_3$ complex, clearly confirming the net antiaromatic nature of Al_4Li_4. Datta and Pati[183c] also performed a σ−π separation analysis of the energies in Al_4Li_4, and they showed that the π distortion prevails over the σ equalization. Thus, Al_4Li_4 is net antiaromatic, even though the π antiaromaticity exceeds the σ aromaticity by just 1 kcal/mol.

The discovery of aromaticity, antiaromaticity, and conflicting aromaticity in all-metal clusters clearly demonstrated that these concepts are capable of explaining structure, stability, chemical bonding, and other molecular properties of many metal, metalloid, and even nonmetal clusters. It has been shown that aromaticity and antiaromaticity in metal clusters frequently have a multiple nature and even a conflicting nature, which is different from that found in common organic molecules. However, much more work needs to be done to firmly establish these concepts as valuable chemical bonding models in clusters of main group clusters.

8. All-Metal Aromatic Clusters as Building Blocks of Molecules and Solids

8.1. Robinson's $R_3Ga_3^{2-}$ Aromatic Organometallic Compounds

In 1995 Robinson and co-workers[44] reported the synthesis of the first organometallic compound, $Na_2[(Mes_2C_6H_3)Ga]_3$ (Mes = 2,4,6-$Me_3C_6H_2$), containing an aromatic triangular ring out of three gallium atoms embedded in a large organometallic compound shown in Figure 37.

On the basis of electron counting and the 60° Ga−Ga−Ga angle, Robinson and co-workers concluded that their compound is a π aromatic system.[44] In follow-up works[45−47] Robinson teamed up with Schaefer, and they confirmed computationally using model compounds that this compound indeed contains two π electrons and thus fulfilled the $4n + 2$ requirement for π aromatic molecules. The π MO calculated for the $K_2[GaH]_3$ model compound is shown in Figure 38. The π electron cloud of $K_2[GaH]_3$ is very similar to that of the prototypical hydrocarbon $C_3H_3^+$. In 1996 Robinson and co-workers reported[45] the analogous potassium compound, $K_2[(Mes_2C_6H_3)Ga]_3$ (Mes = 2,4,6-$Me_3C_6H_2$), containing the a similar

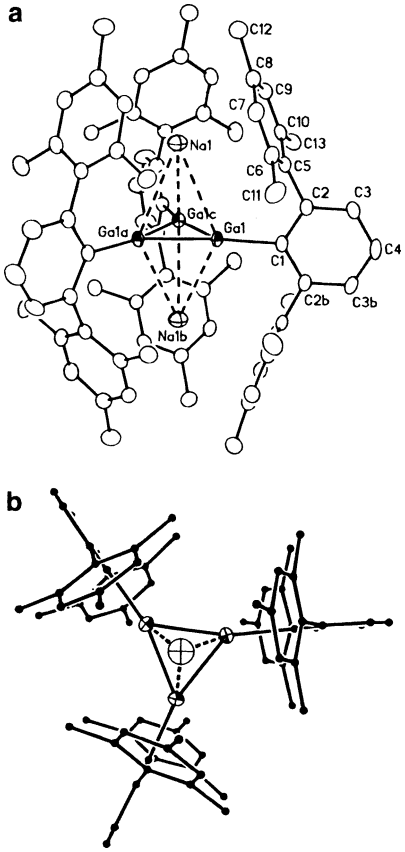

Figure 37. (a) Molecular structure of $Na_2[(Mes_2C_6H_3)Ga]_3$ (thermal ellipsoids are shown at 35% probability level). Selected bond distances (angstroms) and angles (degrees): Ga(1)−Na(1), 3.329(2); Ga(1)−C(1), 2.037(3); Ga(1)−Ga(1a), 2.441(1), Ga(1)−Na(1b), 3.229(2); C(1)−Ga(1)-Ga(1a), 166.3(1); C(1)−Ga(1)-Ga(1c), 133.7(1); Ga(1a)-Ga(1)−Ga(1c), 60.0(1); Na(1)−Ga(1)-Na(1b); 128.2(1), Ga(1)−Na(1)-Ga(1a); 44.4(1). (b) View of $Na_2[(Mes_2C_6H_3)Ga]_3$ along the Na−Na vector.[44] (Reprinted with permission from ref 44. Copyright 1994 American Chemical Society.)

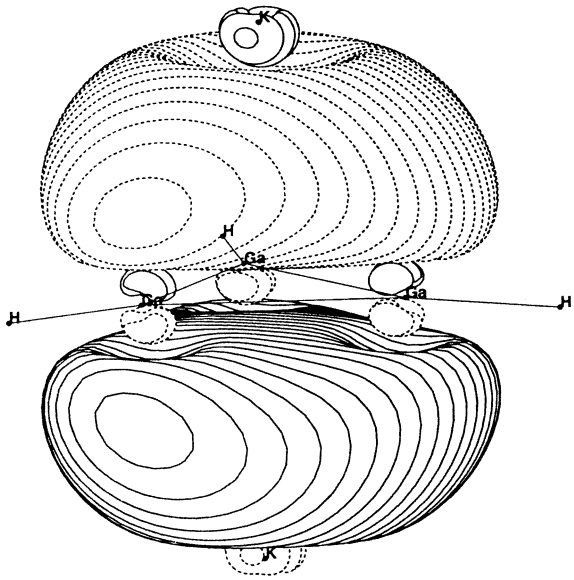

Figure 38. π molecular orbital of $K_2[GaH]_3$.[45] (Reprinted with permission from ref 45. Copyright 1996 American Chemical Society.)

Ga_3 aromatic unit. Robinson and Schaefer[47] also explored aromaticity in a series of model heterocompounds containing $[C_2Ga]$, $[CGa_2]$, $[Si_2Ga]$, and $[SiGa_2]$ aromatic units. The large negative NICS indices suggested that all of these species are indeed aromatic. In 1999 Robinson[48] published a short review on gallium compounds including discussions on aromatic organometallic compounds.

8.2. Power's $R_2Ga_4^{2-}$ Aromatic Organometallic Compound with π Aromaticity and σ Antiaromaticity

In 2001 Twamley and Power reported the synthesis of a truly remarkable compound, $K_2[Ga_4(C_6H_3\text{-}2,6\text{-}Trip_2)_2]$ (Trip = C_6H_2-2,4,6-^{i}Pr$_3$), containing an almost perfect square made of four gallium atoms (Figure 39). Although a compound $(AlBr.Net_3)_4$ containing a planar square Al_4 cluster was reported in 1994 by Schnockel and co-workers,[184] the Schnockel compound is not an aromatic system. Chemical bonding analysis performed for a model compound $(AlCl.NH_3)_4$ by Kuznetsov and Boldyrev[185] clearly showed that after localizing the MOs in the model compounds, four 2c-2e Al−Al bonds (96% localization) were obtained. In both the model compound $(AlCl.NH_3)_4$ and Schnockel's compound $(AlBr.Net_3)_4$, chemical bonding in the Al_4 square can be explained using classical 2c-2e Al−Al bonds. Thus, these compounds are not aromatic or antiaromatic.

We, as well as Phillips and Power,[51,52] performed analyses on the chemical bonding of the Power compound using quantum chemical calculations of model systems. It was concluded that the Ga_4 square in the Power compound has two completely delocalized π-electrons, and thus it is π-aromatic. However, the Ga_4 square does not have enough electrons to form four 2c-2e Ga−Ga σ-bonds. Six σ electrons are available for forming σ bonds in the Ga_4 square, making it σ antiaromatic (Figure 30b), and its structure should be rhombus (see section 7.4). How-

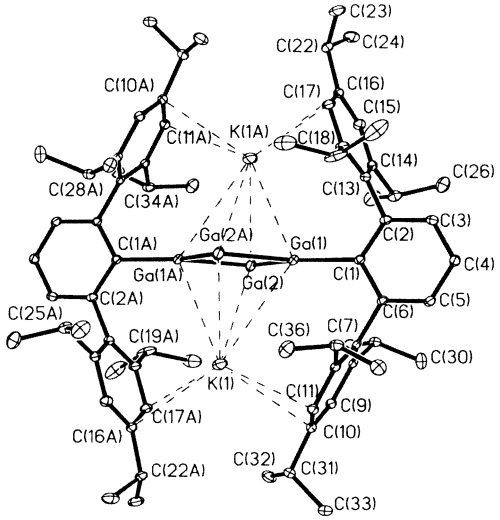

Figure 39. Structure of $K_2[Ga_4(C_6H_3\text{-}2,6\text{-}Trip_2)_2]$ (H atoms are not shown). Selected interatomic distances (angstroms) and angles (degrees): Ga(1)−Ga(2), 2.4623(4); Ga(1)−Ga(2A), 2.4685(3); Ga(1)−C(1), 2.0058(19); Ga(1)−K(1), 3.8017(6); Ga(2)−K(1), 3.8330(6); K(1)−C(11), 3.323(2), K(1)−C(16A), 3.327(2); K(1)−C(17A), 3.268(2); C(1)−Ga(1)-Ga(2), 139.33(6); C(1)−Ga(1)-Ga(2A), 133.44(6), Ga(2)−Ga(1)-Ga(2A), 87.222; Ga(1)−Ga(2)-Ga(1A), 92.778(11); C(6)−C(1)-C(2), 117.82(17).[49] (Reprinted with permission from ref 49. Copyright 2000 Wiley.)

ever, experimental data and results of calculations on the model systems clearly show that the Ga_4 unit possesses an almost perfect square structure. The reason the Ga_4 clusters are an almost perfect squares in the Power compound and in the corresponding model systems is due to contributions from hybridization at the two Ga atoms coordinated by carbon from the ligands. This hybridization works in opposite directions of the rhombus distortion due to the σ antiaromaticity and accidentally almost completely offsets the rhombus distortion. Thus, for the first time a compound containing an all-metal cluster, which is simultaneously π aromatic and σ antiaromatic (at least from the electron-counting point of view), was made in the solid state. This unusual molecule has shown that all-metal clusters with conflicting aromaticity are viable molecular building blocks and may be incorporated in many more novel compounds.

8.3. Tetraatomic Aromatic Species of Group V and VI Elements: M_4^{2-} (M = N, P, As, Sb, Bi) and M_4^{2+} (M = O, S, Se, Te)

In 1977 Cisar and Corbett[58] reported the synthesis of a remarkable compound 2,2,2-crypt-potassium terabismuthide (−2), $(C_{18}H_{36}N_2O_6K^+)_2Bi_4^{2-}$, containing an aromatic all-metal Bi_4^{2-} unit, which is valent isoelectronic to the classical aromatic $C_4H_4^{2-}$ dianion with a σ framework (four 2e-2c C−C bonds and four 2e-2c C−H bonds) and six π electrons.[186−190] Sekiguchi and co-workers[168] synthesized recently a dilithium salt of tetrakis(trimethylsilyc)cyclobutadiene dianion, which provided experimental verification of the aromatic nature of the six π electron cyclobutadiene dianion. In 1984 Critchlow and Corbet[57] reported another potassium-crypt salt of tetraantimonide-(2−), (2,2,2-crypt-K+)$_2Sb_4^{2-}$, containing the aromatic Sb_4^{2-} dianion.

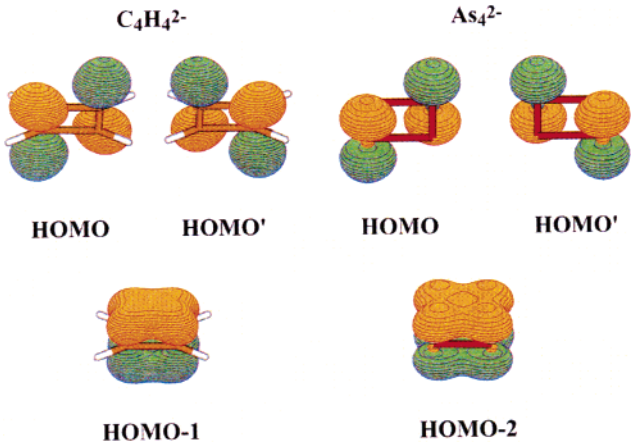

Figure 40. π orbitals of $C_4H_4^{2-}$ and As_4^{2-}.[191] (Reprinted with permission from ref 191. Copyright 1985 American Chemical Society.)

We have examined tetraatomic group V aromatic clusters (Pn_4^{2-}), P_4^{2-}, As_4^{2-}, and Sb_4^{2-}, both theoretically and experimentally.[191] Experimentally, we produced Pn_4^{2-} species stabilized by one Na^+ cation in the form of $NaPn_4^-$ and obtained their PES spectra in a cluster beam in the gas phase. Theoretically, for the bare Pn_4^{2-} dianions we found two low-lying isomers: a square planar structure and a distorted tetrahedral ("roof"-like) structure, with the square structure being more stable. Our calculated Sb−Sb bond length (2.822 Å) in the square structure was close to the experimental values (2.749 and 2.751 Å) reported by Critchlow and Corbet.[57] Excellent agreement between ab initio and experimental PES spectra for NaP_4^-, $NaAs_4^-$, and $NaSb_4^-$ was achieved, confirming the theoretical structures of these species, which consist of a square planar Pn_4^{2-} capped by Na^+ in a pyramidal structure. Molecular orbital analysis showed that indeed all of the Pn_4^{2-} species possess six π electrons (Figure 40). Jin et al.[192] recently reported a theoretical study of MP_4 (M = Be, Mg, and Ca) and M'_2P_4 (M′ = Li, Na, K) clusters and confirmed the aromatic nature of P_4^{2-} in all of these species. Kraus et al.[193] has in fact synthesized a compound $Cs_2P_4{\cdot}2NH_3$, containing an aromatic P_4^{2-} cluster.

The isoelectronic series of group VI chalcogen dications, Ch_4^{2+} (Ch = Te, Se, S, O), have also been studied.[53−56,194−211] The existence of the Se_4^{2+} and Te_4^{2+} dications in solution was reported by Gillespie and co-workers in 1968.[194−196] Subsequent analysis of vibrational spectra and magnetic circular dichroism strongly suggested that these species have a square planar structure. In 1972 Corbett and co-workers[197] reported the synthesis and crystal structure of $Te_4^{2+}(AlCl_4^-)_2$ and showed directly that the Te_4^{2+} unit indeed has a nearly perfect square structure, with the Te−Te bonds being 2.6599(6) and 2.6633(16) Å. In subsequent publications, new compounds containing S_4^{2+} have been reported.[198−200] Theoretical analyses[201−209] of the chemical bonding in S_4^{2+}, Se_4^{2+}, and Te_4^{2+} have confirmed that all of these species are aromatic with six π electrons. Burford et al.[210] reviewed the studies of the Ch_4^{2+} (Ch = Te, Se) dications in 1989. Very recently, the lightest member of this family, the O_4^{2+} dication, has been

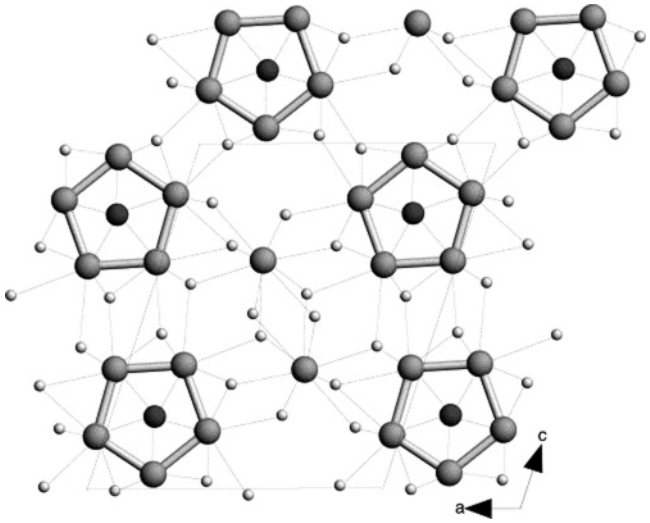

Figure 41. Crystal structures of Na_8BaPb_6, Na_8BaSn_6, and Na_8EuSn_6, showing the pentagonal $Pb(Sn)_5$ rings.[62] (Reprinted with permission from ref 62. Copyright 2004 American Chemical Society.)

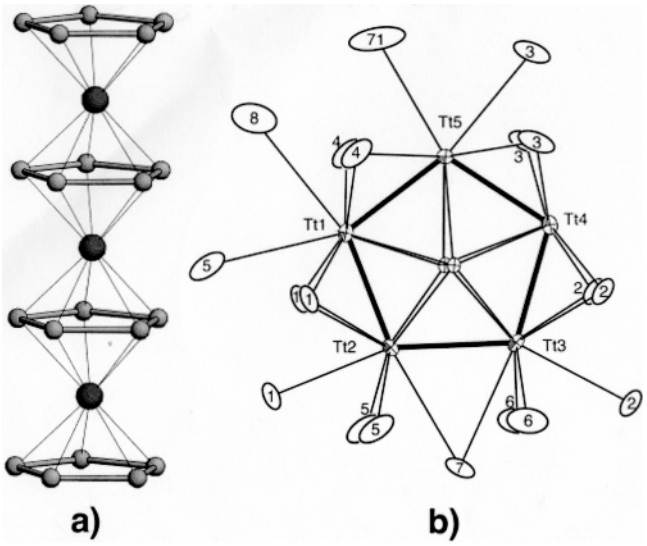

Figure 42. Crystal structures of Na_8BaPb_6, Na_8BaSn_6, and Na_8EuSn_6, showing the stacking of the pentagonal $Pb(Sn)_5$ rings.[62] (Reprinted with permission from ref 62. Copyright 2004 American Chemical Society.)

studied[211] theoretically and has been shown to be the first all-oxygen aromatic species.

The above discussion shows that tetraatomic aromatic clusters of groups V and VI elements with six π electrons and a classical σ framework (four lone pairs located at every atom and four 2c-2e bonds) are well established in chemistry. They can be metal clusters such as Bi_4^{2-}, metalloid clusters such as Sb_4^{2-}, As_4^{2-}, and Te_4^{2+}, or nonmetal clusters such as P_4^{2-}, Se_4^{2+}, S_4^{2+}, and O_4^{2+}. The isoelectronic and isovalent nature of all these species holds, and the change of the nature of the atoms from nonmetal to metalloid and further to metal does not affect the nature of the chemical bonding and the aromaticity in any of these species.

8.4. Pentaatomic Aromatic Species of Group IV and V Elements: M_5^- (M = N, P, As, Sb, Bi) and M_5^{6-} (Ge, Sn, Pb)

Todorov and Sevov[62] recently reported the syntheses and structural characterization of several very unusual all-metal aromatic compounds: Na_8BaPb_6, Na_8BaSn_6, and Na_8EuSn_6. Instead of hexaatomic building blocks from Pb_6 or Sn_6 as the molecular formulas may suggest, detailed analyses revealed that these three compounds exhibit truly unexpected structures (Figures 41 and 42). The three compounds in fact are built of columns of pentagonal aromatic rings (Sn_5^{6-} or Pb_5^{6-}) stacked exactly on top of each other. The alkaline or rare-earth cations are found exactly halfway between the ring planes in a ferrocene-like geometry. The isolated Sn^{4-} or Pb^{4-} monatomic anions are positioned within the plane of the pentagonal rings. Thus, instead of using all six Sn or Pb atoms to form cluster building blocks, these three compounds contain aromatic pentagonal Sn_5^{6-} or Pb_5^{6-} building blocks and the sixth Sn or Pb atom is positioned separately. These compounds are unequivocal proof of the importance of aromaticity in the formation of the Sn_5^{6-} or Pb_5^{6-} building blocks and provide hope that many more compounds with all-metal aromatic building blocks may be synthesized in the future.

The aromaticity in these systems can be easily understood from simple electron counting. In both Sn_5^{6-} or Pb_5^{6-} hexaanions there are 26 valence electrons. Ten of the 26 electrons are lone pairs at each Sn or Pb atom in the pentagonal ring; another 10 electrons form five 2c-2e Sn−Sn or Pb−Pb σ-bonds; and the remaining 6 electrons from three π bonds responsible for the π aromaticity in these hexaanions. Although the electronic structure in both Sn_5^{6-} or Pb_5^{6-} has not yet been studied in detail theoretically, they are valence isoelectronic to the aromatic Pn_5^- (Pn = N, P, As, Sb, Bi) anions, the electronic structure of which has been well understood.[60,61]

In 1994 Gausa et al.[212,213] reported an experimental and theoretical study of the Bi_5^- metal cluster. From the LCAO-LDA calculations they concluded that Bi_5^- has a perfect planar pentagonal structure with a VDE of 3.6 eV, which is substantially higher than the experimental value of 2.89 eV. These authors explained this poor agreement between the experimental and theoretical VDE to be due to the lack of relativistic effects in their calculations. On the basis of isovalent and isostructural analogy between Bi_5^- and $C_5H_5^-$, they concluded that Bi_5^- may be viewed as aromatic with six π electrons. They pointed out that the high first VDE is proof that this system is aromatic. In 2002 we[214] obtained the PES spectra of four Pn_5^- species, including Bi_5^-, and examined their electronic structure and chemical bonding in more detail. In our work well-resolved spectra were obtained at several photon energies (355, 266, and 193 nm) and were used as fingerprints in the identification of global minimum structures for the Pn_5^- clusters. Our measured VDE for Bi_5^- was 2.87 ± 0.02 eV, consistent with the value by Gausa et al.[212,213]

For the metalloid Sb_5^- cluster, Gausa et al. obtained much better agreement between their theoretical (3.7 eV) and experimental (3.8 eV) VDE. We obtained much richer PES spectra for Sb_5^- (Figure

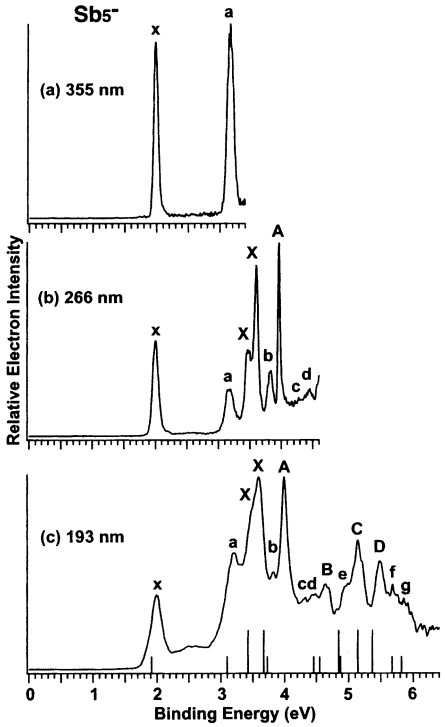

Figure 43. Photoelectron spectra of Sb_5^- at (a) 355 nm, (b) 266 nm, and (c) 193 nm. The longer vertical bars mark the calculated VDEs from the D_{5h} ground state of Sb_5^-, and the shorter vertical bars mark those from the C_{2v} low-lying isomer.[214] (Reprinted with permission from ref 214. Copyright 2002 American Chemical Society.)

43).[214] Our calculations revealed two low-lying isomers for Sb_5^-. The pentagonal and aromatic structure (D_{5h}) is the global minimum with a bicapped tetrahedral isomer (C_{2v}) being 8.2 kcal/mol [CCSD(T)/3-21G*+2s2p1d//B3LYP/3-21G*+2s2p1d] above the global minimum. Our ab initio PES spectra calculated at the OVGF/3-21G*+2s2p1d level of theory were found to be in excellent agreement with the experimental data (Figure 43c and Table 13). The complexicity of the experimental PES spectra was explained nicely by the existence of the low-lying C_{2v} isomers. To prove aromaticity in the global minimum of Sb_5^-, we analyzed its MOs and compared them with the prototypical hydrocarbon molecular anion $C_5H_5^-$ (Figure 44). The three aromatic π MOs are identical in both anions, except that their orders differ. On the basis of this similarity and good agreement between the experimental and theoretical VDEs we concluded that the Sb_5^-, as well as the other valence isoelectronic planar pentagonal species of group V elements, are aromatic with six π electrons.

Another aromatic metalloid cluster, As_5^-, and aromatic nonmetal clusters P_5^- and N_5^- have been studied extensively.[214−223] We reported PES spectra of As_5^- and proved theoretically that the pentagonal D_{5h} ($^1A_1'$) structure is the global minimum.[214] The bicapped tetrahedral isomer was found to be 20.0 kcal/mol [CCSD(T)/6-311+G(2df)//CCSD(T)/6-311+G*] above the global minimum and did not contribute to the PES spectra. The first VDE was measured to be 3.75 ± 0.05 eV, in excellent agreement with the theoretical value of 3.75 eV. Bowen and co-workers[215] obtained previously a PES spectrum of As_5^- using

Table 13. Experimental and Theoretical Vertical Detachment Energies (VDE) in Sb_5^- (Adapted from Reference 214)

			D_{5h}		C_{2v}	
exptl feature	exptl ADE[a]	exptl VDE[a]	MO	VDE (theor)[b]	MO	VDE (theor)[b]
X	3.46 (3)	3.46 (3)	$1e_1''$	3.42 (0.87)		
X′		3.60 (3)				
A		3.97 (2)	$2e_1'$	3.68 (0.88)		
B		4.65 (5)	$1a_2''$	4.84 (0.78)		
C		5.14 (4)	$2a_1'$	5.15 (0.88)		
D		5.48 (4)	$2e_2'$	5.37 (0.83)		
x	1.99 (3)	1.99 (3)			$3b_1$	1.90 (0.88)
a		3.17 (2)			$3b_2$	3.08 (0.89)
b		3.82 (2)			$6a_1$	3.72 (0.88)
c		4.32 (5)			$1a_2$	4.45 (0.89)
d		4.44 (5)			$2b_1$	4.55 (0.86)
e		4.95 (5)			$5a_1$	4.86 (0.87)
f		5.70 (5)			$4a_1$	5.69(0.86)
g		5.87 (5)			$2b_2$	5.81 (0.93)

[a] Numbers in parentheses represent experimental uncertainty in the last digits. [b] VDEs were calculated at the OVGF/3-21G*+2s2p1d//B3LYP/3-21G*+2s2p1d level of theory for Sb_5^- structures. Numbers in parentheses indicate pole strength, which characterizes the validity of the one-electron detachment picture.

2.497 eV photons and reported an EA for As_5 to be >1.7 eV. The energy of the 2.497 eV photons was clearly insufficient to detach an electron from the pentagonal As_5^- anion. Their observed photoelectron signals were due to either very weakly populated low-lying isomers or fragments of As_5^-. De Proft et al.[222] reported ring current and NICS calculations for the planar pentagonal structure of As_5^-. They found that at a height of $1a_0$ the map of the ring current shows a classical example of a diatropic current that agrees with the high negative NICS index (−19.5 ppm), but this feature persists all the way down to the molecular plane. Thus, it is not solely a conventional π current. The orbital analysis reveals that the current density at $1a_0$ has approximately equal contributions from four π electrons and four σ electrons. In the molecular plane, the π current vanishes, but the ring current from σ electrons remains as a strong diatropic circulation at the molecular periphery. A flat NICS height profile indicates cooperation of σ electrons in the overall diatropicity of the current density pattern.

Scherer[223,224] synthesized a sandwich compound $[CpFe(As_5)Fe(C_5Me_5)]PF_6$ containing a planar aromatic As_5^-, with As−As bond lengths in the range of 2.319−2.333 Å compared to our calculated value 2.35 Å [CCSD(T)/6-311+G*] for the isolated As_5^- (D_{5h}, $^1A_1'$).[214] Rheingold and co-workers reported preparation and crystallographic characterization of a remarkable triple-decker sandwich $CpMo(\eta\text{-}(\eta^4\text{-}As_5)\text{-}MoCp$ compound containing a planar As_5 ring.[61] They interpreted this structure as having a As_5^{4-} ion. Indeed, a substantial elongation of two of five As−As bonds by 0.4 Å supports this assignment. It would be interesting to probe this tetraanion (stabilized by three cations perhaps) by PES and by ab initio calculations to determine if this tetraanion is in fact a π antiaromatic or σ antiaromaric species.

The PES spectrum of the P_5^- anion was first recorded with a photon energy of 4.66 eV by Jones

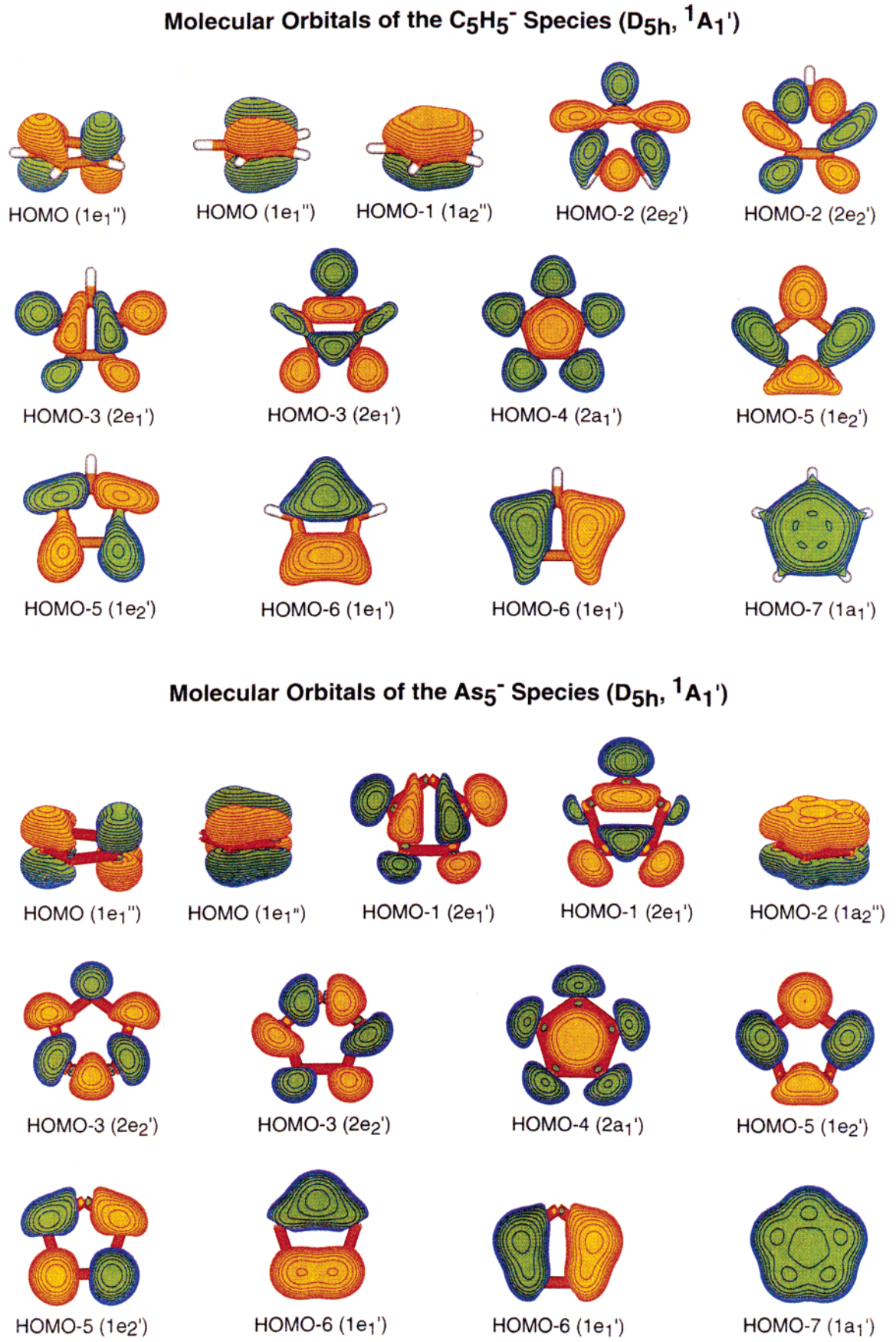

Figure 44. Molecular orbital pictures of $C_5H_5^-$ (D_{5h}, $^1A_1'$) and As_5^- (D_{5h}, $^1A_1'$).[214] (Reprinted with permission from ref 214. Copyright 2002 American Chemical Society.)

et al.[218] They determined a very high first VDE (4.04 eV) for P_5^-. In our work[214] we obtained the PES spectra of P_5^- at both 266 nm (4.661 eV) and 193 nm (6.424 eV). In agreement with the previous results

we found a very high first VDE (4.05 ± 0.03 eV) for P_5^-. We also observed three more peaks at higher binding energies, which were assigned on the basis of ab initio calculations and were used to confirm the planar pentagonal structure for P_5^-. The bicapped tetrahedral isomer was found to be 33.4 kcal/mol [CCSD(T)/6-311+G(2df)//CCSD(T)/6-311+G*] above the pentagonal global minimum and did not contribute to the experimental PES spectra. Aromaticity of P_5^- has been discussed on the basis of NICS calculations by Schleyer and co-workers[221] and on the basis of current density maps by De Proft et al.[222] They found that as in As_5^-, both π and σ electrons contribute to the P_5^- ring current. The cyclic P_5^- has been isolated in alkali metal salts[216,217] and has been incorporated in several mixed sandwich complexes, [(η^5-C_5Me_5)Fe(η^5-P_5)], [(η^5-C_5Me_5)$_2$Fe(η^5-P_5)], and [(η^5-C_5Me_5)Cr_2(η^5-P_5)],[225−227] and recently the carbon-free sandwich complex [Ti(η^5-P_5)$_2$]$^-$ was prepared and characterized.[219]

The lightest member of the group V pentagonal aromatic cluster is N_5^-, which was recently identified mass spectrometrically by Christe and co-workers.[228] This all-nitrogen aromatic species has been extensively studied computationally,[229−244] but experimental spectroscopic data are not yet available.

8.5. Aromatic Hg_4^{6-} Cluster in the Na_3Hg_2 Amalgam

A wide range of alkali metal amalgams is now known with different stoichiometries and structures.[245,246] Low mercury content amalgams contain isolated Hg atoms or clusters solvated by the alkali atoms, whereas high mercury content amalgams tend to have network structures with the alkali atoms occupying interstitial positions. A substantial amount of charge transfer is believed to occur from the alkali-metal atoms to mercury in the amalgams. One particular sodium−mercury amalgam Na_3Hg_2 attracted our attention after our discovery of the first all-metal aromatic Al_4^{2-} cluster.[68] It has been known since 1954 that this amalgam contains Hg_4^{6-} square units as its building blocks (Figure 45).[247] However, why Hg_4^{6-} is a particularly stable building block for the amalgams and why it assumes a perfect square structure are questions that were not understood. Corbett was the first to examine these questions using molecular orbital calculations.[248] We have obtained a key insight into chemical bonding in Hg_4^{6-} through the recent discovery of aromaticity in all-metal clusters.[52,68,71,72] Through model calculations, we showed that the square planar Hg_4^{6-} is isoelectronic to the all-metal aromatic cluster Al_4^{2-} and that its structure and stability can in fact be attributed to aromaticity.[85]

Because the purpose of the Na_6Hg_4 calculations was not to determine its global minimum structure, but rather to examine how the presence of Na^+ cations would influence the MOs and bonding in Hg_4^{6-}, it was important to ensure that the Hg_4 unit in the Na_6Hg_4 model would have the same symmetry as in Hg_4^{6-}. Our geometry optimization with the D_{4h} symmetry restriction led to the square Hg_4 unit with

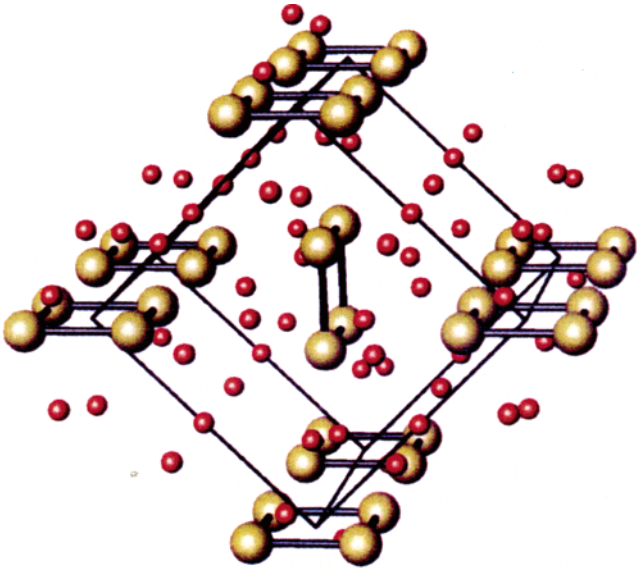

Figure 45. Crystal structure of Na_3Hg_2, showing the Hg_4 square units (yellow) and Na (red).[85] (Reprinted with permission from ref 85. Copyright 2001 Wiley.)

Hg−Hg distances in the range of 2.9−3.1 Å, depending on the methods used. These calculated Hg−Hg bond lengths in the model Na_6Hg_4 cluster are actually very close to the value of 3.0 Å for the square Hg_4 cluster in the Na_3Hg_2 crystal.[247] The bond lengths in the model Na_6Hg_4 cluster are also very close to the optimized Hg−Hg bond length (2.9−3.1) in a linear Na−Hg−Hg−Na molecule.

Figure 46a displays the seven valence MOs of the square planar Hg_4^{6-}, and Figure 46b displays those for the Na_6Hg_4 model cluster. Comparing Figure 46b to Figure 46a, one sees clearly that the same set of occupied MOs is present in both cases. The counterions appear to have little effect on the occupied MOs of the Hg_4^{6-} building block; they alter slightly the MO ordering. The MOs shown in Figure 46a are identical to those of Al_4^{2-},[68] except for the slight difference in ordering among the top three MOs, which are bonding combinations of the valence p orbitals. The bottom four MOs are combinations of the valence s orbitals, which are essentially lone pairs in both Hg_4^{6-} and Al_4^{2-} with little s−p mixing. On the basis of the similar valence MOs and structures in Hg_4^{6-} and Al_4^{2-}, we concluded that Hg_4^{6-} should also be considered to be a mutiple aromatic all-metal cluster.[85] To further confirm the aromatic nature of Hg_4^{6-}, we compared its MOs and bonding to those of an aromatic hydrocarbon $C_4H_4^{2+}$, as shown in Figure 45c. $C_4H_4^{2+}$ has four more valence electrons than Hg_4^{6-}. We observed that except for the degenerate HOMO-1 in $C_4H_4^{2+}$, the remaining seven valence MOs of $C_4H_4^{2+}$ are nearly identical to those of Hg_4^{6-}, with its characteristic aromatic π HOMO.

It should be stressed that a mercury atom has a closed shell electron configuration ($6s^2$) and that neutral Hg_4 is a van der Waals cluster (the bottom four MOs of Figure 46a or Figure 46b provide no net bonding). Hence, the structural and electronic stability of the square planar Hg_4^{6-} and Al_4^{2-} should be attributed not only to π aromaticity due to the presence of the two π electrons in the $1a_{2u}$ orbital but

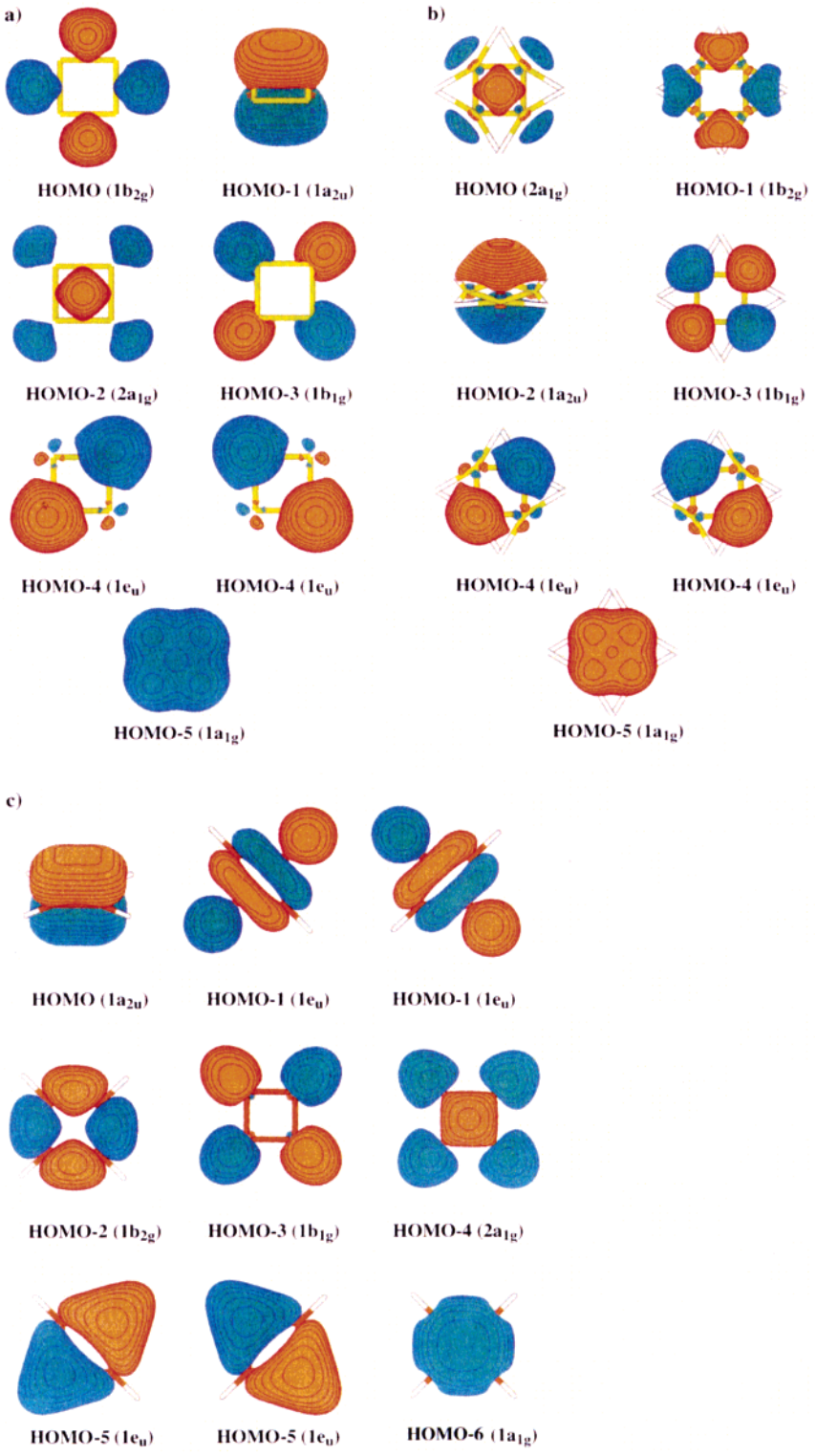

Figure 46. Molecular orbital pictures of square planar Hg_4^{6-} (a) and Na_6Hg_4 (b), compared with those of the aromatic hydrocarbon, $C_4H_4^{2+}$ (c).[85] (Reprinted with permission from ref 85. Copyright 2001 Wiley.)

also to σ aromaticity due to the occupation of the two four-center σ bonding orbitals, $1b_{2g}$ and $2a_{1g}$. The finding of aromaticity in Hg_4^{6-} establishes a solid bridge between our gas-phase studies of multiply aromatic clusters and bulk materials containing such species. It is a pleasant surprise that such an insight can be obtained into ancient and well-known materials such as amalgams using the concept of aromaticity in all-metal systems.

9. Challenges in the Future

We have shown that the concepts of aromaticity and antiaromaticity can be valuable tools in explaining structure, stability, chemical bonding, and other molecular properties of many isolated metal clusters, as well as metal clusters incorporated in organometallic compounds or in solid materials. Although the number of studies dedicated to aromaticity in all-

metal systems is still by far much smaller than for organic molecules, one new feature is emerging. Metal clusters frequently have multiple aromaticity, multiple antiaromaticity, or conflicting aromaticity.

We expect that aromaticity in all-metal or other inorganic systems will continue to attract attention of the chemical community. For future studies we see the following challenges.

1. First of all, new criteria or references about overall aromaticity or antiaromaticity need to be developed for systems with conflicting aromaticity (simultaneously σ aromatic and π antiaromatic or σ antiaromatic and π aromatic).

2. The concepts of aromaticity and antiaromaticity need to be extended into transition metal clusters. Here there is an opportunity to probe two new types of aromaticity and antiaromaticity: δ aromaticity and δ antiaromaticy formed from d-AOs of transition metal atoms, analogous to the δ bond between two transition metal atoms. Another possibility is ϕ aromaticity and ϕ antiaromaticity formed by f-AOs of the lanthanide and actinide elements. Although the d- and f-AOs are usually localized and show less tendency toward chemical bonding, there may be favorable and strongly bonded systems among the vast metal clusters that can be made with these elements. With these additional types of aromaticity and antiaromaticity the possibilities and varieties of their simultaneous presence in a given cluster are even greater, posing more challenges for developing criteria to characterize overall aromaticity or antiaromaticity in a given cluster system.

3. Aromaticity and antiaromaticity may be extended into 3D all-metal systems and may be integrated with other chemical bonding models. The first steps have already been made, as reviewed by Chen and King in the current issue. Considering the fact that the majority of main group clusters and especially transition metal clusters have 3D structures, we believe that this may be a rich field of future studies.

4. The concepts of aromaticity and antiaromaticity may be useful in explaining chemical bonding in bulk metal and metal alloys, connecting ideas in chemistry with those in solid-state physics. We have demonstrated that for alloys with well-defined building blocks, such as Na_3Hg_2, aromaticity is already useful in explaining the structure and stability of the building blocks. However, we need to develop chemical ideas to explain chemical bonding in 3D networks. One way to attack this problem may be to consider fusions of small aromatic units into 2D and 3D networks.

5. New findings of aromaticity in all-metal systems are also applicable to nonmetal clusters. We have recently demonstrated that multiple aromaticity and antiaromaticity can be used to explain the structures and bonding in silicon[153] and boron clusters.[158,249−254] Further advances in this direction will help in the design of new ligands in chemistry.

6. One of the future challenges for understanding aromaticity in metal clusters and in solid metal and alloys will be an analysis of their reactivity. Recently, two papers[103,255] by H. Li and co-workers have been published on computational gas-phase reactivity of some all-metal aromatic species. Certainly, experimental studies on reactivity of all-metal systems are highly desirable.

7. Eventually, the goal of advancing the concepts of aromaticity and antiaromaticity in new territories and chemical systems should be to help develop a unified chemical bonding theory, which will provide us with the ability to intelligently design new materials with special properties and to better understand chemistry including catalysis and even biologically important processes.

10. Acknowledgments

We thank many talented students and postdoctoral associates in both the Utah State and Washington State groups who have contributed to the topics of this review, including Dr. Aleksey E. Kuznetsov, Dr. Anastassia N. Alexandrova, Grant D. Geske, Nathan A. Cannon, Ben M. Elliott, Kelley A. Birch, Dmitry Zubarev, and Eldon Koyle (Utah State University) and Xi Li and Dr. Hua-Jin Zhai (Washington State University). We specifically thank Dr. Anastassia Alexandrova and Dr. Hua-Jin Zhai for their contributions to and help with the development of this review. We are grateful to the principal sponsors of our research—the National Science Foundation (NSF) and the Petroleum Research Fund (PRF) administered by the American Chemical Society. The experimental work carried out at Washington State University was primarily supported by a grant from the NSF (DMR-0095828 and DMR-0503384) and was performed at the W. R. Wiley Environmental Molecular Sciences Laboratory, a national user facility sponsored by the Department of Eenergy's (DOE) Office of Biological and Environmental Research and located at Pacific Northwest National Laboratory, operated for DOE by Battelle. The theoretical work was carried out at Utah State University and was primarily supported by three grants from the PRF-ACS (35255-AC6, 38242-AC6, and 43101-AC6) and from the NSF (CHE-0404937). A.I.B. is grateful to the W. R. Wiley Environmental Molecular Science Laboratory and the Chemical Science Division, Pacific Northwest National Laboratory for the hospitality and support during the preparation of this review.

11. Abbreviations

2c-2e = two-center two-electron bond
3D = three-dimensional
ADE = adiabatic detachment energy
AO = atomic orbital
ARCS = aromatic ring current shielding
B3LYP = hybrid method, a mixture of Hartree−Fock exchange with density functional exchange correlation
BE = binding energy
CASSCF = complete active-space self-consistent field
CCSD(T) = coupled-cluster method with all single and double excitations with noniterative inclusion of triple excitations
CEP = effective core potential
DFT = density functional theory
ELF = electron localization function

EPT = electron propagator theory
GEGA = gradient embedded genetic algorithm
HF = Hartree−Fock
HOMO = highest occupied molecular orbital
IR = infrared
KE = kinetic energy
LUMO = lowest unoccupied molecular orbital
MO = molecular orbital
MP2 = second-order Møller−Plesset pertubation theory
MPn = nth-order Møller−Plesset pertubation theory
MRCISD = multireference singles plus doubles configuration interaction
NICS = nucleus-independent chemical shift
NICS-CMO = NICS index of each canonical MO
NMR = nuclear magnetic resonance
NPA = natural population analysis
OVGF = outer valence Green function
PES = photoelectron spectroscopy
RE = resonance energy
ROVGF = restricted OVGF
SVP = split-valence basis sets augmented with polarization functions
TD-B3LYP = time-dependent B3LYP
TZ2P = triple-ζ quality basis set plus double-polarization functions
TZVPP = valence triple-ζ basis set augmented with two d and one f polarization function
UCCSD(T) = unrestricted CCSD(T)
UOVGF = unrestricted OVGF
UV = ultraviolet
VB = valence bond
VDE = vertical detachment energy
ZPE = zero point energy

12. References

(1) Kekulé, A. *Bull. Soc. Chim. Fr. (Paris)*, **1865**, *3*, 98.
(2) Special edition on aromaticity. Schleyer, P. v. R., Guest Ed. *Chem. Rev.* **2001**, *101* (5).
(3) Special edition on heterocycles. Katritzky, A. R., Guest Ed. *Chem. Rev*. **2004**, *104* (5).
(4) Randic, M. *Chem. Rev*. **2003**, *103*, 3449.
(5) Harvey, R. G. *Polycyclic Aromatic Hydrocarbons*; Wiley-VCH: New York, 1997.
(6) Shaik, S.; Shurki, A.; Danovich, D.; Hiberty, P. C. *J. Mol. Struct. (THEOCHEM)* **1997**, *398*, 155.
(7) Schleyer, P. v. R.; Jiao, H. *Pure Appl. Chem*. **1996**, *38*, 209.
(8) Minkin, V. I.; Glukhovtsev, M. N.; Simkin, B. Ya. *Aromaticity and Antiaromaticity. Electronic and Structural Aspects*; Wiley: New York, 1994.
(9) Gutman, I.; Cyvin, S. J. *Introduction to the Theory of Benzenoid Hydrocarbons*; Springer-Verlag: Berlin, Germany, 1989.
(10) Lloyd, D. *The Chemistry of Conjugate Cyclic Compounds*; Wiley: Chichester, U.K., 1989.
(11) Dias, J. R. *Handbook of Polycyclic Hydrocarbons. Part A. Benzenoid Hydrocarbons*; Elsevier: Amsterdam, The Netherlands, 1987.
(12) Cyvin, S. J.; Gutman, I. *Kekule Structures in Benzenoid Hydrocarbons*; Springer-Verlag: Berlin, Germany, 1988.
(13) Garrat, P. J. *Aromaticity*; Wiley: New York, 1986.
(14) 4th International Symposium on the Chemistry of Novel Aromatic Compounds, Jerusalem, 1981; Agranat, I., Guest Ed. *Pure Appl. Chem.* **1982**, *54*, 927.
(15) Aihara, J.-I. *Pure Appl. Chem.* **1982**, *54*, 1115.
(16) Balaban, A. T. *Pure Appl. Chem.* **1980**, *52*, 1409, and references therein.
(17) International Symposium on Aromaticity, Dubrovnik, 1979; Graovac, A., Trinajstic, N., Guest Eds. *Pure Appl. Chem.* **1980**, *52*, 1397.
(18) Lewis, D.; Peters, D. *Facts and Theories of Aromaticity*; Macmillan: London, U.K., 1975.
(19) *Clar E. The Aromatic Sextet*; Wiley: London, U.K., 1972.
(20) Bergman, E. D., Pullman, B., Eds. *Aromaticity, Pseudoaromaticity, Antiaromaticity*; Israel Academy of Science and Humanities: Jerusalem, Israel, 1971.
(21) Nyulaszi, L. *Chem. Rev*. **2001**, *101*, 1229.
(22) Minkin, V. I.; Minyaev, R. M. *Chem. Rev*. **2001**, *101*, 1247.
(23) Katritzky, A. R.; Jug, K.; Oniciu, D. C. *Chem. Rev*. **2001**, *101*, 1421.
(24) *Metallocenes*; Togni, A., Haltermann, R. L., Eds.; Wiley-VCH: New York, 1998.
(25) Cotton, F. A.; Wilkinson, G.; Murillo, C. A.; Bochmann, M. *Advanced Inorganic Chemistry*, 6th ed.; Wiley: New York, 1999.
(26) Li, J.; Bursten, B. E. *J. Am. Chem. Soc.* **1997**, *119*, 9021, and references therein.
(27) Urnézius, E.; Brennessel, W. W.; Cramer, C. J.; Ellis, J. E.; Schleyer, P. v. R. *Science* **2002**, *295*, 832.
(28) Xu, Z.-F.; Xie, Y.; Feng, W.-L.; Schaefer, H. F., III. *J. Phys. Chem. A* **2003**, *107*, 2716, and references therein.
(29) Lein, M.; Frunzke, J.; Frenking, G. *Inorg. Chem.* **2003**, *42*, 2504, and references therein.
(30) King, R. B. *Chem. Rev.* **2001**, *101*, 1119, and references therein.
(31) Schleyer, P. v. R.; Subramanian, G.; Jiao, H.; Najafian, K.; Hofmann, M. Are Boron Compounds Aromatic? An Analysis of their Magnetic Properties. In *Advances in Boron Chemistry*; Siebert, W., Ed.; The Royal Society of Chemistry: Cambridge, U.K., 1997; p 3.
(32) Kroto, H. W. *Pure Appl. Chem*. **1990**, *62*, 407.
(33) (a) Zanasi, R.; Fowler, P. W. *Chem. Phys. Lett.* **1995**, *238*, 270. (b) Fowler, P. W.; Collins, D. J.; Austin, S. J. *J. Chem. Soc., Perkin 2* **1993**, 275. (c) Fowler, P. W.; Lazzeretti, P.; Malagoli, M.; Zanasi, R. *Chem. Phys. Lett*. **1991**, *179*, 174. (d) Fowler, P. W.; Lazzeretti, P.; Zanasi, R. *Chem. Phys. Lett*. **1990**, *165*, 79.
(34) Buhl, M.; Hirsch, A. *Chem. Rev*. **2001**, *101*, 1153.
(35) Thorn, D. L.; Hoffmann, R. *Nouv. J. Chim.* **1979**, *3*, 39.
(36) Bleeke, J. R. *Chem. Rev.* **2001**, *101*, 1205, and references therein.
(37) Elliot, G. P.; Roper, W. R.; Waters, J. M. *J. Chem. Soc., Chem. Commun.* **1982**, 811.
(38) Bleeke, J. R.; Xie, Y.-F.; Peng, W.-J.; Chiang, M. *J. Am. Chem. Soc.* **1989**, *111*, 4118.
(39) Bleeke, J. R.; Behm, R.; Xie, Y.-F.; Clayton, T. W., Jr.; Robinson, K. D. *J. Am. Chem. Soc.* **1994**, *116*, 4093.
(40) Bleeke, J. R.; Behm, R.; Xie, Y.-F.; Chiang, M. Y.; Robinson, K. D.; Beatty, A. M. *Organometallics* **1997**, *16*, 606, and references therein.
(41) Profilet, R. D.; Fanwick, P. E.; Rothwell, I. P. *Angew. Chem., Int. Ed.* **1992**, *31*, 1261.
(42) Riley, P. N.; Profilet, R. D.; Salberg, M. M.; Fanwick, P. E.; Rothwell, I. P. *Polyhedron* **1998**, *17*, 773.
(43) Bursten, B. E.; Fenske, R. F. *Inorg. Chem.* **1979**, *18*, 1760.
(44) Li, X.-W.; Pennington, W. T.; Robinson, G. H. *J. Am. Chem. Soc.* **1995**, *117*, 7578.
(45) Li, X.-W.; Xie, Y.; Schreiner, P. R.; Gripper, K. D.; Crittendon, R. C.; Campana, C. F.; Schaefer, H. F., III; Robinson, G. H. *Organometallics* **1996**, *15*, 3798.
(46) Xie, Y.; Schreiner, P. R.; Schaefer, H. F., III; Li, X.-W.; Robinson, G. H. *J. Am. Chem. Soc.* **1996**, *118*, 10635.
(47) Xie, Y.; Schreiner, P. R.; Schaefer, H. F., III.; Li, X.-W.; Robinson, G. H. *Organometallics* **1998**, *17*, 114.
(48) Robinson, G. H. *Acc. Chem. Res.* **1999**, *32*, 773, and references therein.
(49) Twamley, B.; Power, P. P. *Angew. Chem., Int. Ed.* **2000**, *39*, 3500.
(50) Kuznetsov, A. E.; Boldyrev, A. I.; Li, X.; Wang, L. S. *J. Am. Chem. Soc.* **2001**, *123*, 8825.
(51) Phillips, A. D.; Power, P. P. *J. Cluster Sci.* **2002,** *13*, 569.
(52) Power, P. P. Multiple Bonding Between Heavier Group 13 Elements. *Struct. Bonding* **2002**, *103*, 58.
(53) Gillespie, R. J.; Passmore, J. *Acc. Chem. Res.* **1971**, *4*, 413.
(54) Brown, I. D.; Crump, D. B.; Gillespie, R. J.; Santry, D. F. *Chem. Commun.* **1968**, 963.
(55) Brown, I. D.; Crump, D. B.; Gillespie, R. J. *Inorg. Chem.* **1971**, *10*, 2319.
(56) Gillespie, R. J.; Pez, G. P. *Inorg. Chem.* **1969**, *8*, 1229.
(57) Critchlow, S. C.; Corbett, J. D. *Inorg. Chem.* **1984**, *23*, 770.
(58) Cisar, A.; Corbett, J. D. *Inorg. Chem.* **1977**, *16*, 2482.
(59) Adolphson, D. G.; Corbett, J. D.; Merryman, D. J. *J. Am. Chem. Soc.* **1976**, *98*, 7234.
(60) Scherer, O. J. *Angew. Chem., Int. Ed*. **1990**, *29*, 1104.
(61) Rheingold, A. L.; Foley, M. J.; Sullivan, P. J. *J. Am. Chem. Soc*. **1982**, *104*, 4727.
(62) Todorov, I.; Sevov, S. C. *Inorg. Chem*. **2004**, *43*, 6490.
(63) (a) King, R. B.; Rouvray, D. H. *J. Am. Chem. Soc.* **1977**, *99*, 7834. (b) Aihara, J. *J. Am. Chem. Soc*. **1978**, *100*, 3339. (c) Aihara, J. *Inorg. Chem*. **2001**, *40*, 5042.
(64) King, R. B. *Inorg. Chem.* **2002**, *41*, 4722.
(65) Wade, K, *Adv. Inorg. Chem. Radiochem*, **1976**, *18*, 1.
(66) King, R. B. *Inorg. Chem.* **1991**, *30*, 4437.
(67) Li, J. *J. Cluster Sci.* **2002**, *13*, 137.
(68) Li, X.; Kuznetsov, A. E.; Zhang, H. F.; Boldyrev, A. I.; Wang, L. S. *Science* **2001**, *291*, 859.
(69) (a) Juselius, J.; Straka, M.; Sundholm, D. *J. Phys. Chem. A* **2001**, *105*, 9939. (b) Lin, Y.-C.; Juselius, J.; Sundholm, D.; Gauss, J. *J. Chem. Phys.* **2005**, *122*, 214308.
(70) Zhan, C.-G.; Zheng, F.; Dixon, D. A. *J. Am. Chem. Soc.* **2002**, *124*, 14795.
(71) Boldyrev, A. I.; Kuznetsov, A. E. *Inorg. Chem.* **2002**, *41*, 532.
(72) Li, X.; Zhang, H. F.; Wang, L. S.; Kuznetsov, A. E.; Cannon, N. A.; Boldyrev, A. I. *Angew. Chem., Int. Ed.* **2001**, *40*, 1867.

(73) Chi, X. X.; Li, X. H.; Chen, X. J.; Yuang, Z. S. *J. Mol. Struct. (THEOCHEM)* **2004**, *677*, 21.
(74) Zhao, C.; Balasubramanian, K. *J. Chem. Phys.* **2004**, *120*, 10501.
(75) Kuznetsov, A. E.; Boldyrev, A. I. *Struct. Chem.* **2002**, *13*, 141.
(76) (a) Tanaka, H.; Neukermans, S.; Janssens, E.; Silverans, R. E.; Lievens, P. *J. Am. Chem. Soc*. **2003**, *125*, 2862. (b) Alexandrova, A. N.; Boldyrev, A. I.; Zhai, H.-J.; Wang, L. S. *J. Phys. Chem. A* **2005**, *109*, 562. (c) Wannere, C. S.; Corminboeuf, C.; Wang, Z.-X.; Wodrich, M. D.; King, R. B.; Schleyer, P. v. R. *J. Am. Chem. Soc.* **2005**, *127*, 5701.
(77) Tsipis, A. C.; Tsipis, C. A. *J. Am. Chem. Soc*. **2003**, *125*, 1136.
(78) Mercero, J. M.; Ugalde, J. M. *J. Am. Chem. Soc*. **2004**, *126*, 3380.
(79) Kong, Q.; Chen, M.; Dong, J.; Li, Z.; Fan, K.; Zhou, M. *J. Phys. Chem*. *A* **2002**, *106*, 11709.
(80) Kuznetsov, A. E.; Zhai, H. J.; Wang, L. S.; Boldyrev, A. I. *Inorg. Chem.* **2002**, *41*, 6062.
(81) Gausa, M.; Kaschner, R.; Lutz, H. O.; Seifert, G.; Meiwes-Broer, K.-H. *Chem. Phys. Lett.* **1994**, *230*, 99.
(82) Gausa, M.; Kaschner, R.; Seifert, G.; Faehmann, J. H.; Lutz, H. O.; Meiwes-Broer, K.-H. *J. Chem. Phys*. **1996**, *104*, 9719.
(83) Lein M.; Frunzke, J.; Frenking, G. *Angew. Chem., Int. Ed*. **2003**, *42*, 1303.
(84) Zhai, H.-J.; Wang, L. S.; Kuznetsov, A. E.; Boldyrev, A. I. *J. Chem. Phys. A* **2002**, *106*, 5600.
(85) Kuznetsov, A. E.; Corbett, J. D.; Wang, L. S.; Boldyrev, A. I. *Angew. Chem., Int. Ed*. **2001**, *40*, 3369.
(86) Fowler, P. W.; Havenith, R. W. A.; Steiner, E. *Chem. Phys. Lett*. **2001**, *342*, 85.
(87) Fowler, P. W.; Havenith, R. W. A.; Steiner, E. *Chem. Phys. Lett*. **2002**, *359*, 530.
(88) Chen, Z.; Corminboeuf, C.; Heine, T.; Bohmann, J.; Schleyer, P. v. R. *J. Am. Chem. Soc*. **2003**, *125*, 13930.
(89) Havenith, R. W. A.; van Lenthe, J. H. *Chem. Phys. Lett*. **2004**, *385*, 198.
(90) Santos, J. C.; Tiznado, W.; Contreras, R.; Fuentealba, P. *J. Chem. Phys*. **2004**, *120*, 1670.
(91) Kuznetsov, A. E.; Birch, K. A.; Boldyrev, A. I.; Li, X.; Zhai, H. J.; Wang, L. S. *Science* **2003**, *300*, 622.
(92) Havenith, R. W. A.; Fowler, P. W.; Steiner, E.; Shetty, S.; Kanhere, D.; Pal, S. *Phys. Chem. Chem. Phys*. **2004**, *6*, 285.
(93) Shetty, S.; Kanhere, D. G.; Pal, S. *J. Phys. Chem. A* **2004**, *108*, 628.
(94) Santos, J. C.; Andres, J.; Aizman, A.; Fuentealba, P. *J. Chem. Theory Comput*. **2005**, *1*, 83.
(95) Ritter, S. K. *Chem. Eng. News* **2003**, *81* (50), 23.
(96) Krygowski, T. M.; Cyranski, M. K.; Czarnocki, Z.; Häfelinger, G.; Katritzky, A. R. *Tetrahedron* **2000**, *56*, 1783.
(97) Krygowski, T. M.; Cyranski, M. K. *Chem. Rev*. **2001**, *101*, 1385.
(98) Wang, L. S.; Cheng, H. S.; Fan, J. *J. Chem. Phys*. **1995**, *102*, 9480.
(99) Wang, L. S.; Wu, H. In *Advances in Metal and Semiconductor Clusters, IV. Cluster Materials*; Duncan, M. A., Ed.; JAI Press: Greenwich, CT, 1998; pp 299−343.
(100) Thomas, O. C.; Zheng, W.; Bowen, K. H., Jr. *J. Chem. Phys*. **2001**, *114*, 5514.
(101) Rao, B. K.; Jena, P. *J. Chem. Phys*. **2000**, *113*, 1508.
(102) Dhavale, A.; Kanhere, D. G.; Blundell, S. A.; Zope, R. R. *Phys. Rev. B* **2002**, *65*, 085402.
(103) Hu, X.; Li, H.; Liang, W.; Han, S. *Chem. Phys. Lett*. **2004**, *397*, 180.
(104) (a) Alexandrova, A. N.; Boldyrev, A. I.; Fu, Y.-J.; Yang, X.; Wang, X.-B.; Wang, L. S. *J. Chem. Phys.* **2004**, *121*, 5709. (b) Alexandrova, A. N.; Boldyrev, A. I. *J. Chem. Theory Comput*. **2005**, *1*, 566.
(105) Parr, R. G.; Yang, W. *Density-Functional Theory of Atoms and Molecules*; Oxford University Press: Oxford, U.K., 1989.
(106) Becke, A. D. *J. Chem. Phys.* **1993**, *98*, 5648.
(107) Perdew, J. P.; Chevary, J. A.; Vosko, S. H.; Jackson, K. A.; Pederson, M. R.; Singh, D. J.; Fiolhais, C. *Phys. Rev. B* **1992**, *46*, 6671.
(108) Gaussian 03 (revision A.1). Frisch, M. J.; Trucks, G. M.; Schlegel, H. B.; Scuseria, G. E.; Robb, M. A.; Cheeseman, J. R.; Montgomery, J. A.; Vreven, T., Kudin, K. N.; Burant, J. C.; Millam, J. M.; Iyengar, S. S.; Tomasi, J.; Barone, V.; Mennucci, B.; Cossi, M.; Scalmani, G.; Rega, N.; Petersson, G. A.; Nakatsuji, H.; Kitao, O.; Nakai, H.; Klene, M.; Li, X.; Knox, J. E.; Hratchian, H. P.; Cross, J. B.; Adamo, C.; Jaramillo, J.; Gomperts, R.; Stratmann, R. E.; Yazyev, O.; Austin, A. J.; Cammi, R.; Pomelli, C.; Ochterski, J. W.; Ayala, P. Y.; Morokuma, K.; Voth, G. A.; Salvador, P.; Dannenberg, J. J.; Zakrzewski, V. G.; Dapprich, S.; Daniels, A. D.; Strain, M. C.; Farkas, O.; Malick, D. K.; Rabuck, A. D.; Raghavachari, K.; Foresman, J. B.; Ortiz, J. V.; Cui, Q.; Baboul, A. G.; Clifford, S.; Cioslowski, J.; Stefanov, B. B.; Liu,.; Liashenko, A.; Piskorz, P.; Komaromi, I.; Martin, R. L.; Fox, D. J.; Keith, T.; Al-Laham, M. A.; Peng, C. Y.; Nanayakkara, A.; Challacombe, M.; Gill, P. M. W.; Johnson, B. G.; Chen, W.; Wang, M. W.; Gonzales, C.; Pople, J. A. Gaussian, Inc.: Pittsburgh, PA, 2003.
(109) Deaven, D. M.; Ho, K. M. *Phys. Rev. Lett*. **1995**, *75*, 288.
(110) Alexandrova, A. N.; Boldyrev, A. I. Unpublished results.
(111) Koopmans, T. *Physica* **1933**, *1*, 104.
(112) Linderberg, J.; Ohrn, Y. *Propagators in Quantum Chemistry*; Wiley: Hoboken NJ, 2004.
(113) Pickup, B. T.; Goscinki, O. *Mol. Phys*. **1973**, *26*, 1013.
(114) Simons, J.; Smith, W. D. *J. Chem. Phys*. **1973**, *58*, 4899.
(115) Cederbaum, L. S. *J. Phys. B* **1975**, *8*, 290.
(116) Niessen, W. von; Shirmer, J.; Cederbaum, L. S. *Comput. Phys. Rep*. **1984**, *1*, 57.
(117) Zakrzewski, V. G.; Ortiz, J. *V. Int. J. Quantum Chem., Quantum Chem. Symp*. **1994**, *28*, 23.
(118) (a) Zakrzewski, V. G.; Ortiz, J. V. *Int. J. Quantum Chem.* **1995**, *53*, 583. (b) Ortiz, J. V. *Int. J. Quantum Chem., Quantum Chem. Symp*. **1989**, *23*, 321. (c) Lin, J. S.; Ortiz, J. V. *Chem. Phys. Lett*. **1990**, *171*, 197.
(119) (a) Zakrzewski, V. G.; Ortiz, J. V.; Nichols, J. A.; Heryadi, D.; Yeager, D. L.; Golab, J. T. *Int. J. Quantum Chem.* **1996**, *60*, 29. (b) Ortiz, J. V. *Adv. Quantum Chem*. **1999**, *35*, 33.
(120) Krishnan, R.; Binkley, J. S.; Seeger, R.; Pople, J. A. *J. Chem. Phys*. **1980**, *72*, 650.
(121) Frisch, M. J.; Head-Gordon, M.; Pople, J. A. *Chem. Phys. Lett*. **1990**, *166,* 281, and references therein.
(122) Cizek, J. *Adv. Chem. Phys*. **1969**, *14*, 35.
(123) Purvis, G. D., III; Bartlett, R. J. *J. Chem. Phys*. **1982**, *76*, 1910.
(124) (a) Raghavachari, K.; Trucks, G. W.; Pople, J. A.; Head-Gordon, M. *Chem. Phys. Lett*. **1989**, *157*, 479. (b) Scuseria, G. E.; Schaefer, H. F., III. *J. Chem. Phys.* **1989**, *90*, 3700, and references therein.
(125) Dewar, M. J. S. *Bull. Soc. Chim. Belg*. **1979**, *88*, 957.
(126) Dewar, M. J. S.; McKee, M. L. *Pure Appl. Chem*. **1980**, *52*, 1431.
(127) Cremer, D.; Gauss, J. *J. Am. Chem. Soc*. **1986**, *108*, 7467, and references therein.
(128) Cremer, D. *Tetrahedron* **1988**, *44*, 7427, and references therein.
(129) Unverzagt, M.; Subramanian, G.; Hofmann, M.; Schleyer, P. v. R., Harms, K.; Massa, W.; Berndt, A. *Angew. Chem., Int. Ed*. **1997**, *36*, 1469.
(130) Prasang, C.; Hofmann, M.; Geiseler, G.; Massa, W.; Berndt, A. *Angew. Chem., Int. Ed*. **2002**, *41*, 1526.
(131) Prasang, C.; Mlodzianowska, A.; Sahin, Y.; Hofmann, M.; Geiseler, G.; Massa, W.; Berndt, A. *Angew. Chem., Int. Ed*. **2002**, *41*, 3380.
(132) Pyykko, P.; Zhao, Y. *Mol. Phys*. **1990**, *70*, 701, and references therein.
(133) Pyykko, P. *Phys. Scr.* **1990**, *T33*, 52, and references therein.
(134) Pyykko, P.; Zhao, Y. *J. Phys. Chem.* **1990**, *94*, 7753, and references therein.
(135) Wang, X. B.; Wang, L. S. *Nature* **1999**, *400*, 245.
(136) Wang, L. S.; Wang, X. B. *J. Phys. Chem. A* **2000**, *104*, 1978, and references therein.
(137) Scheller, M. K.; Compton, R. N.; Cederbaum, L. S. *Science* **1995**, *270*, 1160, and references therein.
(138) Simons, J.; Skurski, P.; Barrios, R. *J. Am. Chem. Soc*. **2000**, *122*, 11893, and references therein.
(139) Becke, A.; Edgecombe, K. *J. Chem. Phys*. **1990**, *92*, 5397.
(140) Silvi, B.; Savin, A. *Nature* **1994**, *371*, 683.
(141) Silvi, B. *Phys. Chem. Chem. Phys*. **2004**, *6*, 256.
(142) Savin, A.; Silvi, B.; Colonna, F. *Can. J. Chem*. **1996**, *74*, 1088.
(143) . Savin, A.; Becke, A.; Flad, D.; Nesper, R.; Preuss, H.; Schnering, H. v. *Angew. Chem., Int. Ed. Engl.* **1991**, *30*, 409.
(144) Schaad, L. J.; Hess, B. A., Jr. *Chem. Rev*. **2001**, *101*, 1465.
(145) Schleyer, P. v. R.; Maerker, C.; Dransfeld, A.; Jiao, H.; Hommes, N. J. R. *J. Am. Chem. Soc*. **1996**, *118*, 6317.
(146) Boldyrev, A. I.; Simons, J.; Li, X.; Chen, W.; Wang, L. S. *J. Chem. Phys*. **1999**, *110*, 8980.
(147) Feng, P. Y.; Balasubramanian, K. *Chem. Phys. Lett*. **1999**, *301*, 458.
(148) Archibong, E. F.; St-Amant, A.; Goh, S. K.; Marynick, D. S. *J. Phys. Chem. A* **2002**, *106*, 5932.
(149) Feng, P. Y.; Balasubramanian, K. *Chem. Phys. Lett*. **1998**, *288*, 1.
(150) Archibong, E. F.; St-Amant, A.; Goh, S. K.; Marynick, D. S. *Chem. Phys. Lett.* **2002**, *361*, 411.
(151) Archibong, E. F.; St-Amant, A. *J. Phys. Chem. A* **2002**, *106*, 7390.
(152) Balasubramanian, K.; Zhu, X. *J. Chem. Phys*. **2001**, *115*, 8858.
(153) Zhai, H. J.; Kuznetsov, A. E.; Boldyrev, A. I.; Wang, L. S. *ChemPhysChem*, **2004**, *5*, 1.
(154) Li, X.; Wang, X. B.; Wang, L. S. *Phys. Rev. Lett*. **1998**, *81*, 1909.
(155) Wu, H.; Li, X.; Wang, X. B.; Ding, C.-F.; Wang, L. S. *J. Chem. Phys*. **1998**, *109*, 449.
(156) Villata, P. W.; Leopold, D. G. Unpublished data quoted in ref 157.
(157) Baeck, K. K.; Bartlett, R. J. *J. Chem. Phys*. **1998**, *109*, 1334.
(158) Zhai, H. J.; Wang, L. S.; Alexandrova, A. N.; Boldyrev, A. I.; Zakrzewski, V. G. *J. Phys. Chem*. *A* **2003**, *107*, 9319.
(159) Boldyrev, A. I. Unpublished data.
(160) Bishop, D. M.; Chaillet, M.; Larrieu, K.; Pouchan, C. *Mol. Phys.* **1984**, *51*, 179.

(161) (a) Alexandrova, A. N.; Boldyrev, A. I. *J. Phys. Chem. A* **2003**, *107*, 554. (b) Havenith, R. W. A.; De Proft, F.; Fowler, P. W.; Geerlings, P. *Chem. Phys. Lett*. **2005**, *407*, 391.
(162) Ivanic, J.; Marsden, C. J.; Hassett, D. M. *J. Chem. Soc., Chem. Commun*. **1993**, 822.
(163) Cremer, D.; Binkley, J. S.; Pople, J. A.; Hehre, W. *J. J. Am. Chem. Soc*. **1974**, *96*, 6900.
(164) Beckman, H.-O.; Koutecky, J.; Bonacuc-Koutecky, V. *J. Chem. Phys*. **1980**, *73*, 5182.
(165) Glukhovtsev, M. N.; Schleyer, P. v. R.; Stein, A. *J. Phys. Chem*. **1993**, *97*, 5541.
(166) Balci, M.; McKee, M. L.; Schleyer, P. v. R. *J. Phys. Chem. A* **2000**, *104*, 1246.
(167) Zandwijk, G. v.; Janssen, R. A. J.; Buck, H. M. *J. Am. Chem. Soc.* **1990**, *112*, 4155.
(168) Sekiguchi, A.; Matsuo, T.; Watanabe, H. *J. Am. Chem. Soc*. **2000**, *122*, 5652.
(169) Kuznetsov, A. E.; Boldyrev, A. I. *Chem. Phys. Lett*. **2004**, *388*, 452.
(170) Kaplan, I. G.; Dolgounitcheva, O.; Watts, J. D.; Ortiz, J. V. *J. Chem. Phys*. **2002**, *117*, 3687.
(171) Reuse, F.; Khana, S. N.; Coulon, V. de.; Buttet, J. *Phys. Rev. B* **1989**, *39*, 12911.
(172) Reuse, F.; Khana, S. N.; Coulon, V. de.; Buttet, J. *Phys. Rev. B* **1990**, *41*, 11743.
(173) Thomas, O. C.; Zheng, W.; Xu, S.; Bowen, K. H., Jr. *Phys. Rev. Lett*. **2002**, *89*, 213403.
(174) Chacko, S.; Kanhere, D. G.; Paranjape, V. V. *Phys. Rev. A* **2004**, *70*, 023204.
(175) *Chem. Eng. News* **2003**, *81* (51), 45.
(176) Baird, N. C. *J. Am. Chem. Soc*. **1972**, *94*, 4941.
(177) Raghavachari, K.; Logovinsky, V. *Phys. Rev. Lett*. **1985**, *55*, 2853.
(178) Honea, E. C.; Ogura, A.; Murray, C. A.; Raghavachari, K.; Sprenger, W. O.; Jarrold, M. F.; Brown, W. L. *Nature* **1993**, *366*, 42.
(179) Li, S.; Van Zee, R. J.; Weltner, W. Jr.; Raghavachari, K. *Chem. Phys. Lett*. **1995**, *243*, 275.
(180) Fulara, J.; Freivogel, P.; Grutter, M.; Maier, J. P. *J. Phys. Chem*. **1996**, *100*, 18042.
(181) Shiota, Y.; Kondo, M.; Yoshizawa, K. *J. Chem. Phys*. **2001**, *115*, 9243.
(182) Shaik, S.; Shurki, A.; Danovich, D.; Hiberty, P. C. *Chem. Rev*. **2002**, *101*, 1501.
(183) (a) Datta, A.; Pati, S. K. *J. Phys. Chem. A* **2004**, *108*, 9527. (b) Datta, A.; Pati, S. K. *J. Am. Chem. Soc*. **2005**, *127*, 3496. (c) Datta, A.; Pati, S. K. *J. Chem. Theory Comput*. **2005**, *1*, 824.
(184) Mocker, M.; Robl, C.; Schnockel, H. *Angew. Chem., Int. Ed*. **1994**, *33*, 1754.
(185) Kuznetsov, A. E.; Boldyrev, A. I. *Inorg. Chem*. **2002**, *41*, 3596.
(186) Clark, T.; Wilhelm, D.; Schleyer, P. v. R. *Tetrahedron Lett.* **1982**, *23*, 3457.
(187) Hess, B. A., Jr.; Ewig, C. S.; Schaad, L. J. *J. Org. Chem*. **1985**, *50*, 5869.
(188) Skancke, A. *Nouv. J. Chim*. **1985**, *9*, 577.
(189) Zandwijk, G. v.; Janssen, R. A. J.; Buck, H. M. *J. Am. Chem. Soc*. **1990**, *112*, 4155.
(190) Balci, M.; McKee, M. L.; Schleyer, P. v. R. *J. Phys. Chem. A* **2000**, *104*, 1246.
(191) Kuznetsov, A. E.; Zhai, H.-J.; Wang, L. S.; Boldyrev, A. I. *Inorg. Chem.* **2002**, *41*, 6062.
(192) Jin, Q.; Jin, B.; Xu, W. G. *Chem. Phys. Lett.* **2004**, *396*, 398.
(193) Kraus, F.; Aschenbrenner, J. C.; Korber, N. *Angew. Chem., Int. Ed*. **2003**, *42*, 4030.
(194) Gillespie, R. J.; Barr, J.; Kapoor, R.; Malhotra, K. C. *Can. J. Chem*. **1968**, *46*, 149.
(195) Gillespie, R. J.; Barr, J.; Crump, D. B.; Kapoor, R.; Ummat, P. K. *Can. J. Chem*. **1968**, *46*, 3607.
(196) Barr, J.; Gillespie, R. J.; Kapoor, R.; Pez, G. P. *J. Am. Chem. Soc*. **1968**, *90*, 6855.
(197) Couch, T. W.; Lokken, D. A.; Corbett, J. D. *Inorg. Chem*. **1972**, *11*, 357.
(198) Gillespie, R. J.; Passmore, J.; Ummat, P. K.; Vaidya, O. C. *Inorg. Chem*. **1971**, *10*, 1327.
(199) Passmore, J.; Sutherland, G.; White, P. S. *J. Chem. Soc., Chem. Commun*. **1980**, 330.
(200) Cameron, T. S.; Dionne, I.; Jenkins, H. D. B.; Parsons, S.; Passmore, J.; Roobottom, H. K. *Inorg. Chem*. **2000**, *39*, 2042, and references therein.
(201) Tanaka, K.; Yamabe, T.; Teramae, H.; Fukui, K. *Inorg. Chem*. **1979**, *18*, 3591.
(202) Kao, J. *J. Mol. Struct*. **1980**, *63*, 293.
(203) Tang, T.-H.; Bader, R. F. W.; MacDougall, P. J. *Inorg. Chem*. **1985**, *24*, 2047.
(204) Skrezenek, F. L.; Harcourt, R. D. *Theor. Chim. Acta* **1985**, *67*, 271.
(205) Saethre, L. J.; Gropen, O. *Can. J. Chem*. **1992**, *70*, 348.
(206) Sannigrahi, M.; Grein, F. *Can. J. Chem*. **1994,** *72*, 298.
(207) Krossing, I.; Passmore, J. *Inorg. Chem*. **1999**, *38*, 5203.
(208) Jenkins, H. D. B.; Jitariu, L. C.; Krossing, I.; Passmore, J.; Suontamo, R. *J. Comput. Chem*. **2000**, *21*, 218.
(209) Tuononen, H. M.; Suontamo, R.; Valkonen, J.; Laitinen, R. S. *J. Phys. Chem. A* **2004**, *108*, 5670.
(210) Burford, N.; Passmore, J.; Sanders, J. C. P. In *From Atoms to Polymers. Isoelectronic Analogies*; Liebman, J. F., Greenburg, A., Eds.; VCH: New York, 1989; pp 53−108.
(211) Elliott, B. M.; Boldyrev, A. I. *J. Phys. Chem. A* **2005**, *109*, 236.
(212) Gausa, M.; Kaschner, R.; Lutz, H. O.; Seifert, G.; Meiwes-Broer, K.-H. *Chem. Phys. Lett*. **1994**, *230*, 99.
(213) Gausa, M.; Kaschner, R.; Seifert, G.; Faehrmann, J.-H.; Lutz, H. O.; Meiwes-Broer, K.-H. *J. Chem. Phys.* **1996**, *104*, 9719.
(214) Zhai, H. J.; Wang, L. S.; Kuznetsov, A. E.; Boldyrev, A. I. *J. Phys. Chem. A* **2002**, *106*, 5600.
(215) Lippa, T. P.; Xu, S.-J.; Lyapustina, S. A.; Nilles, J. M.; Bowen, K. H. *J. Chem. Phys.* **1998**, *109*, 10727.
(216) Baudler, M.; Akpapoglou, S.; Ouzounis, D.; Wasgestian, F.; Meinigke, B.; Budzikiewicz, H.; Munster, H. *Angew. Chem., Int. Ed. Engl.* **1988**, *27*, 280.
(217) Baudler, M.; Duster, D.; Ouzounis, D. *Z. Anorg. Allg. Chem*. **1987**, *544*, 87.
(218) Jones, R. O.; Gantefor, G.; Hunsicker, S.; Pieperhoff, P. *J. Chem. Phys*. **1995**, *103*, 9549.
(219) Urnezius, E.; Brennessel, W. W.; Cramer, C. J.; Ellis, J. E.; Schleyer, P. v. R. *Science* **2002**, *295*, 832.
(220) Beck, V.; Cowley, A. R.; O'Hare, D. *Organometallics* **2004**, *23*, 4265.
(221) Dransfeld, A.; Nyulaszi, L.; Schleyer, P. v. R. *Inorg. Chem*. **1998**, *37*, 4413.
(222) De Proft, F.; Fowler, P. W.; Havenith, R. W. A.; Schleyer, P. v. R.; Lier, G. V.; Geerlings, P. *Chem. Eur. J.* **2004**, *10*, 940.
(223) Scherer, O. J. *Angew. Chem., Int. Ed. Engl.* **1990**, *29*, 1104.
(224) Scherer, O. J. *Acc. Chem. Res*. **1999**, *32*, 751.
(225) Scherer, O. J.; Bruck, T. *Angew. Chem., Int. Ed. Engl.* **1987**, *26*, 59.
(226) Scherer, O. J.; Schwalb, J.; Wolmershauser, G.; Kaim, W.; Gross, R. *Angew. Chem., Int. Ed. Engl.* **1986**, *25*, 363.
(227) Chamizo, J. A.; Ruiz-Mazon, M.; Salcedo, R.; Toscano, R. A. *Inorg. Chem*. **1990**, *29*, 879.
(228) Vij, A.; Pavlovich, J. G.; Wilson, W. W.; Vij, V.; Christe, K. O. *Angew. Chem., Int. Ed*. **2002**, *41*, 3051.
(229) Sana, M.; Leroy, G.; Nguyen, M. T.; Elguero, J. *Neuv. J. Chim*. **1979**, *3*, 607.
(230) Nguyen, M. T.; Sana, M.; Leroy, G.; Elguero, J. *Can. J. Chem*. **1983**, *61*, 1435.
(231) Nguyen, M. T.; McGinn, M. A.; Hegarty, A. F.; Elguero, J. *Polyhedron* **1985**, *4*, 1721.
(232) Glukhovtsev, M. N.; Schleyer, P. v. R.; Maerker, C. *J. Phys. Chem*. **1993**, *97*, 8200.
(233) Ostrovskii, V. A.; Eurasalimskii, G. B.; Shcherbinin, M. B. *Russ. J. Org. Chem*. **1995**, *31*, 1284.
(234) Glukhovtsev, M. N.; Jiao, H.; Schleyer, P. v. R. *Inorg. Chem*. **1996**, *35*, 7124.
(235) Perera, S. A.; Bartlett, R. J. *Chem. Phys. Lett.* **1999**, *314*, 381.
(236) Bartlett, R. J. *Chem. Ind*. **2000**, 140.
(237) Gagliardi, L.; Pyykko, P. *J. Am. Chem. Soc*. **2001**, *123*, 9700.
(238) Lein, M.; Frunzke, J.; Timoshkin, A.; Frenking, G. *Chem. Eur. J*. **2001**, *7*, 4155.
(239) Nguyen, M. T.; Ha, T.-K. *Chem. Phys. Lett*. **2001**, *335*, 311.
(240) Gagliardi, L.; Orlandi, G.; Evangelisti, S.; Roos, B. O. *J. Chem. Phys*. **2001**, *114*, 10733.
(241) Fau, S.; Bartlett, R. J. *J. Phys. Chem. A* **2001**, *105,* 4096.
(242) Gagliardi, L.; Pyykko, P. *J. Phys. Chem. A* **2002**, *106*, 4690.
(243) Fau, S.; Wilson, K. J.; Bartlett, R. J. *J. Phys. Chem. A* **2002**, *106,* 4639.
(244) Dixon, D. A.; Feller, D.; Christe, K. O.; Wilson, W. W.; Vij, A.; Vij, V.; Jenkins, D. B.; Olson, R. M.; Gordon, M. S. *J. Am. Chem. Soc*. **2004**, *126*, 834.
(245) Deiseroth, H.-J. *Prog. Solid State Chem*. **1997**, *25*, 73.
(246) Deiseroth, H.-J. In *Molecular Clusters of the Main Group Elements*; Driess, M., Noth, H., Eds.; Wiley-VCH: New York, 2004; pp 169−187.
(247) Nielsen, J. W.; Baenziger, N. C. *Acta Crystallogr*. **1954**, *7*, 277.
(248) Corbett, J. D. *Inorg. Nucl. Chem. Lett*. **1969**, *5*, 81.
(249) Zhai, H.-J.; Wang, L. S.; Alexandrova, A. N.; Boldyrev, *J. Chem. Phys*. **2002**, *117*, 7917.
(250) Alexandrova, A. N.; Boldyrev, A. I.; Zhai, H.-J.; Wang, L. S.; Sheiner, E.; Fowler, P. W. *J. Phys. Chem. A* **2003**, *107*, 1359.
(251) Zhai, H.-J.; Alexandrova, A. N.; Birch, K. A.; Boldyrev, A. I.; Wang, L. S. *Angew. Chem., Int. Ed.* **2003**, *42*, 6004.
(252) Zhai, H.-J.; Kiran, B.; Li, J.; Wang, L. S. *Nat. Mater.* **2003**, *2*, 827.
(253) Alexandrova, A. N.; Boldyrev, A. I.; Zhai, H.-J.; Wang, L. S. *J. Phys. Chem. A* **2004**, *108*, 3509.
(254) Kuznetsov, A. E.; Boldyrev, A. I. *Struct. Chem*. **2002**, *13*, 141.
(255) Hu, X.; Li, H.; Liang, W.; Han, S. *Chem. Phys. Lett*. **2005**, *402*, 539.

CR030091T